1984

Polarized crystal optical spectra of Magnus-type salts

Michael Lee Rodgers
Iowa State University

Rodgers, Michael Lee

POLARIZED CRYSTAL OPTICAL SPECTRA OF MAGNUS-TYPE SALTS

Iowa State University PH.D. 1984

Polarized crystal optical spectra of Magnus-type salts

by

Michael Lee Rodgers

A Dissertation Submitted to the
Graduate Faculty in Partial Fulfillment of the
Requirements for the Degree of
DOCTOR OF PHILOSOPHY

Department: Chemistry
Major: Inorganic Chemistry

Approved:

Signature was redacted for privacy.

In Charge of Major Work

Signature was redacted for privacy.

For the Major Department

Signature was redacted for privacy.

For the Graduate College

Members of the Committee:

Signature was redacted for privacy.

Iowa State University
Ames, Iowa

1984

TABLE OF CONTENTS

INTRODUCTION

The green crystalline compound, tetrammineplatinum(II) tetrachloroplatinate(II) was first described by Magnus in 1828 (1), hence it is commonly known as Magnus' Green Salt (MGS). Among the most surprising characteristics of MGS is its color: the two complex ions from which MGS forms, $PtCl_4^{2-}$ and $Pt(NH_3)_4^{2+}$, are red and colorless, respectively. That MGS is green, rather than red, indicates the existence of an interionic interaction within the compound in addition to the usual electrostatic attraction of oppositely charged ions.

Over the years, a considerable body of research has been offered in attempts to explain the unusual interionic interaction present in MGS. The first clue to the nature of the interaction came in 1932, when Cox et al. (2) showed that MGS crystallizes in long chains of alternating cations and anions, with a Pt-Pt distance of only 3.21 A. Although the wrong space group was used in that research, the discovery of the unusually short Pt-Pt distance served to focus the attention of later work on possible interactions between the metal centers.

In 1951, Yamada (3) obtained crude crystal spectra of MGS and found that the dichroism of the salt was "abnormal", i.e., absorption along the z axis was more intense than along the x,y plane. He noted that the reverse is usually found in the spectra of planar molecules. Yamada concluded that a direct interaction between Pt atoms was responsible for the green color of MGS.

Godycki and Rundle (4) made the first theoretical study applicable to MGS in 1953, based on the analogous compound, bis-(dimethylglyoximato)nickel(II). This study suggested that the hybridization of the metal atom was changed from dsp^2 to d^2sp^3, on going from free ions to the crystal. Evidence collected by Yamada and Tsuchida (5), indicating that the dichroism of bis-(dimethylglyoximato)nickel(II) was similar to that of MGS, lent support to Godycki and Rundle's theory.

A crystal structure of MGS was published in 1957 by Atoji, Richardson, and Rundle (6). This work showed that MGS crystallizes in a tetragonal cell, with space group P_4/mnc, and that the Pt-Pt distance is 3.24 A. Figure 1 shows the relationship of the ions within a single chain. The structure of a polymorph of MGS, Magnus' Pink Salt (MPS), was also studied in this work. MPS is less stable than MGS; it occasionally forms as a pink powder during the precipitation of MGS. While single crystals of MPS were too small to permit a complete structure determination, powder patterns revealed that the Pt-Pt distance was greater than 5 A. MPS is the color of isolated $PtCl_4^{2-}$ ions, and the green color of MGS is related to the close approach of the platinum atoms in MGS.

Yamada and Tsuchida (7) studied the effect of the Pt-Pt distance on the color of several Magnus-type salts by measuring the dichroism of salts in which the ammonia ligands were replaced by methylamine, and higher alkylamines. Increasing the size of the ligand was expected

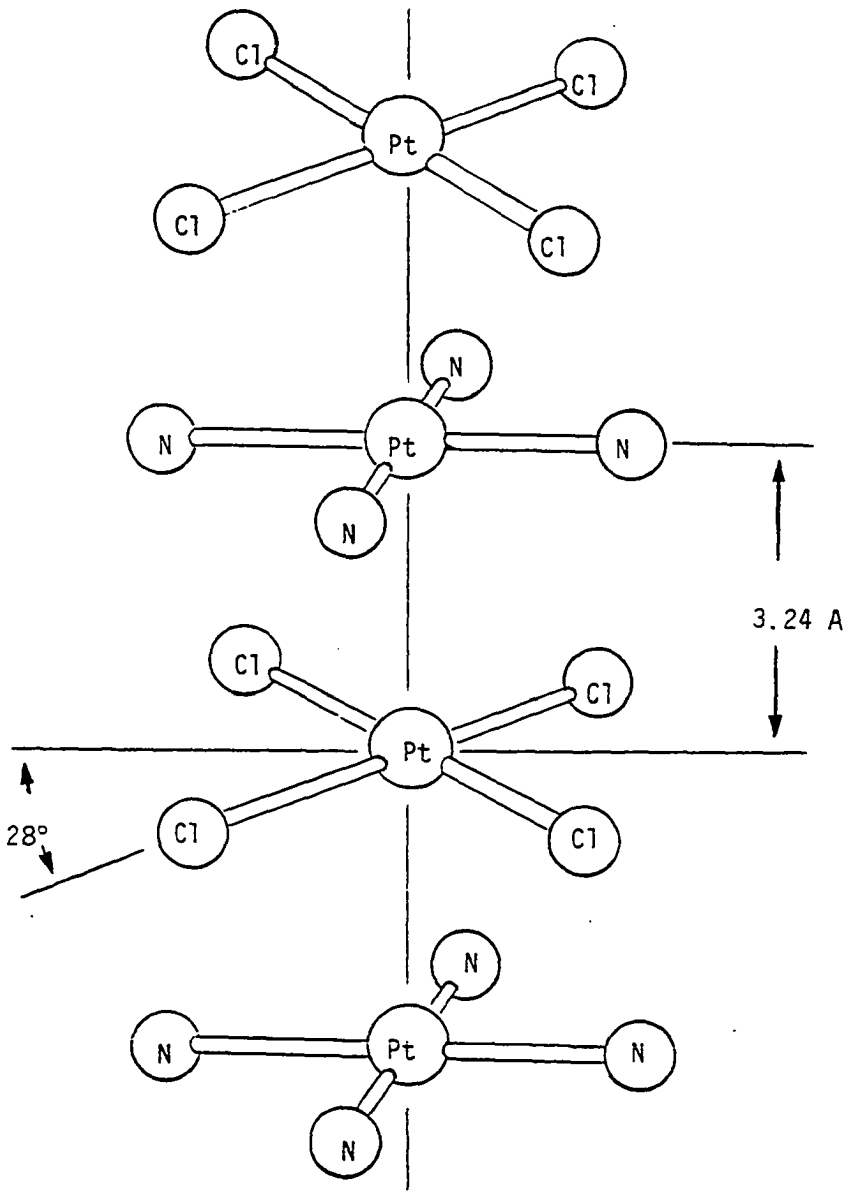

Figure 1. Structure of MGS, after Reference 6.

to result in a larger Pt-Pt distance, accompanied by a change from "abnormal" to "normal" dichroism. Indeed, Yamada and Tsuchida found that, in addition to MGS, only $Pt(CH_3NH_2)_4PtCl_4$ possessed the green color and "abnormal" dichroism; the other salts were pink with "normal" dichroism.

In the early 1960s, Miller presented unit cell constants for many Magnus-type salts, including both platinum and palladium salts (8), and attempted to correlate the intermetallic distances measured with the color of the compounds. Miller first proposed that the green color characteristic of MGS could be used as a positive diagnostic test for metal-metal interaction in any Magnus-type salt. Additional data, in the form of reflectance spectra for eighteen Magnus-type salts (9) led Miller to amend his original proposal: "The absence of an abnormal color certainly does not preclude the existence of an interaction, although it is likely to be weak in such cases."

Miller also noted that the transition energies depend on the metal used in the cation, as well as the interionic distance. The transitions of compounds with platinum cations generally occur at lower energy than those in compounds having palladium cations with the same ligands, even though the interionic distances are nearly identical.

Based on his observation of a broad band in the infrared (~6500 cm^{-1}) for several compounds, Miller attempted to explain the metal-metal interaction in terms of band theory: $5d_z2$ (hybridized

with 6s) orbitals mixed to form delocalized "crystal orbitals" along the crystal's c-axis. While this theory accounted for the peak in the IR for two of the compounds, it failed to explain why the peak was absent in most of the other compounds studied. The theory was later discounted by the work of Fishman and Interrante (10), who used perdeutero-MGS to show that the IR peak was due to hydrogen stretching overtones, and by the work of Mehran and Scott (11), who showed that the semiconducting properties of MGS are due to "extrinsic" defects, rather than "intrinsic" band formation.

Most modern treatments of the Magnus-type salts view their spectra as modifications of the spectra for the $PtCl_4^{2-}$ ion. Research done on the $PtCl_4^{2-}$ ion and K_2PtCl_4 is therefore pertinent to any discussion of the electronic structure of the Magnus-type salts.

Yamada recorded crystal spectra for K_2PtCl_4 (12) in 1951, but the resolution of his instrument in the visible region of the spectrum was not good, due to excessive convergence in the microscope optics that he used, according to Martin (13).

Solution spectra for $PtCl_4^{2-}$ ion and several chloroammine complexes were obtained by Chatt, Gamlen, and Orgel (14). These authors used molecular orbital and ligand field theory to develop an orbital energy diagram for the d-electrons, pictured as Scheme A in Figure 2. They predicted that the orbital with $d_{x^2-y^2}$ character is the lowest unoccupied molecular orbital: it is the most destabilized d-orbital because it points directly at the ligands. The authors also

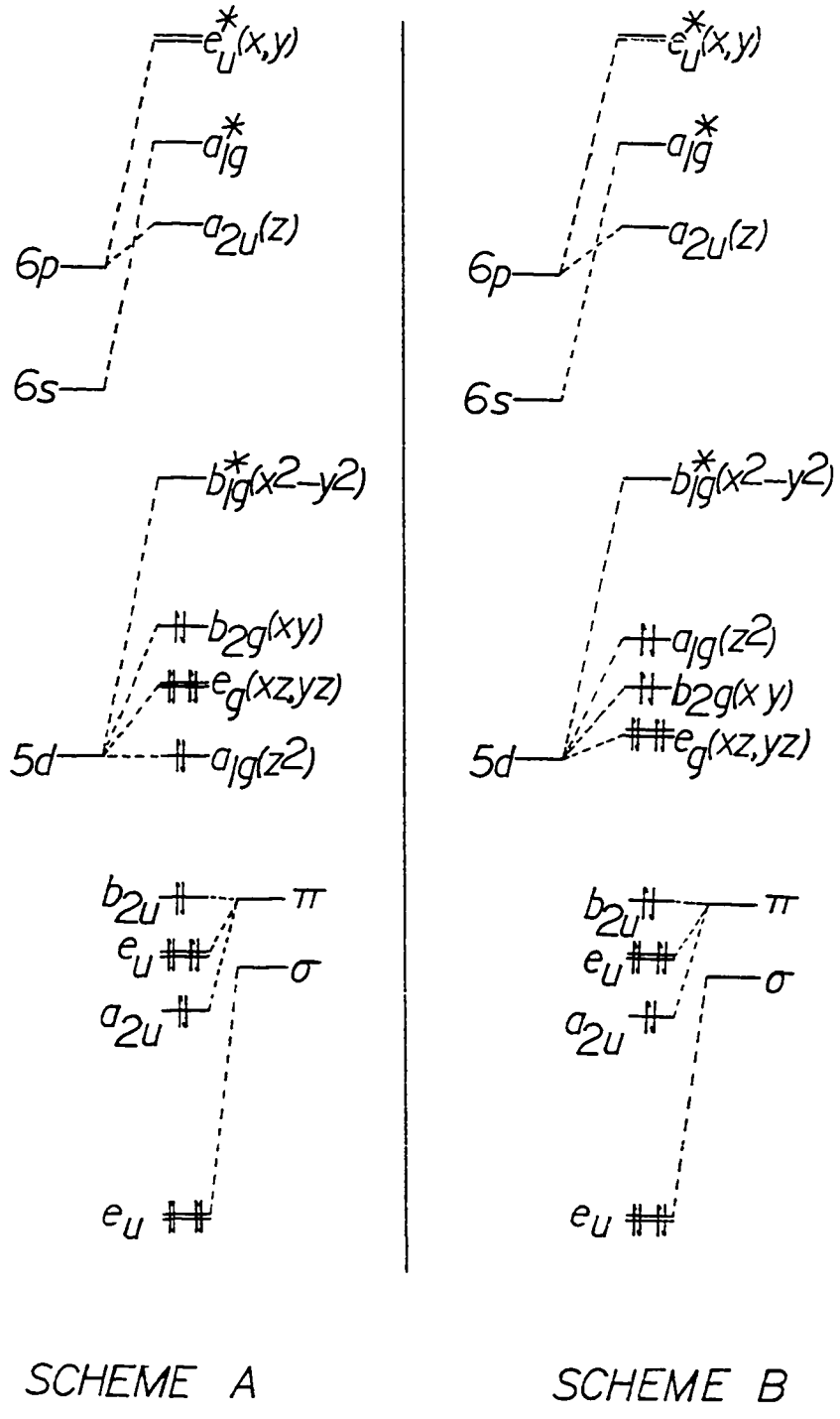

Figure 2. Two proposed energy-level diagrams for the $PtCl_4^{2-}$ system

predicted, on the basis of ligand field theory, that the orbitals with d_{xy} character would be at higher energy than the $d_{xz,yz}$ pair. They could not, however, provide any substantive arguments for the placement of the d_z2 orbital; they could only guess that the d_z2 orbital was more stable than the $d_{xz,yz}$ pair.

Chatt et al. (14) also proposed that relatively intense triplet $\leftarrow$ singlet transitions would be observed because of platinum's strong spin-orbit coupling. An intense allowed transition was also observed at 46,400 cm^{-1} and given the assignment $p \leftarrow d$.

Theoretical treatments of $PtCl_4^{2-}$ ion are greatly simplified by the strict D_{4h} symmetry of the ion. Unfortunately, the theoretical studies have not yet reached the level of sophistication required to provide unambiguous grounds on which to assign the electronic transitions.

Fenske, Martin, and Ruedenberg (15), using a point-charge, or point-dipole crystal field approach which included electron-electron repulsions and spin-orbit coupling, proposed the order $d_{x^2-y^2} > d_{xy} > d_{z^2} > d_{xz,yz}$ for the energies of the d orbitals. Ballhausen and Gray (16) proposed the same order using a molecular orbital model that emphasized assignment of the π-L $\leftarrow$ d transitions. Semiempirical molecular orbital studies by Basch and Gray (17), and Cotton and Harris (18) produced the d-orbital ordering first suggested by Chatt et al. (14). Without new experimental evidence, however, a preferred d-orbital ordering could not be chosen.

The new experimental evidence came essentially from two sources: 1) high-quality polarized absorption spectra for single crystals of K_2PtCl_4 were obtained by Martin et al. (19) at both room temperature and 15K, and 2) Magnetic Circular Dichroism (MCD) spectra for $PtCl_4^{2-}$ were obtained by Martin, Foss et al. (20) and McCaffrey, Schatz, and Stephens (21).

The room temperature polarized absorption spectra of K_2PtCl_4 exhibit relative band intensities and locations that are quite similar to those exhibited by the $PtCl_4^{2-}$ solution spectrum. From these observations, it was concluded that crystal effects are small, and that the transitions observed in the crystal spectra are essentially those of the free $PtCl_4^{2-}$ ion.

The most important feature of the crystal spectra is the absence of a band at 26,400 cm^{-1} in the c (z) polarization. The band appears in the a (x,y) polarization only. Such a situation is predicted by the selection rules for vibronic transitions in a D_{4h} system (see Appendix A). Only one spin-allowed vibronic transition, $^1A_{2g} \leftarrow {}^1A_{1g}$ is vibronically allowed in the a (x,y) direction, but forbidden in the c (z) direction. Therefore, the transition in K_2PtCl_4 observed at 26,400 cm^{-1} can be unambiguously assigned to $^1A_{2g} \leftarrow {}^1A_{1g}$. The d_{xy} orbital has b_{2g} symmetry which, when the symmetry product is taken with the $d_{x^2-y^2}$* b_{1g} orbital, yields the $^1A_{2g}$ state. Therefore, the $^1A_{2g} \leftarrow {}^1A_{1g}$ transition is an excitation of an electron from the orbital with d_{xy} character to the orbital with $d_{x^2-y^2}$* character, $^1A_{2g} \leftarrow {}^1A_{1g}$

$(d_{x^2-y^2}{}^* \leftarrow d_{xy})$.

The low temperature polarized absorption also revealed vibrational structure in x,y-polarization from 20,000 cm^{-1} to 27,000 cm^{-1}, and in z polarization from 20,000 cm^{-1} to 26,000 cm^{-1}. The structure in z-polarization is much weaker than that in x,y-polarization over the region 23,000 cm^{-1} to 27,000 cm^{-1}, although the x,y polarized structure is weakest in the region around 20,000 cm^{-1}. Such structure is characteristic of the Franck-Condon effect (13). At very low temperatures, the $PtCl_4^{2-}$ ion will be in the lowest state possible for each of the nine vibrations of the electronic ground state. If the force constants for the nontotally-symmetric vibrations are similar for the ground and excited states, transitions will occur from the ground state to the first excited vibrational states in the excited electronic state for the vibronically active mode. The average separation between peaks was 270-290 cm^{-1}, which was consistent with some decrease in the symmetric stretching frequency that is 335 cm^{-1} in the ground state.

Now, if the situation described above holds, the temperature dependence of the oscillator strength of a band is given by (13)

$$f(T) = f(T=0)\coth(h\nu_i/2kT) \qquad (1)$$

where ν_i is the frequency of the exciting asymmetric vibration. Martin et al. (19) found the oscillator strength of the bands at room temperature to be 2-3 times the strengths at liquid helium temperatures. Equation (1) yielded vibrational frequencies of 140-

220 cm^{-1} for the observed ratios of oscillator strengths, f(298)/f(15). The calculated frequencies tend to support the vibronic model because the ground state bending frequencies lie in that range.

The Magnetic Circular Dichroism spectrum for $PtCl_4^{2-}$ (20,21) permitted the unambiguous assignment of the $^1E_g \leftarrow {}^1A_{1g}$ transition. One of the degenerate e_g states is excited by left-circularly polarized light; the other by right-circularly polarized light. The two states are split by the Zeeman effect in the magnetic field, giving rise to the so-called "A-term" in the MCD spectrum. The A-term is characterized by a sign change at the wavelength of the band's maximum absorbance.

Martin, Foss et al. (20) found such an A-term at 30,300 cm^{-1} in the MCD spectrum of a K_2PtCl_4 solution. Thus, the absorption peak appearing in both polarizations of the crystal spectra at about 29,500 cm^{-1} has been assigned to $^1E_g \leftarrow {}^1A_{1g}$.

McCaffery, Schatz, and Stephens (21) recorded MCD spectra for $PtCl_4^{2-}$ in the region of allowed transitions (~ 40,000 cm^{-1}), and found that the band appearing in the absorption spectra as a shoulder at 43,400 cm^{-1} provided an MCD A-term, while the peak at 46,400 cm^{-1} provided a B-term. From those findings, McCaffery, Schatz, and Stephens concluded that the transition at 43,400 cm^{-1} was $^1E_u \leftarrow {}^1A_{1g}$ ($d_{x^2-y^2}{}^* \leftarrow \pi$ -L), with a $^1A_{2u} \leftarrow {}^1A_{1g}$ ($6p_z \leftarrow d_{xz,yz}$) transition possibly present as well. The transition at 46,000 cm^{-1} was assigned only to $^1A_{2u} \leftarrow {}^1A_{1g}$ ($d_{x^2-y^2}{}^* \leftarrow \pi$ or $6p_z \leftarrow d_{z^2}$).

The two assignments made from the new experimental evidence

generally served to restrict the range of reasonable values obtained from theoretical calculations. However, since neither the polarized absorption spectra, nor the MCD spectra could be used to distinguish the $^1B_{1g} \leftarrow {}^1A_{1g}$ transition (the transition is vibronically allowed in both the x,y and z directions, and is nondegenerate), considerable controversy remained over its placement, and hence over the placement of the a_{1g} (d_z2) orbital in the energy-level diagram for $PtCl_4^{2-}$.

Scattered-wave Xα calculations performed by Messmer et al. (22), like most other theoretical calculations performed by earlier workers (17,18), supported the assignment of $^1B_{1g} \leftarrow {}^1A_{1g}$ to the shoulder at 36,500 cm^{-1} in the crystal spectra. A ligand-field calculation by Vanquickenborne and Ceulemans (23) arrived at the same assignment using a correction parameter to account for mixing of the platinum $5d_z2$ and 6s orbitals. This assignment is often rationalized by invoking the participation of the platinum d_{xy}, d_{xz}, d_{yz} orbitals in π-bonding with the chloride p orbitals. The three d orbitals therefore have some π-antibonding character. The d_z2 orbital, on the other hand, is limited to mixing with the 6s orbital, hence the d_z2 is primarily nonbonding.

Elding and Olsson (24) recorded the solution spectra for the series $PtCl_n(H_2O)_{4-n}^{2-n}$ (n= 0,1,2,3,4) and the two related series $PdCl_n(H_2O)_{4-n}^{2-n}$ and $PdBr_n(H_2O)_{4-n}^{2-n}$ (n= 0,1,2,3,4). Their spectra showed that the transition at 37,500 cm^{-1} in $PtCl_4^{2-}$, which corresponds to the shoulders at 36,500 cm^{-1} in the K_2PtCl_4 crystal spectra, experiences

a blue shift comparable to that experienced by the allowed transitions, on going from n=4 to n=0 in the series. The blue shift over the series are only about one-third as great for $^1E_g \leftarrow {}^1A_{1g}$ and $^1A_{2g} \leftarrow {}^1A_{1g}$ as for the allowed transitions; on this basis, the authors concluded that the transition at 37,500 cm^{-1} was not a d-d transition at all. Rather, it was a $^1B_{1u} \leftarrow {}^1A_{1g}$ symmetry-forbidden transition ($a_{2u} \leftarrow b_{2g}$, d_{xy}) allowed by a b_{2g} vibration. The assignment is supported by the fairly high intensity of the band. The change in intensity as the molecular point symmetry is lowered also supports the assignment: the transition is symmetry-forbidden in all complexes of the series except cis-$PtCl_2(H_2O)_2$, where it is allowed under the C_{2v} point group. The spectra show a transition at 44,500 cm^{-1} for the cis-complex, but no corresponding absorption in trans-$PtCl_2(H_2O)_2$, where the band is forbidden.

With the shoulder at 37,500 cm^{-1} assigned to $^1B_{1u} \leftarrow {}^1A_{1g}$, Elding and Olsson placed the $^1B_{1g} \leftarrow {}^1A_{1g}$ transition at about the same energy as $^1E_g \leftarrow {}^1A_{1g}$, 30,200 cm^{-1}. This means, of course, that the $d_{xz,yz}$ pair, and the d_z2 orbital would all have roughly the same energy. This ordering had been considered earlier by Martin et al. (19), but the ordering $d_{xz,yz} < d_z2$ was favored instead, because semiempirical calculations (19,25) placed the $^1B_{1g} \leftarrow {}^1A_{1g}$ transition at about 35,000 cm^{-1}, and a Gaussian component was detected in both polarizations of the crystal spectra. Symmetry predicts that $^1B_{1g} \leftarrow {}^1A_{1g}$ is both xy- and z-polarized.

More recently, Tuszynski and Gliemann applied ligand field theory,

including electron-electron repulsions and spin-orbit coupling, to the square-planar system (26). Their attempt to fit the calculations to the observed spectra for K_2PtCl_4, K_2PtBr_4, K_2PdCl_4, $K_2PdBr_4.H_2O$, $K_2Pt(SCN)_4$, and $K_2Pd(SCN)_4$ was made by considerably reducing the values for the Slater-Condon parameters F_2 and F_4 relative to the values used by previous workers (17,19,27).

Noting that the crystal spectra are very similar to the solution spectra for the six compounds studied, and that the square planar complexes are normal to the plane in which no intermolecular interactions occur, Tuszynski and Gliemann performed the calculations for a single complex ion. In such a system, the energy ordering of the one-electron terms is determined by the ratio, D_s/D_q. The authors argued that D_s/D_q should be between 1 and 3 for platinum complexes and between 2 and 4 for palladium complexes, depending on the set of orbital wavefunctions used to calculate D_s/D_q. The value of D_s/D_q obtained from the ligand field calculations is about 1.5 for the platinum complexes, and about 2.2 for the palladium complexes. The authors therefore maintained that the smaller values for F_2 and F_4 were reasonable.

A total of about 12 transitions were obtained from the calculations for K_2PtCl_4. Of these, seven were in quantitative agreement with observed transitions. The other five corresponded to weak spin-forbidden transitions not observed in the crystal spectra. Transition assignments were made according to Scheme B in Figure 2. The $^1B_{1g} \leftarrow {}^1A_{1g}$ transition is assigned to the peak at 21,000 cm^{-1} in the observed

spectra for K_2PtCl_4. Such an assignment places the $^3B_{1g} \leftarrow {}^1A_{1g}$ spin-forbidden transition in the very weak peak at 17,500 cm^{-1}, apparently discounting the argument of other workers (14) that large spin-orbit coupling effects for platinum greatly enhance the intensities of the spin-forbidden transitions.

The ^3E_g states are placed at about 24,000 cm^{-1} by the calculations. The observed band in this region is much more intense in x,y-polarization than in z-polarization. The authors attribute the higher intensity in the x,y polarization to mixing of the A_2' component (from the D_4' double group necessary to treat electron spin) of ^3E_g with the nearby $^1A_{2g}$ state. If the $^1B_{1g}$ transition were placed at 36,500 cm^{-1}, however, the peaks at 24,000 cm^{-1} would correcpond to $^3B_{1g}$ transitions, which possess no A_2' component to account for the intensity difference of the two polarizations.

Quantitative fits of the calculated energies to the experimentally observed peaks were reported for all complexes studied except $K_2Pt(SCN)_4$. The authors suggested that the ligand field approximation may be "too rough" to apply quantitatively to $K_2Pt(SCN)_4$. Nevertheless, qualitative assignments were made that were consistent with those made for the other complexes.

Research on the problem of the green color of MGS continued as the spectroscopic data collected for the $PtCl_4^{2-}$ system became more and more extensive. High-quality polarized crystal spectra and other data became available for MGS and related compounds; the data tended to support

the view, suggested by Day et al. in 1965 (28) that the unusual color was due to a perturbation of the transitions of the anion by the cation, rather than a direct metal-metal interaction, as Miller (8,9) and Yamada (12) proposed.

Day et al. (28,29) recorded single-crystal polarized spectra at room temperature for K_2PtCl_4, K_2PdCl_4, $Pt(NH_3)_4PtCl_4$, $Pt(CH_3NH_2)_4PtCl_4$, and $Pt(CH_3CH_2NH_2)_4PtCl_4$, and diffuse reflectance spectra for a total of 35 compounds related to MGS. Unfortunately, the single-crystal spectra show evidence of incomplete polarization, perhaps due to light convergence in the condensing lens of their microspectrophotometer, and scattering of light as a result of surface defects on the crystal.

Nevertheless, Day et al. noticed that the bands due to the anion absorption shifted progressively to higher energies as the metal-metal separation increased from the 3.25 A in MGS to 4.13 A in K_2PtCl_4, over the series $Pt(NH_3)_4PtX_4$, $Pt(CH_3NH_2)_4PtX_4$, $Pt(CH_3CH_2NH_2)_4PtX_4$, K_2PtCl_4, where X= Cl, Br, or SCN. The vibronic mechanism was invoked for the MGS system (just as it had been for the K_2PtCl_4 system (14)) to assign the electronic states to the observed transitions. The schemes shown in Figure 2 were considered to be the two most likely orderings, although Day et al. did not attempt to single out either of the orderings as the correct one, stating only that the $^{1,3}A_{2g} \leftarrow {}^1A_{1g}$ was assumed to lie beneath the x,y polarization of the $^{1,3}E_g$ or $^{1,3}B_{1g} \leftarrow {}^1A_{1g}$ peak at 24,900 cm^{-1} for MGS.

The intensity of a vibronic transition is "borrowed" from an

allowed transition, and the degree of the vibronic transition's intensity enhancement will be greatest if the vibronic and allowed transitions occur at similar energies. Thus, the intensities of the d-d transitions in the systems studied should be greater in MGS than in those salts with a larger metal-metal spacing, argued Day, et al. Such an effect was observed: the lowest energy allowed transitions in z-polarization occurred at progressively lower energies -- and thus occurred closer to the d-d bands -- as the metal-metal distance decreased. A corresponding rise in the intensities of the z-polarized d-d bands was noted in the series. The intensities of the x,y-polarized bands (which were not enhanced by a nearby allowed transition) dropped slightly over the same series.

The perturbing effect of the cation d_z2 electrons on the anion transitions was also suggested. Because the d_z2 and $d_{xz,yz}$ orbitals on the anion are oriented in the direction of the d_z2 orbital on the cation, these orbitals are destabilized to a much greater extent than is the d_{xy} orbital, which is oriented in the plane perpendicular to the d_z2 orbital on the cation. Thus, the red shift of the $^{1,3}E_g\ (d_{xz,yz}) \leftarrow {}^1A_{1g}$ and $^{1,3}B_{1g}\ (d_z2) \leftarrow {}^1A_{1g}$ bands should decrease as the cation d_z2 and the anion $d_{xz,yz}$ and d_z2 orbitals are separated; such a progression was observed both for increasing ammine size in $Pt(A)_2PtX_4$, $Pd(A)_4PtX_4$ (A= NH_3, CH_3NH_2, $CH_3CH_2NH_2$; X= Cl, Br, SCN), and for different metal centers: Pt-Pt > Pd-Pt > Pt-Pd > Pd-Pd.

Anex and coworkers (30) obtained single-crystal polarized

reflectance spectra for $Pt(A)_4PtCl_4$, where A= NH_3, CH_3NH_2, and $CH_3CH_2NH_2$. These spectra showed an intense allowed transition in the ultraviolet (34,400 - 39,900 cm^{-1}) in z-polarization. The observation of the transition provided support for the proposal of Day, et al., that the intensities of the z-polarized d-d transitions were enhanced by the red-shift of an intense allowed transition as the Pt-Pt distance decreased in the series.

Calculations of the extinction coefficients for the absorption bands corresponding to the observed reflectance peaks, by means of the Kramers-Kronig analysis, allowed a further test of the vibronic mechanism proposed by Day, et al. According to the vibronic theory, intensity of the d-d bands will be controlled by both the magnitude of the allowed transition's intensity, and the difference in energy between the allowed and vibronic bands. In general, the relative intensities of the d-d bands tended to increase or decrease as expected over the range of energy differences and allowed transition intensities in the series.

Further study of the allowed transitions by Anex and Takeuchi (31) indicated that the transition in the Magnus-type salts corresponds to a mostly z-polarized transition observed at about 44,000 cm^{-1} in the polarized single-crystal reflection spectra of K_2PtCl_4 (about 46,000 cm^{-1} in the solution spectrum). The transition was assigned as a $5d_z2 \leftarrow 6_{pz}$ transition centered on the Pt. Interestingly, a peak at similar energies observed for K_2PdCl_4, was assigned as a $d_{x^2-y^2}{}^* \leftarrow \sigma$

ligand-to metal charge transfer, due to its predominantly x,y polarization.

Despite the new insight gained by Day et al., and Anex et al., the electronic structure of the Magnus-type salts still presented several problems. While the work of Day et al., and Anex et al. showed that the visible transitions were probably vibronic in origin, their work failed to rule out the possibility of interionic electron transfer transitions. Furthermore, the $^1B_{1g} \leftarrow {}^1A_{1g}$ ($d_z2 \leftarrow d_{x^2-y^2}*$) transition, which proved to be so elusive in the K_2PtCl_4 system, had not been unambiguously assigned in the MGS spectra.

The possibility of interionic electron transfer states in the Magnus-type salts was realized after Martin and coworkers (32) detected sharp peaks at 33,100 cm^{-1} and 39,100 cm^{-1} in the single-crystal polarized absorption spectra of $Pt(en)Cl_2$, which they attributed to ionized exciton states. Transitions from the d_{xz} and ligand-π orbitals from one $Pt(en)Cl_2$ unit into a d_{xy} ($\sigma*$) orbital on an adjacent $Pt(en)Cl_2$ unit were proposed for the two bands. Intermolecular (interionic) electron transfers can occur where there is considerable overlap of the orbitals on neighboring molecules (ions).

The possibility of strong crystal interactions, suggested by the strong dichroism and green color of MGS, led Martin and coworkers to test for the presence of a nonvibronic band in MGS which could be attributed to an interionic electron transfer process, similar in nature to the intermolecular electron-transfer transition in $Pt(en)Cl_2$

(33).

To test for the presence of a nonvibronic band in the spectra of MGS, Martin and coworkers recorded single-crystal polarized absorption spectra for MGS at 15K and 300K. Vibronic bands will decrease in intensity as temperature is lowered because the amplitude of the exciting vibration decreases as the temperature decreases. The intensity of allowed transitions (including interionic electron transfers), on the other hand, remain fairly constant as temperature changes; the intensity appears to increase because the allowed band narrows at lower temperatures, giving a higher peak maximum with little change in integrated intensity. By comparing the heights of the peaks at 15K with the heights at 300K, Martin et al., concluded that all of the observed peaks in the visible region were vibronic in origin, and had simply been subject to large crystal effects. These results confirmed the proposals of Day et al. (28), and others (30,31).

A peak corresponding to the $^1B_{1g} \leftarrow {}^1A_{1g}$ transition was not found; Martin et al. suggested that either the peak occurs at 30,000 cm^{-1} with an intensity much lower than that of the other d-d transitions, or it occurs above the limits of detection by their instruments, 32,000 cm^{-1}. The possibility that the weak peak at 23,000 cm^{-1} was due to $^3B_{1g} \leftarrow {}^1A_{1g}$ was used to place $^1B_{1g} \leftarrow {}^1A_{1g}$ at 30,000 cm^{-1} or higher. Unless the $^1B_{1g} \leftarrow {}^1A_{1g}$ transition has a significantly higher intensity at 30,000 cm^{-1} than the intensity of the $^3B_{1g} \leftarrow {}^1A_{1g}$ transition placed at 23,000 cm^{-1}, it is unlikely that the shoulder observed at 30,000 cm^{-1}

is the $^1B_{1g}$ state.

The present research was performed with the hope of acheiving two goals: (1) the assignment of the $^1B_{1g} \leftarrow {}^1A_{1g}$ transition in the Magnus-type salts, and (2) the rationalization and assignment of several allowed transitions of moderate intensity observed by Martin (34) in $Pt(en)_2PdCl_4$, and $Pt(NH_3)_4PdCl_4$.

If electron-electron repulsions are the primary sources of orbital energy perturbation in the crystal, the d_z2 orbital will be most perturbed as a result of a close metal-metal spacing (28). The $d_{xz,yz}$ pair will be somewhat perturbed, while the $d_{x^2-y^2}$* and d_{xy} orbitals will be perturbed very little, due to the orbitals' orientations with respect to the d_z2 orbital on the neighboring ion. It should therefore be possible, if a series of Magnus-type salts is chosen for which the metal-metal spacings are known and are distributed over a wide range of distances, to identify the $^1B_{1g} \leftarrow {}^1A_{1g}$ ($d_{x^2-y^2}$* $\leftarrow$ d_z2) transition in the single-crystal spectra as the one that displays the largest energy shift as the metal-metal spacing changes. The $^1E_g \leftarrow {}^1A_{1g}$ ($d_{x^2-y^2}$* $\leftarrow$ $d_{xz,yz}$) peak should display a moderate energy shift over the series, while the $^1A_{2g} \leftarrow {}^1A_{1g}$ ($d_{x^2-y^2}$* $\leftarrow$ d_{xy}) peak should display very little shift over the series. For all three d-d transitions, $d_{x^2-y^2}$* is the lowest unoccupied molecular orbital; it should not experience a significant change in energy as the metal-metal spacing changes. The energy shifts observed will therefore reflect perturbations in the energies of the filled d orbitals only, and the

$^1B_{1g}$ transition should then be distinguishable from the other d-d bands.

The use of the Magnus-type salts makes possible the appearance of d-d bands arising from the d-orbitals on the cation metal atom. Such d-d bands are expected to be well above the region of the anion d-d transitions in the Magnus-type salts because the d-d bands for $Pt(NH_3)_4Cl_2$, as recorded by Isci and Mason (35), appear at energies in excess of 37,000 cm^{-1}, well above the d-d region in K_2PtCl_4. If the cation d-d transitions are observed at all, they should be in the region of allowed transitions in the spectra of the Magnus-type salts, and thus readily distinguished from the allowed bands by the temperature dependence of their intensities.

Of course, the success of the experiment as outlined depends on the cooperation of the Magnus-type salts: if the $^1B_{1g}$ transition is of such low intensity as to be undetectable, or it lies at an energy beyond the spectrophotometer's limit of detection, or if electron-electron repulsions are not the main perturbation in the crystal, the $^1B_{1g}$ transition cannot be easily identified by comparison of the polarized absorption spectra of a series of salts.

By using thin crystals which tend to compensate for the high extinction coefficients of allowed transitions (even the transitions of moderate intensity have extinction coefficients well above those associated with vibronic transitions) by reducing the path length of the polarized light through the sample, it should be possible to systematically detect the allowed transitions of moderate intensity

over the full range of compounds studied. Rationalizations for the occurrence of several distinct allowed transitions observed will be accomplished by comparison with known transitions in K_2PtCl_4, $Pt(en)Cl_2$, and other similar systems.

EXPERIMENTAL

Preparation of Crystals

Magnus' Green Salt was prepared according to the reaction:

$$Pt(NH_3)_4Cl_{2(aq)} + K_2PtCl_{4(aq)} \rightarrow Pt(NH_3)_4PtCl_{4(s)} + 2KCl_{(aq)}$$

The K_2PtCl_4 used in the preparation was obtained from a supply in the laboratory. The $Pt(NH_3)_4Cl_2$ was prepared from K_2PtCl_4 by the following procedure:

$$K_2PtCl_4 + 4NH_3 \rightarrow Pt(NH_3)_4Cl_2 + 2KCl$$

K_2PtCl_4 (0.05 g) was dissolved in a minimum of water. Concentrated aqueous NH_3 was then added until a precipitate of MGS formed. The reaction mixture was heated until the MGS disappeared and nearly all of the liquid evaporated. The remaining liquid was added to 500 ml of a solution consisting of 45% diethyl ether, 45% acetone, and 10% ethanol. The white precipitate was collected by suction filtration. After drying in air, the white $Pt(NH_3)_4Cl_2$ powder was stored in a desiccator containing a little aqueous NH_3 to minimize possible ligand exchange reactions.

Crystals of MGS suitable for spectroscopic studies were prepared by allowing the $Pt(NH_3)_4^{2+}$ and $PtCl_4^{2-}$ ions to slowly combine in aqueous solution. Two methods were used to slow the mixing of aqueous ions enough to allow good crystal formation:

a. very small quantities (~ 1 mg) of $Pt(NH_3)_4Cl_2$ and K_2PtCl_4 were dissolved in 0.1 ml of water on opposite corners of a 2 in x 2 in glass plate. Two drops of water were placed

in the center of the plate without coming in contact with either of the solutions at the corners. Upon covering the plate with a clean 2 in x 2 in plate, the two solutions slowly mixed in the center of the plates. The plates were stored in a humid container for two to four days. The plates were dried by removing them from the humid container. The larger crystals were then removed from the plate by floating them free of the glass with a drop of water, and lifting them from the water on the tip of a needle. On two occasions, Magnus's Pink Salt formed between the plates along with MGS. The salt appeared as a pink powder; no crystals large enough for spectroscopic studies were obtained.

b. A "crystal grower", shown in Figure 3, was loaded by placing a dilute solution (0.001 M) of K_2PtCl_4 in one of the end compartments, and a dilute solution of $Pt(NH_3)_4Cl_2$ in the other end compartment. Water or dilute KCl solution (to inhibit slow ligand exchange at the $PtCl_4^{2-}$ ions.) was placed in the middle compartment. After several days, crystals formed on the glass frits separating the three compartments. The crystals were scraped off the frits with a wire; the solutions and the crystals were poured into a Petri dish for further inspection.

Preparation of the nineteen other Magnus-type salts of interest was accomplished in much the same manner as the preparation of MGS:

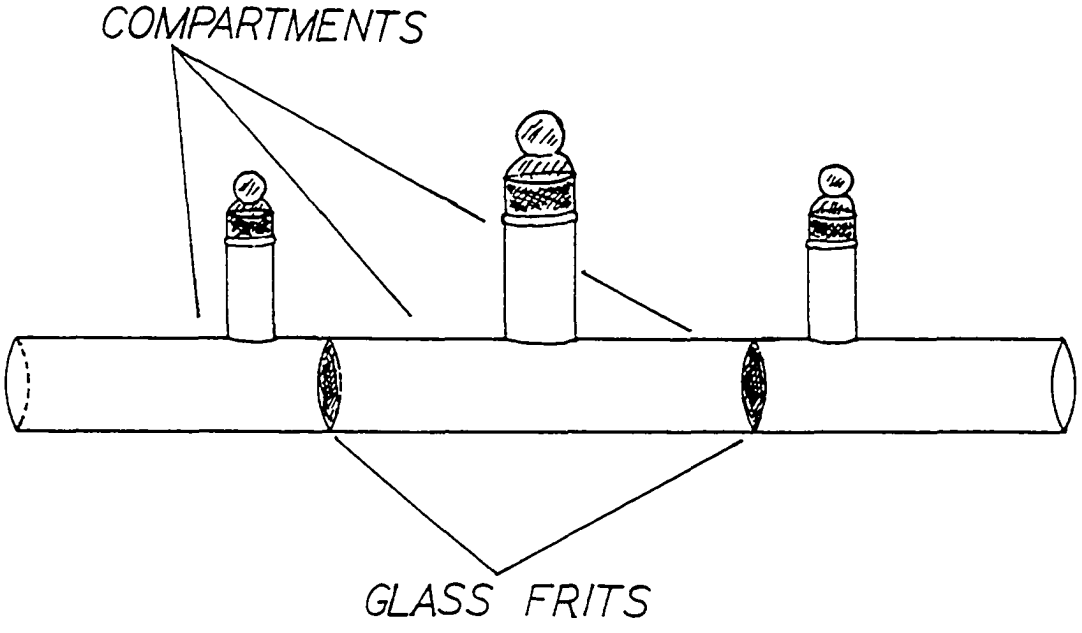

Figure 3. The "crystal grower"

the starting materials were either synthesized in the laboratory or obtained from laboratory stock, then they were slowly mixed, following the two procedures for mixing outlined above. Care was taken to react only those starting materials having the same halogen, i.e., the anions of the +2 complex must be Cl^- when the -2 complex has chloride ligands, and the anions of the +2 complex must be Br^- when the -2 complex has bromide ligands. This rule was followed to prevent the possible formation of mixed-halogen Magnus-type salts.

Table 1 lists the starting materials and products for each of the twenty Magnus-type salts under consideration. The two columns on the right in Table 1 show the method (glass plates, crystal grower) by which spectroscopic-quality crystals were obtained for each salt.

The Rb_2PtBr_4 that provided the $PtBr_4^{2-}$ anion was obtained from laboratory stock. The $Pt(NH_3)_4Br_2$, $Pt(CH_3NH_2)_4Cl_2$, $Pt(CH_3NH_2)_4Br_2$ $Pt(en)_2Cl_2$ (en= ethylenediamine, $NH_2CH_2CH_2NH_2$), $Pt(en)_2Br_2$, $Pd(NH_3)_4Cl_2$, $Pd(NH_3)_4Br_2$, $Pd(en)_2Cl_2$, and $Pd(en)_2Br_2$ starting materials were all synthesized by the same method used to obtain $Pt(NH_3)_4Cl_2$, with Pd substituted for Pt, CH_3NH_2 or ethylenediamine substituted for NH_3, and Br substituted for Cl, as appropriate. Attempts to synthesize $Pd(CH_3NH_2)_4Cl_2$ and $Pd(CH_3NH_2)Br_2$ by this procedure resulted in very poor yields of an impure product unsuitable for use in the Magnus-type salt synthesis.

K_2PdCl_4 was prepared by the reactions:

$$Pd + 2HNO_3 + 4HCl \rightarrow H_2PdCl_{4(aq)} + 2NO_{2(g)} + 2H_2O$$

Table 1. Preparation of the Magnus-type salts

Cation Source	Anion Source	Product	CG[a]	P[b]
$Pt(NH_3)_4Cl_2$	K_2PtCl_4	$Pt(NH_3)_4PtCl_4$	x	x
$Pt(NH_3)_4Cl_2$	K_2PdCl_4	$Pt(NH_3)_4PdCl_4$	x	x
$Pt(NH_3)_4Br_2$	Rb_2PtBr_4	$Pt(NH_3)_4PtBr_4$	x	x
$Pt(NH_3)_4Br_2$	K_2PdBr_4	$Pt(NH_3)_4PdBr_4$		x
$Pt(CH_3NH_2)_4Cl_2$	K_2PtCl_4	$Pt(CH_3NH_2)_4PtCl_4$	x	x
$Pt(CH_3NH_2)_4Cl_2$	K_2PdCl_4	$Pt(CH_3NH_2)_4PdCl_4$	x	x
$Pt(CH_3NH_2)_4Br_2$	Rb_2PtBr_4	$Pt(CH_3NH_2)_4PtBr_4$	x	x
$Pt(CH_3NH_2)_4Br_2$	K_2PdBr_4	$Pt(CH_3NH_2)_4PdBr_4$		x
$Pt(en)_2Cl_2$	K_2PtCl_4	$Pt(en)_2PtCl_4$	x	x
$Pt(en)_2Cl_2$	K_2PdCl_4	$Pt(en)_2PdCl_4$	x	x
$Pt(en)_2Br_2$	Rb_2PtBr_4	$Pt(en)_2PtBr_4$		x
$Pt(en)_2Br_2$	K_2PdBr_4	$Pt(en)_2PdBr_4$	x	x
$Pd(NH_3)_4Cl_2$	K_2PtCl_4	$Pd(NH_3)_4PtCl_4$		x
$Pd(NH_3)_4Cl_2$	K_2PdCl_4	$Pd(NH_3)_4PdCl_4$		x
$Pd(NH_3)_4Br_2$	Rb_2PtBr_4	$Pd(NH_3)_4PtBr_4$		x
$Pd(NH_3)_4Br_2$	K_2PdBr_4	$Pd(NH_3)_4PdBr_4$		x
$Pd(en)_2Cl_2$	K_2PtCl_4	$Pd(en)_2PtCl_4$	x	x
$Pd(en)_2Cl_2$	K_2PdCl_4	$Pd(en)_2PdCl_4$	x	x
$Pd(en)_2Br_2$	Rb_2PtBr_4	$Pd(en)_2PtBr_4$		x
$Pd(en)_2Br_2$	K_2PdBr_4	$Pd(en)_2PdBr_4$		x

[a]Crystal Grower.

[b]Plates.

passing through the crystal in the two polarization directions. If, however, the incident plane-polarized light is aligned parallel to one of the polarization directions, the magnitude of the electric vector parallel to the other polarization direction will be zero, giving transmitted light polarized in one direction only. Two polarized absorption spectra for a crystal can therefore be obtained by aligning the incident radiation vector parallel to each of the crystal's polarization directions.

Polarizing Microscope

In order to obtain good polarized spectra, the crystal must be single, and the polarization directions must be known.

If the crystal is not single (i.e., the unit cells within the crystal are not all related by a simple translation), each set of translationally related unit cells in the crystal will possess its own pair of polarization directions. The spectra of such crystals will consist of contributions from each polarization direction, and the spectra are considered to be "impure".

If a single crystal is selected, the polarization directions of the crystal must be determined so that the plane-polarized light incident on the crystal may be aligned parallel to each polarization direction. Failure to align the incident polarized light with the crystal's polarization directions also produces "impure" spectra.

In these experiments, single crystals were identified, and polarization directions were found with the aid of a polarizing

microscope.

The polarizing microscope, as Figure 4 shows, is essentially an ordinary optical microscope equipped with a pair of polarizers and other accessories that operate on the properties of polarized light. Unpolarized light from a lamp is polarized by the polarizer; the polarized light then passes through the crystal mounted on a microscope slide on the rotating stage. Accessories such as a quartz wedge or a 1/4 wave mica plate can be inserted into the light path to study interference effects. These accessories were seldom used in this research. A second polarizer, called the analyzer, can be inserted above the stage in order to admit only light polarized perpendicular to the plane of the light admitted by the polarizer -- hence the method of "crossed polarizers" is employed by the polarizing microscope. The behavior of an anisotropic crystal between crossed polarizers is demonstrated in Figure 5.

Polarization directions of the crystals were found by placing the crystal between crossed polarizers in a position corresponding to its fixed orientation in the light path of the spectrophotometer. Rotating the crystal on the stage until the crystal extinguishes (i.e., no light is transmitted perpendicular to the polarizer's plane of polarization) aligned one of the crystal's polarization directions parallel to the analyzer's plane of polarization, and thus provides the angle at which the spectrophotometer's polarizers must be tilted in order for the incident polarized light to be parallel to

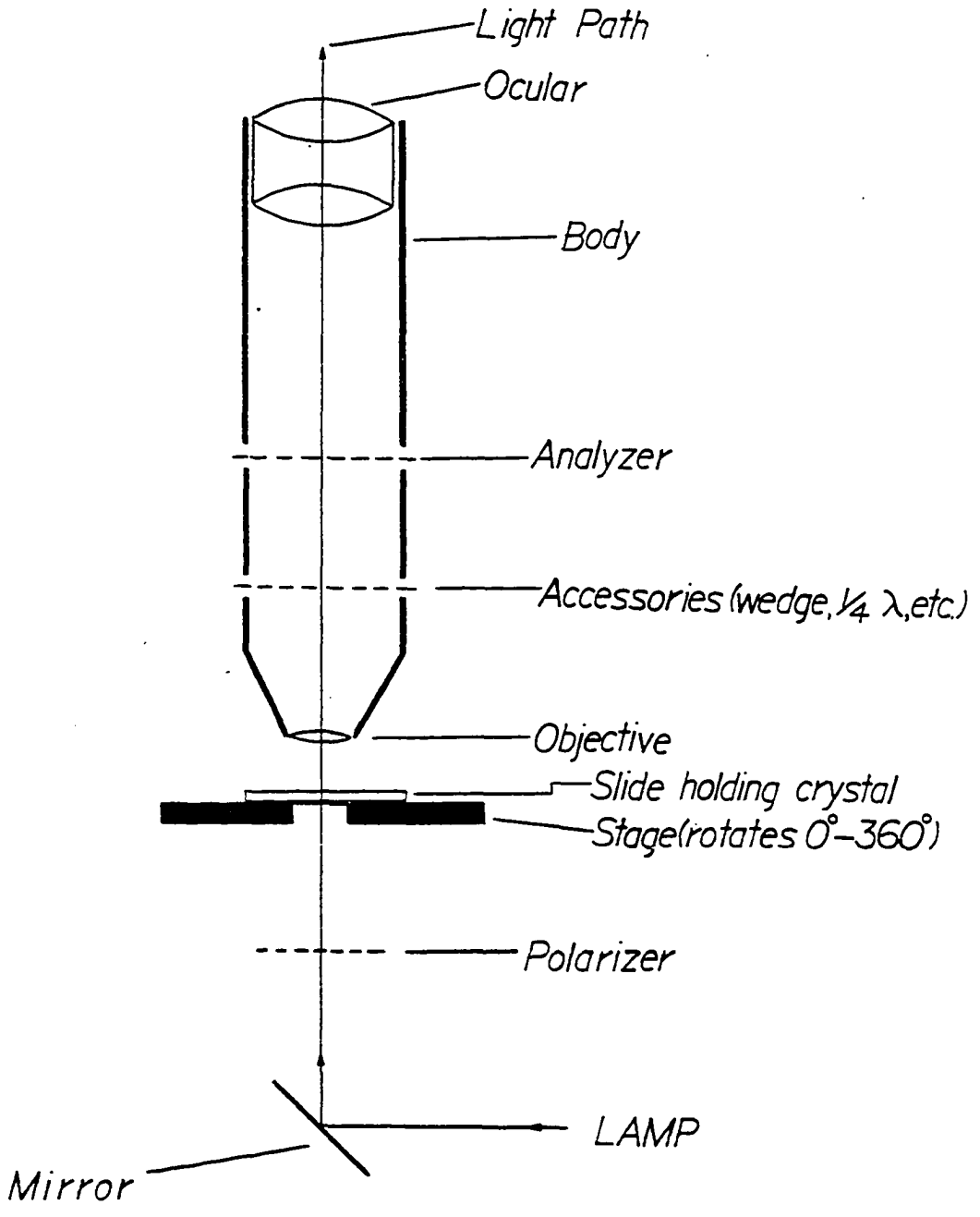

Figure 4. The polarizing microscope, showing major components

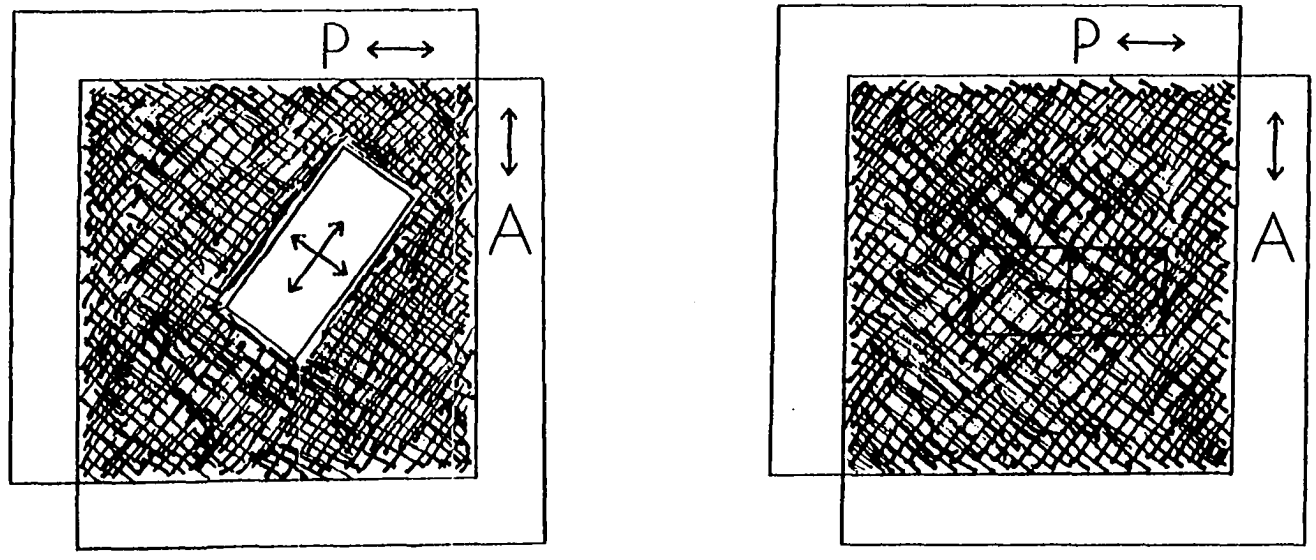

Crystal aligned so that some light is transmitted by crossed polarizers

Crystal is aligned with extinction directions ⊥ to crossed polarizers: no light is transmitted

Figure 5. Behavior of a crystal under crossed polarizers

one of the crystal's polarization directions. Of course, the crystal's other polarization direction is 90 deg. from the first. By this method, polarization directions were measured to an accuracy of approximately ± 1 deg.

Although identifying a crystal's polarization directions could be done by relating the polarization angles to a morphological feature of the crystal (such as an edge), it was actually more convenient to mount the crystal in a sample holder before obtaining the polarization directions.

Pinholes in Platinum Sheets

After selecting a single crystal of suitable dimensions, the crystal was mounted over a small hole cut into a 1 cm by 1 cm piece of 0.006 in. Pt sheet. The dimensions of the hole were such that the crystal completely covered the hole, so that no light was transmitted that did not actually pass through the crystal.

The holes were made by denting the sheet, then abrading the raised surface with No. 600 emery paper. The sheet was dented and sanded up to twenty times in order to make a single hole. A fine-point sewing needle was used to make dents for round holes; the edge of a new razor blade was used to make dents for slits. The long, narrow slits took fullest advantage of the surface area of the needle-like crystals, allowing a maximum surface for light to pass through the crystals to the detector. By this method, holes as small as 20 μm in diameter were obtained.

The crystals were affixed to the Pt sheet by means of a very thin layer of high-vacuum grease spread adjacent to the hole.

The Pt sheet bearing the crystal was then clamped into a brass sample holder that fit into the cryostat. Two crystals could be mounted in each sample holder: the crystals were placed so that rotating the sample holder by 90 deg. along its vertical axis would exchange the crystals in the light beam.

Helium Cryostat

A liquid helium cryostat, Andonian model MHD-3L-30N was used to obtain crystal spectra at temperatures ranging from room temperature (normally 300K) to 5K. A jet of cold He vapor, obtained from the controlled vaporization of liquid He, cooled the crystal and sample holder. The temperature of the sample was regulated by controlling the rate of flow at the sample, and by heating the vapor before it reached the sample by means of a small resistance heater placed around the helium transfer tube. The temperature was measured by a platinum resistance thermometer at temperatures above 30K, and by a germanium resistance thermometer below 30K. Under normal operating conditions, the cryostat retained liquid He long enough to deep the sample chamber at 6K for about four hours. Often, it was possible to record the spectra for both crystals in the sample holder quickly enough to obtain spectra for a second pair of crystals before the liquid helium supply in the cryostat was exhausted. The cold sample was simply removed after warming to about 25K; a second sample holder was inserted in its place

and cooled to the 5K operating temperature over a period of about 40 minutes. In this manner, up to four crystals could be studied each time the cryostat was filled with liquid helium.

The Spectrophotometer

The system used to record the polarized absorption spectra was built around a Cary 14 double-beam recording spectrophotometer, as shown in Figure 6. Light from 650 watt tungsten lamp was polarized by Glan-Taylor calcite polarizers in both the sample and reference compartments. A Cary model 1460215 phototube, sensitive to 850 nm, served as the system's detector. A digital interface converted data to digital form and transferred the data to an IBM model 29 keypunch for punched-card output. The electronic ratio detector, when combined with manual selection of neutral-density reference screens, gave the system a range of about three absorbance units.

After obtaining punched data for the crystal spectra, the crystals were removed from the pinholes and baselines were recorded. The crystal and baseline data were then submitted to the Iowa State University Computation Center, where baselines were subtracted and spectra were plotted, using the SIMPLOTTER.

In order to assure reproducibility of recorded results, spectra were measured at both room temperature and 6K for a total of six to ten crystals for each of the twenty salts studied. By measuring spectra for crystals over an extended range of thicknesses for each crystal (~3 μm to ~100 μm), maximum advantage of the system's absorbance range

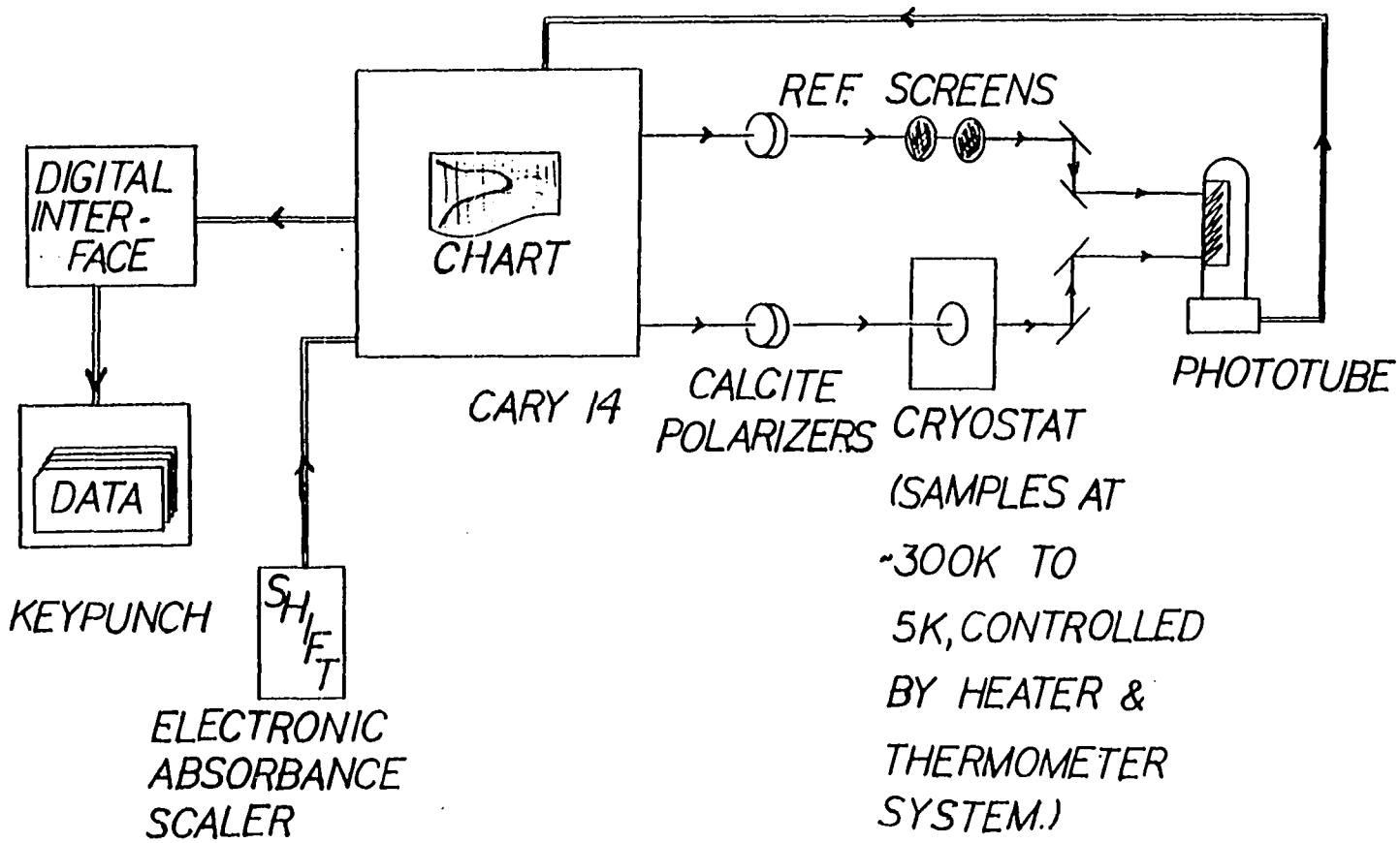

Figure 6. Schematic of the system used to obtain polarized crystal spectra at room temperature and 6K

was taken.

Crystallographic Indexing

Sixteen of the twenty compounds studied were indexed by X-ray diffraction from single crystals. Knowledge of the crystals' unit cells permits one to determine the spectroscopic face of representative crystals. The unit cell data also helps verify the identity of the compounds studied by comparison to previous work (8,9). Finally, the unit cell data provides the molarity of the crystals, from which extinction coefficients may be calculated.

To index a crystal, a single crystal of about 0.2 mm in length was affixed to the end of a small glass fiber. The fiber was inserted into a 1/2 inch section of copper tubing, which was subsequently mounted on a goniometer head. The crystal and goniometer head were sketched in a notebook so that a crystal face could be related to the axes of the unit cell. The goniometer head was then placed on the Ames Laboratory diffractometer, a computer-controlled, four-circle instrument maintained by Dr. R. A. Jacobson and his research group. The crystal was then indexed using ALICE (37), a computer program that controls the diffractometer during indexing.

After ALICE produced a reliable set of cell constants, the spectroscopic face was identified by a trial-and-error determination of the set of Miller indices which brought the face of the crystal into the diffracting position.

ALICE reports directly the volume of the unit cell. The number

of formula units per cell was determined from the estimated density of the crystal, the formula weight, and the volume of the cell. The molarity of the crystal was then calculated from the volume and the number of formula units per cell.

X-Ray Structure Determination

The structure of MGS has been known for some time (6). Those Magnus-type salts with ammonia or methylamine ligands were assumed to have crystal structures similar to that of MGS because all those salts, like MGS, possess tetragonal (or nearly so) cells. The salts with ethylenediamine ligands possess triclinic unit cells, however, so similarity of structure with MGS could not be as readily assumed. An attempt was therefore made to determine the crystal structure of $Pt(en)_2PdCl_4$, as a representative of the triclinic compounds.

The crystal of $Pt(en)_2PdCl_4$ that was mounted and indexed previously to give the unit cell constants, was remounted and indexed using the equipment and methods described in the "Crystallographic Indexing" section. After the unit cell was obtained, data were collected for 2659 reflections in the hkl, $h\bar{k}l$, $hk\bar{l}$, and $h\bar{k}\bar{l}$ octants. Mo-Kα radiation with a wavelength of 0.70964 A was used.

A scintillation counter was used to detect the reflection peaks; the intensity of each peak was determined by performing a series of 0.01 deg. steps in omega until the observed count was within the standard deviation, σ, of the background count. To monitor changes in intensity due to instrument drift or modifications in the crystal's

structure, the intensities of a set of standard reflections were measured after every 75 reflections. The data were written onto a computer disk, from which a data tape was made for transfer of the data to the Iowa State Computation Center.

A total of 1244 independent reflections were observed with intensities greater than the limit for statistical significance, i.e., $|Fo| \geq 3\,\sigma\,(Fo)$. These independent reflections were used in the structure determination calculations.

The data were corrected for both absorption and Lorentz-polarization effects. Refined unit cell constants were obtained from program LATT (38) for ±20 values of 22 independent reflections. The final cell parameters were: a= 11.711(7) A, b= 8.480(6) A, c= 6.801(2) A, α=96.10 (4) deg., β= 91.08(4) deg., γ= 106.74(8) deg., and V= 642.3(2) A^3. A Wilson plot indicated the presence of an inversion center in the cell; $P\bar{1}$ was selected as the space group of the crystal. Z= 2 for the cell.

A Patterson map was obtained from the corrected intensity data. From this map, vectors for the two Pt atoms and one Cl atom were determined; these vectors were subsequently used as initial atom positions in ALLS (39), a least-squares program that generates data for electron density maps by fitting observed and calculated structure factors. Values for atomic scattering factors and anomalous dispersion corrections were built into the program. ALLS calculated discrepancy factors R (unweighted) and R_w (weighted) for each iteration, where $R = \Sigma||F_o| - |F_c||/\Sigma|F_o|$ and $R_w = \{\Sigma w(|F_o| - |F_c|)^2/\Sigma w|F_o|^2\}^{\frac{1}{2}}$.

In these equations, F_o is the observed structure factor, F_c is the calculated structure factor, and $w = 1/\sigma^2$ (Fo), where σ(Fo) is the estimated standard deviation in Fo.

Unfortunately, the electron density maps failed to resolve the carbon atoms in the ethylenediamine units. It was thought that perhaps the cell possessed body-centering, so ALLS was run using the $I\bar{1}$ space group. Using the full-matrix calculation, with positions and anisotropic temperature factors for the Pt, Pd, and Cl atoms, and positions and isotropic temperature factors for N and C atoms varied, R = 0.136, and R_w = 0.165.

Slightly better discrepancy factors were obtained where anisotropic temperature factors were used for Pt, Pd, Cl, and N atoms, and isotropic temperature factors for two C atoms in a full-matrix calculation. Here, R = 0.126, and R_w = 0.147. Holding the position of one carbon atom constant while varying the position of the other carbon resulted in no change from the R and R_w values obtained above.

A full-matrix calculation in $I\bar{1}$, for which positions and anisotropic temperature factors of Pt, Pd, Cl, and N atoms were allowed to vary resulted in the best discrepancy factors obtained: R = 0.125, and R_w = 0.146. However, the C-C distances obtained were 1.55 A and 1.41 A for the two pairs of C-atoms. These distances are expected to be nearly equal for the $Pt(en)_2^{2+}$ ion. Carbon-nitrogen distances are likewise unequal: 1.51 A and 1.27 A for the two pairs.

A return to the primitive unit cell without an inversion center,

P1, provided diverging C-C distances and temperature factors as the carbon atoms were varied isotropically in a block-matrix calculation. $R = 0.140$, $R_w = 0.175$ for this attempt.

Those distances and angles which could be determined with a reasonable degree of confidence from the incomplete structure determination are presented in the Results and Discussion section.

RESULTS AND DISCUSSION

Crystal Indexing

Unit cells were determined from single-crystal indexing data for sixteen of the twenty Magnus-type salts. Table 2 gives the cell dimensions for all twenty salts. The values for $Pd(NH_3)_4PtBr_4$, $Pd(NH_3)_4PdCl_4$, and $Pd(NH_3)_4PdBr_4$ are those of Miller (8), who obtained cell constants from powder photographs. Cell constants for $Pt(NH_3)_4PtCl_4$ were obtained from the crystal structure determination of Atoji, Richardson, and Rundle (6).

Five of the salts indexed in this work were previously indexed by Miller (8,9): $Pt(NH_3)_4PdCl_4$, $Pt(NH_3)_4PtBr_4$, $Pt(CH_3NH_2)_4PtCl_4$, $Pt(CH_3NH_2)_4PtBr_4$, and $Pt(en)_2PdCl_4$. Our cell axes were within 0.02 A of Miller's for every compound except $Pt(CH_3NH_2)_4PtBr_4$, in which case our a,b, and c axis lengths were respectively 0.16 A, 0.15 A, and 0.13 A larger than Miller's. Our constants appear to be the better ones for two reasons. First, the values are quite similar to those obtained for $Pt(CH_3NH_2)_4PdBr_4$, which is expected on the basis of the high degree of similarity evinced by the values for $Pt(CH_3NH_2)_4PtCl_4$ and $Pt(CH_3NH_2)_4PdCl_4$. Second, Miller's c-axis is only 6.61 A. If this were the actual value, $Pt(CH_3NH_2)_4PtBr_4$ would have the smallest c-axis of all the $PtBr_4^{2-}$ salts. The bulky CH_3NH_2 ligand certainly should not give rise to a smaller value for c than is observed in the $Pt(NH_3)_4PtBr_4$ cell; if anything, c should be larger for the methylamine salt. We have assumed, on the basis of structural data, that the metal

Table 2. Cell constants and metal-metal distances for the Magnus-type salts

Salt	a(A)	b(A)	c(A)	α(deg)	β(deg)	γ(deg)	d(M-M)(A)
$Pt(NH_3)_4PtCl_4$[a]	9.03	9.03	6.49	90.0	90.0	90.0	3.25
$Pt(NH_3)_4PdCl_4$	8.967	8.927	6.465	90.0	89.9	90.0	3.23
$Pt(NH_3)_4PtBr_4$	9.279	9.279	6.626	90.0	90.0	90.0	3.31
$Pt(NH_3)_4PdBr_4$	9.317	9.317	6.645	90.1	90.1	89.8	3.32
$Pt(CH_3NH_2)_4PtCl_4$	10.373	10.351	6.486	90.1	89.9	90.0	3.24
$Pt(CH_3NH_2)_4PdCl_4$	10.358	10.358	6.491	90.0	90.0	90.0	3.25
$Pt(CH_3NH_2)_4PtBr_4$	10.711	10.695	6.743	90.0	90.1	90.0	3.37
$Pt(CH_3NH_2)_4PdBr_4$	10.651	10.664	6.695	90.2	90.1	90.0	3.35
$Pt(en)_2PtCl_4$	12.341	8.167	6.826	92.0	94.5	108.9	3.41
$Pt(en)_2PdCl_4$	11.711	8.480	6.801	96.1	91.1	106.7	3.40
$Pt(en)_2PtBr_4$	12.177	8.551	7.015	99.0	89.4	106.2	3.51
$Pt(en)_2PdBr_4$	12.201	8.538	7.051	98.9	89.8	106.1	3.53
$Pd(NH_3)_4PtCl_4$[b]	9.00	9.00	6.50	90.0	90.0	90.0	3.25
$Pd(NH_3)_4PdCl_4$[b]	8.96	8.96	6.49	90.0	90.0	90.0	3.25
$Pd(NH_3)_4PtBr_4$	9.355	9.352	6.664	89.8	90.0	90.2	3.33
$Pd(NH_3)_4PdBr_4$[b]	9.32	9.32	6.66	90.0	90.0	90.0	3.33
$Pd(en)_2PtCl_4$	12.292	8.175	6.819	92.9	95.8	109.4	3.41
$Pd(en)_2PdCl_4$	12.294	8.754	6.870	110.6	82.9	109.9	3.44
$Pd(en)_2PtBr_4$	12.558	8.426	7.096	95.2	96.3	106.1	3.55
$Pd(en)_2PdBr_4$	12.445	8.800	7.104	108.5	83.9	108.0	3.55

[a]Reference 6.

[b]Reference 8.

atoms stack along the c-axis for all of the salts, regardless of whether or not the crystals are tetragonal or triclinic. The metal-metal spacing along the stacking direction is conveniently given as one-half the length of the c-axis.

The metal-metal spacings, d(M-M), are listed in the rightmost column in Table 2. Note that chloride ligands produce spacings on the order of 0.1 A smaller than those produced by bromide ligands for the same cation. The cation ligands also affect d(M-M). While ammonia and methylamine ligands produce similar spacings, ethylenediamine gives spacings that are typically 0.15- 0.2 A higher. Over the entire set of compounds we see d(M-M) values ranging from 3.552 A, in $Pd(en)_2PdBr_4$, to 3.23 A, in $Pt(NH_3)_4PdCl_4$.

Attempted Crystal Structure for $Pt(en)_2PdCl_4$

The unit cells of the ammonia and methylamine salts are tetragonal, or very nearly so, as the unit cell angles in Table 2 indicate. The unit cells of the ethylenediamine, however, are triclinic. It was therefore desirable to solve the complete crystal structure for one of the ethylenediamine salts. A complete crystal structure would be convincing evidence that ion stacking and other structural features are comparable to those in MGS.

$Pt(en)_2PdCl_4$ was selected for single-crystal x-ray diffraction studies, both because Miller had already performed precession measurements on the salt (9), and because the $Pt(en)_2PdCl_4$ crystals were generally large and in abundant supply.

Table 3 provides positions, distances, and angles for a full-matrix calculation in the $I\bar{1}$ space group. The $I\bar{1}$ space group gave the best discrepancy factors, but a complete structural determination still could not be made. It was apparent from the final carbon positions and N-C distances that the ethylenediamine ligands undergo conformational interactions, presumably of a type similar to that illustrated in Figure 7. The result is a "smearing" of electron density over the region occupied by the carbon atoms. From the values for the z-axis positions of Pt, N1, N2, C1, and C2 in Table 3, we note that C1 occupies a position nearly in the plane defined by Pt, N1, and N2, while C2 lies somewhat above the plane. If the ethylenediamine existed in a single conformation, we would expect C1 to lie below the Pt-N1-N2 plane.

Calculations using the atom position data gave Pd-Cl distances d(Pd-Cl) of 2.32 A, which is very close to the values obtained for K_2PdCl_4 (41). The Cl1-Pd-Cl2 angle was 89.3 deg., very close to the strict square-planar arrangement we expected. Distances and angles obtained for the N and C atoms were less reasonable. Values for d(Pt-N1) of 2.05 A and d(Pt-N2) of 2.07 A agree with the values reported for MGS (6). However, the N1-Pt-N2 angle was only 81.1 deg., a significant deviation from the expected square-planar configuration for the $Pt(en)_2^{2+}$ cation. Even more disturbing were the unequal N-C distances: d(N1-C1) = 1.51 A, while d(N1-C1A) = 1.27 A, where C1A is the carbon atom related to C1 by the body center.

Table 3. Atom positions, distances and angles for $Pt(en)_2PdCl_4$ attempted crystal structure

atom(s)	x[a]	y	z	distance(A)	angle(deg.)
Pt	0	0	0		
Pd	0.5	0.5	0.0		
Cl1	0.5238(8)	0.783(1)	0.024(1)		
Cl2	0.7054(7)	0.554(1)	0.002(1)		
N1	0.007(3)	0.245(3)	0.015(5)		
N2	0.818(3)	-0.028(3)	-0.007(5)		
C1	0.893(3)	0.269(5)	-0.006(6)		
C2	0.800(4)	0.37(5)	0.051(6)		
Pt-N1				2.05	
Pt-N2				2.07	
Pd-Cl1				2.32	
Pd-Cl2				2.32	
N1-C1				1.51	
Pd-Pt-N1					92.9
Pt-Pd-Cl1					88.0

N1-Pt-Cl1	25.1
N2-Pt-Cl2	17.8
N1-Pt-N2	81.8
Cl1-Pd-Cl2	89.3

[a]Given in fractional coordinates.

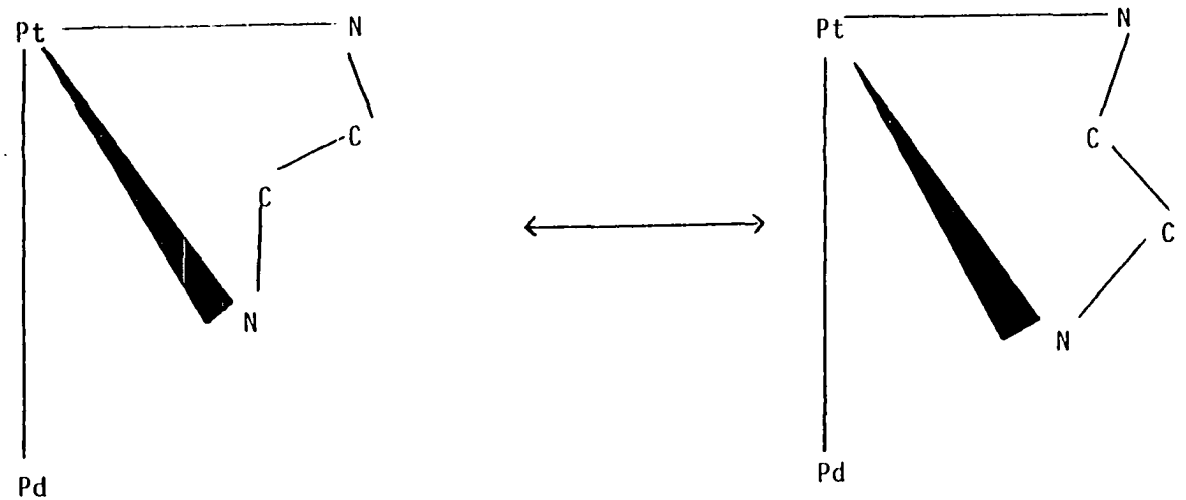

Figure 7. Possible conformational interactions in salts containing $Pt(en)_2^{2+}$ ion

The failure to arrive at a complete solution for the structure of $Pt(en)_2PdCl_4$ is especially unfortunate, since a complete crystal structure is needed to test the explanation for the variation of vibrational structure intensities proposed further on in the Discussion. Nevertheless, the attempt made here does permit us to conclude that the salts with ethylenediamine ligands possess the same kind of ion stacking observed in MGS.

Crystal Spectra

Single-crystal polarized spectra are presented in this section for the twenty salts. The 300K and 6K spectra for the z- and x,y-polarizations of each salt, plotted as Absorbance vs. wavenumbers (cm^{-1}), appear in the text along with the discussion of the series represented by each anion. Except where otherwise noted, z-polarization corresponds to the higher of the two polarization angles for each set of spectra.

Tables 4 through 7 summarize the absorptions observed for each compound. Every absorption included in the table met the requirement that it be observed in the spectra of at least two of the 6-10 crystals of each salt for which spectra were recorded. The practice of choosing crystals for each salt over the widest possible range of thickness (typically, an order of magnitude) reduced the number of observations of both very weak absorptions and very intense absorptions: intense absorptions were usually beyond the spectrophotometer's absorbance range in the thick crystals, and the weak absorptions were obscured by background noise in thin crystals. The two-observation

Table 4. Absorptions observed for the $PdCl_4^{2-}$ series at 6K and 300K[a]

Spectrum		$Pd(en)_2PdCl_4$		$Pd(NH_3)_4PdCl_4$	
		ν, cm^{-1}	ε, $cm^{-1}M^{-1}$	ν, cm^{-1}	ε, $cm^{-1}M^{-1}$
z	6K	16075	5.2 ± 1.3	19100	57.9 ± 8.9
		20700	61.6 ± 7.3	28000	235 ± 15
				34250	466
z	300K	16050	10.3 ± 2.1	19600	114 ± 10
		20900	154 ± 9	28000	304 ± 54
				34000	541
x,y	6K	16075	4.8 ± 1.0	20800	110 ± 18
		20650	107 ± 22	26400	102 ± 33
				31000?	>900
x,y	300K	15950	11.4 ± 1.7	20400	174 ± 28
		20500	202 ± 32	31000?	>900

[a]All wavenumber values are for peak maxima, or the middle of distinct shoulders only.

$Pt(en)_2PdCl_4$		$Pt(CH_3NH_2)_4PdCl_4$		$Pt(NH_3)_4PdCl_4$	
ν, cm^{-1}	ε, $cm^{-1}M^{-1}$	ν, cm^{-1}	ε, $cm^{-1}M^{-1}$	ν, cm^{-1}	ε, $cm^{-1}M^{-1}$
18000	44.1 ± 6.3	14550	48.3 ± 4.7	14200	34.9 ± 5.2
25600	196 ± 16	16500	37 ± 8.8	16100	25.4 ± 8.3
		23200	216 ± 30	22500	195 ± 9.9
18500	110	14900	80	15950	68
26500	225 ± 19	16850	80.9	23500	220
		24500	280		
20000	76.9 ± 6.1	15000	11.2 ± 4.8	14400	4.8 ± 0.5
26100	192 ± 12	20500	147 ± 28	16250?	3
				20200	122 ± 16
19950	154 ± 10	15100	20.7 ± 5.0	15100	7.5
		20050	199 ± 50	19750	233 ± 27

Table 5. Absorptions observed for the $PdBr_4^{2-}$ series at 6K and 300K[a]

Spectrum		$Pd(en)_2PdBr_4$		$Pd(NH_3)_4PdBr_4$	
		ν, cm^{-1}	ε, $cm^{-1}M^{-1}$	ν, cm^{-1}	ε, $cm^{-1}M^{-1}$
z	6K	15700?	5	15300	10.7
		20200	29.0	18700	46.3 ± 13
		29600	640	28200	675
				32100	317
				35100	318
z	300K	15600?	10	18900	101 ± 8
		20250	82.8	28200	713
		29600	560		
x,y	6K	19700	166	19350	134 ± 10
x,y	300K	19300	360	19100	226 ± 31

[a]All wavenumbers are given for peak maxima, or the middle of distinct shoulders only.

$Pt(en)_2PdBr_4$		$Pt(CH_3NH_2)_4PdBr_4$		$Pt(NH_3)_4PdBr_4$	
ν, cm^{-1}	ε, $cm^{-1}M^{-1}$	ν, cm^{-1}	ε, $cm^{-1}M^{-1}$	ν, cm^{-1}	ε, $cm^{-1}M^{-1}$
15300	3.9 ± 2.7	14650	18.1	14100	11.6 ± 4
18000	42.6 ± 7.6	16500	27.4 ± 6.9	15700	15
25000	212 ± 47	19600	15	22000	56.6 ± 6
29600	725	23000	123	24500	83.1 ± 7
		25700	186	28000	735
		29300	741		
18300	151 ± 18	17000	113 ± 13	14000	40
29500	745	23000	162	15850	58.7 ± 16
		29600	704	22500	104
				28050	599
14600	4.5	19250	189 ± 29	14500	5
19200	164 ± 28	22000	124	19350	80.2 ± 5
22000?	<200			22000	100
14400	11.9	18850	332 ± 41	14500	7
18750	334 ± 55			18700	144
22000	237				

Table 6. Absorptions observed for the $PtCl_4^{2-}$ series at 6K and 300K[a]

Spectrum		$Pd(en)_2PtCl_4$		$Pd(NH_3)_4PtCl_4$	
		ν, cm^{-1}	ε, $cm^{-1}M^{-1}$	ν, cm^{-1}	ε, $cm^{-1}M^{-1}$
z	6K	19950	36.2 ± 3.9	18700	27.7
				25200	203
z	300K	19500	70.1 ± 7.3	18700	58.6
				25600	330
x,y	6K	19750	21.4 ± 2.4	19000	13.0
		23000	25.0	26400	81.4
		25000	64.3 ± 5.4		
		27600	84.0 ± 11.5		
x,y	300K	19400	35.7 ± 9.8	18600	13.0
		25000	127 ± 18	26100	135
		27500	135 ± 35		

[a]All wavenumbers are given for peak maxima, or the middle of distinct shoulders only.

$Pt(en)_2PtCl_4$		$Pt(CH_3NH_2)_4PtCl_4$		$Pt(NH_3)_4PtCl_4$	
ν, cm^{-1}	ε, $cm^{-1}M^{-1}$	ν, cm^{-1}	ε, $cm^{-1}M^{-1}$	ν, cm^{-1}	ε, $cm^{-1}M^{-1}$
18200	43.6 ± 6	16700	67.4 ± 7.0	16100	99.4
24900	118 ± 20	21000?	124 ± 30	23000	358
18100	98.1 ± 6	17300	119 ± 10	16700	119
25300	240 ± 26			24000	498
18400	17	17500	15	17400	20.4
22500	35.1	25400	108 ± 17	22400	68.1
25000	61.3	31900	568	25200	140.3
28200	129			31900	764
33650	650				
18000	16.4	18000	20	17400	31.3
25500	118	25300	177 ± 9	25000	184
34600	550	33100	460	33600	679

Table 7. Absorptions observed for the $PtBr_4^{2-}$ series at 6K and 300K[a]

Spectrum		$Pd(en)_2PtBr_4$		$Pd(NH_3)_4PtBr_4$	
		ν, cm^{-1}	ε, $cm^{-1}M^{-1}$	ν, cm^{-1}	ε, $cm^{-1}M^{-1}$
z	6K	18700	38.5	18250	16.9
		26700	326	25000	98
		32000	>400	32000	>400
z	300K	18500	46.2	17700	28.3
		26300	487	24900	160
x,y	6K	18900	32.1	18500	18.8
		22000	75	25000	113
		23850	141	31200	>300
		25900	190		
		31200	>300		
x,y	300K	18250	18.8	18650	46.2
		24150	93.9	23500	254
				25550	326

[a]All wavenumbers are given for peak maxima, or the middle of distinct shoulders only.

$Pt(en)_2PtBr_4$		$Pt(CH_3NH_2)_4PtBr_4$		$Pt(NH_3)_4PtBr_4$	
ν, cm^{-1}	ε, $cm^{-1}M^{-1}$	ν, cm^{-1}	ε, $cm^{-1}M^{-1}$	ν, cm^{-1}	ε, $cm^{-1}M^{-1}$
17400	18.0	16340	23.0	15500	60.4
23800	78.0	22170	60.7	21600	173
26500	171	25000	172	24000?	285
17250	75.0	16580	62.7	15650	107
23800	179 ± 65	22730	156	22500	308
17500	37.5	16340	5.2	16000	19.5
23800	99.0	21740	13.8	21400	70.2
26500	189	23920	110	23600	185
17300	37.5	16640	14.4	16100	27.3
23800	246	23530	167	23300	292

requirement was therefore adopted as a reasonable guard against the inclusion of spurious peaks in Tables 4-7.

Most of the extinction coefficients reported in Tables 4-7 were calculated from the average values over each crystal in which the absorption was observed. The standard deviation

$$s = \sqrt{\frac{\sum_{i=1}^{n} (x_i - x)^2}{n-1}} \qquad (2)$$

is given to the right of each extinction coefficient calculated by this method. In several cases, the extinction coefficients were calculated from the absorbance and thickness data for the crystal that showed the best resolution of spectral features. This method was used only when the salt produced few crystals of spectroscopic quality. Any crystal for which a light leak, or poor polarization might be suspected was eliminated from the calculations of the extinction coefficients.

Despite the care taken to calculate the extinction coefficients from the best data collected, the extinction coefficients are accurate to about ±30%, and as such are probably best considered as estimates only. Much of the error can be attributed to inaccuracy in the measurements of the crystal thicknesses, and to distortions in the baseline when very small pinholes (<40μm) were used.

Crystal thicknesses were measured by standing the crystal on edge under a microscope equipped with a calibrated reticle. Unfortunately, this technique can only measure the thickness at the edge: it cannot

detect variations in the crystal's thickness over the area of the crystal above the pinhole. Many crystals formed with a trough-like shape: the center of the crystal was much thinner than the edges. Other crystals formed as wedges and blades of uneven thickness.

In the case of MGS, however, one crystal was obtained with very flat, optical faces; evidence of which appeared in the form of interference waves brought about by constructive and destructive interference of light reflected from the inner faces of the crystal (33). Precise measurement of the maxima and minima of these interference waves allowed the crystal thickness to be determined by solving for N, the number of wavelengths equalling two crystal thicknesses, in the equation

$$\frac{m + N}{n_m \nu_m} = \frac{N}{n_N \nu_N} \qquad (3)$$

where m is the number of interference waves, ν_m is the wavenumber (cm^{-1}) at wave m, ν_N is the wavenumber at which N is determined, n_m and n_N are the indices of refraction at ν_m and ν_N, respectively. Dispersion effects cause ν_m to vary nonlinearly over the range of the interference waves. To account for this variation, ν_m was fit by a quadratic least-squares treatment on a microcomputer (41), in which ν_m is determined as a function of m, as equation 4 shows:

$$\nu_m = c_0 + c_1 m + c_2 m^2 \qquad (4)$$

In this equation, $c_0 = \nu_N$; c_1 and c_2 are constants determined by the fit. By substituting $\Delta\nu$ for $\nu_m - \nu_N$, then solving equation 4 for m,

and retaining only the first two terms in the binomial expansion, m is expressed in terms of ν, c_1, and c_2:

$$m \cong \frac{\Delta\nu}{c_1} - \frac{c_2(\Delta\nu)^2}{c_1^3} + \ldots. \tag{5}$$

Therefore, we see that

$$\frac{m\nu_N}{\Delta\nu} = \frac{c_0}{c_1} - \frac{c_0 c_2 \Delta\nu}{c_1^3} \tag{6}$$

which also appears as

$$\frac{m\nu_N}{\Delta\nu} = N + \frac{Nc_0}{n_N}\left(\frac{\Delta n}{\Delta\nu}\right) + \frac{N}{n_N}\frac{\Delta n}{\Delta\nu}\Delta\nu \tag{7}$$

from equation 3. The third term of 7 corresponds to the second term in 6, and the first two terms in 7 correspond to the first term in 6:

$$\frac{N}{n_N}\frac{\Delta n}{\Delta\nu} = \frac{c_0 c_2}{c_1^3} \tag{8}$$

and

$$N\{\,1 + \frac{c_0}{n_N}\left(\frac{\Delta n}{\Delta\nu}\right)\,\} = \frac{c_0}{c_1} \tag{9}$$

These two equations provide the expression for N

$$N = \left(\frac{c_0}{c_1}\right)/\left(1 + \frac{c_0}{n}\left(\frac{\Delta n}{\Delta\nu}\right)\right) \tag{10}$$

which yields the approximate expression,

$$N = \frac{c_0}{c_1}\{1 - \frac{c_0}{n_N}\left(\frac{dn}{d\nu}\right)\} \tag{11}$$

In equation 11, $1/n\,dn/d\nu$ can be obtained from the change in the interference wave maxima and minima as the cryatal face is tilted away from the sample beam. Such data are available in the literature (33), allowing reasonably good values for N to be calculated (42). A thickness of 4.0 $\pm$0.1 μm was calculated from the interference waves. This compares

with a value of 5.1 μm obtained from the calibrated reticle technique. It appears that errors of ±20% are readily obtained from the calibrated reticle method.

The extinction coefficients calculated from the absorbances and thickness for the optically flat MGS crystal still have a large error associated with them. The interference waves tended to obscure all but the most intense absorptions, and the baseline was reproducible only to about 0.05 absorbance unit, due to the very small size (about 30 μm x 30 μm) of the crystal over the pinhole. Since the most intense peak measured in the spectra had an absorbance of only 0.45, a ±0.05 baseline absorbance error was quite significant. Fortunately, most crystals for which spectra were obtained were at least 50 μm x 80 μm; in these cases the baseline error tended to be very small.

In general, the locations of the peak maxima observed in this research are in good agreement with those obtained by diffuse reflectance spectroscopy by Miller (9) and Day et al. (28).

Comparison of the room temperature spectra for MGS and $Pt(CH_3NH_2)_4PtCl_4$ (Me-MGS) with single-crystal polarized spectra for those salts obtained by Day et al. shows good agreement of the peak locations for the x,y-polarized peaks below 30,000 cm^{-1} and the z-polarized peaks below 20,000 cm^{-1}. As was stated in the Introduction, however, the z-polarized spectra above 25,000 cm^{-1} reported by Day et al. show signs of incomplete polarization. The spectra for MGS and Me-MGS recorded in this research do not seem to indicate incomplete

polarization. Instead, the absorption rises rapidly from a minimum at about 20,000 cm^{-1}, and at 25,000 cm^{-1} is too intense to be measured by our equipment. Day et al. also reported a shoulder at 23,000 cm^{-1} in the z-polarized spectrum of Me-MGS that is not seen in our spectra, although we so note a questionable shoulder at 21,000 cm^{-1} in z-polarization at 6K.

Several differences in extinction coefficients are noted in Table 8 for MGS and Me-MGS. This is not surprising, in view of the large error in our extinction coefficient values. Even with the large error, however, our values are remarkably similar to those obtained by Day et al. at room temperature.

The spectra reported here for MGS are also consistent with those reported earlier by Martin and coworkers for both room temperature and 15K (34). No disagreement on peak positions was noted, but the extinction coefficients for both x,y-polarized peak at 25,200 cm^{-1} and the z-polarized peak at 16,500 cm^{-1} differ by more than can be accounted for by the large error, as Table 8 indicates. The discrepancy in the extinction coefficients for the z-polarized peak may be explained by the inability of the phototube used by Martin and coworkers to detect light far enough into the red to observe the peak maximum. This explanation, however, does not explain the large discrepancy in the extinction coefficients calculated for the 25,200 cm^{-1} peak in x,y-polarization at 6K.

The limited wavelength range of the phototube used by Martin et al.

Table 8. Comparison of peak maxima and extinction coefficients for MGS and Me-MGS from three sources

Salt	peak	temp., pol.		Reference 28		Reference 34		This work	
				ν_{max}[a]	ε[b]	ν_{max}	ε	ν_{max}	ε
MGS	$^3A_{2g}, ^3E_g$	6K	z			16500	ca.50	16100	61
		300K	z	16500	150	16500	ca.110	16100	124
	$^1A_{2g}, ^1E_g$	6K	x,y			25200	65	25200	140.3
		300K	x,y	24900	170	25200	140	25200	184
Me-MGS	$^3A_{2g}, ^3E_g$	6K	z					16700	67.4
		300K	z	17300	100			16700	124
	$^1A_{2g}, ^1E_g$	6K	x,y					25400	108
		300K	x,y	25200	190			25400	177

[a] units of cm^{-1}.

[b] units of $cm^{-1}M^{-1}$.

also prevented them from observing a very sharp, narrow peak in x,y-polarization for MGS at low temperature. This peak will be discussed in detail in another section.

Recall from the Introduction that the close approach of the cation's d_z2 orbital to the anion's d orbitals should result in the anion's orbitals shifting in energy according to the progression:

$$d_z2 > d_{xz,yz} > d_{x^2-y^2}, d_{xy}$$

The polarized spectra of the five Magnus-type salts having a $PdCl_4^{2-}$ anion, as shown in Figures 8-12, and as summarized in Table 4, indicate shifts in the d-d transition energies that are quite consistent with the behavior predicted as the metal-metal spacings decrease, and thereby raise the energies of the anion d orbitals perturbed by the cation d_z2 orbital. Figure 13 provides a graphic representation of the shifts across the series for all transitions observed.

The x,y-polarized peak at 21,700 cm^{-1} in K_2PdCl_4 assigned by Martin and coworkers to the $^1A_{2g} \leftarrow {}^1A_{1g}$ ($d_{x^2-y^2}{}^* \leftarrow d_{xy}$) transition (36) is seen to shift by only 1500 cm^{-1} from K_2PdCl_4, d(M-M) = 4.112 A (40), to $Pt(NH_3)_4PdCl_4$, d(M-M) = 3.23 A. This transition is identified in the Magnus-type salts by analogy with the $^1A_{2g}$ peak in K_2PdCl_4: the x,y-polarization, the presence of vibrational structure, and the similar effect of temperature on the transition intensity (see Table 9) readily identify the transition in the region of 20,700-cm^{-1} to 20,000 cm^{-1} in the Magnus-type $PdCl_4^{2-}$ salts as the same one that appears at 21,700 cm^{-1} in K_2PdCl_4.

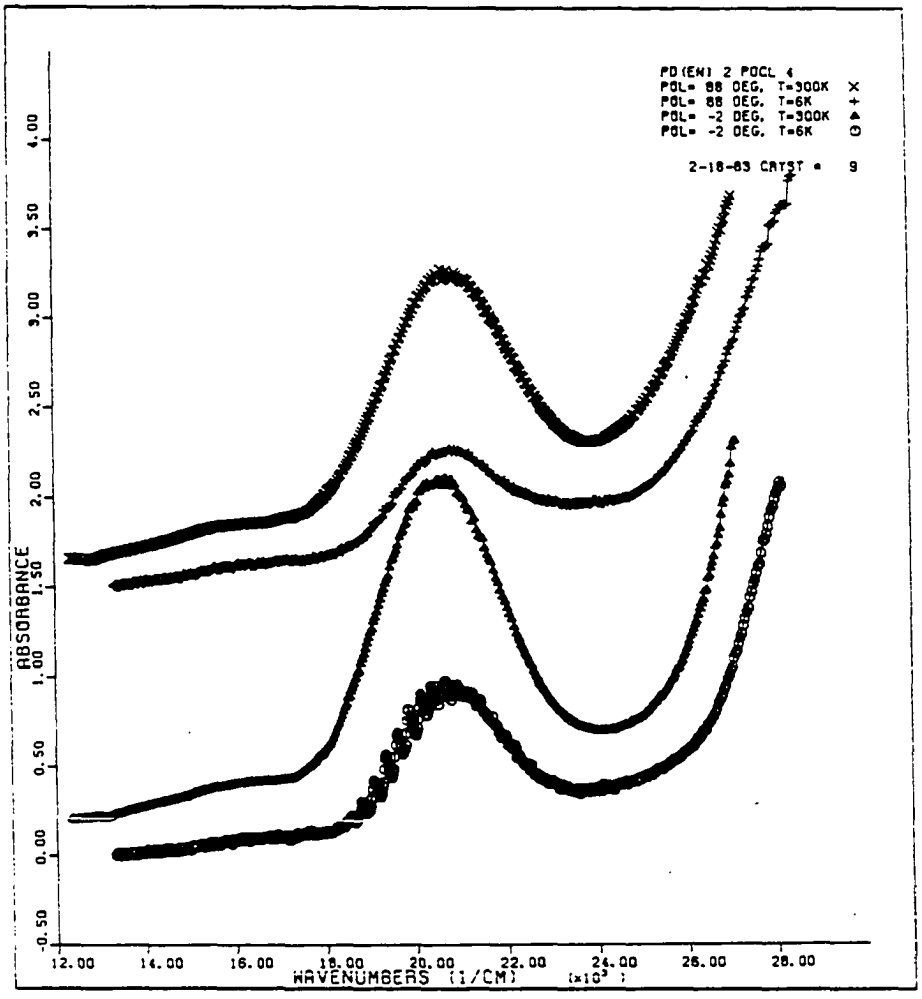

Figure 8. Polarized absorption spectra for $Pd(en)_2PdCl_4$

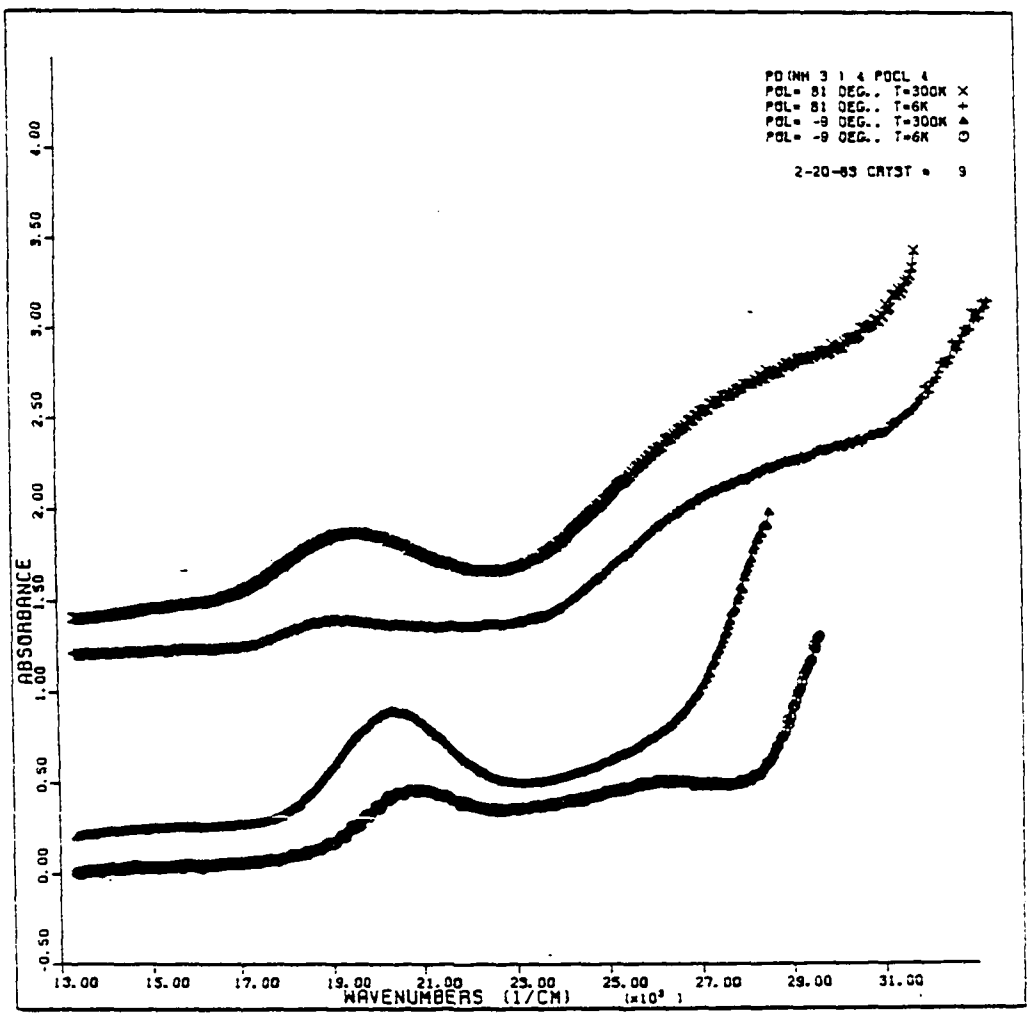

Figure 9. Polarized absorption spectra for $Pd(NH_3)_4PdCl_4$

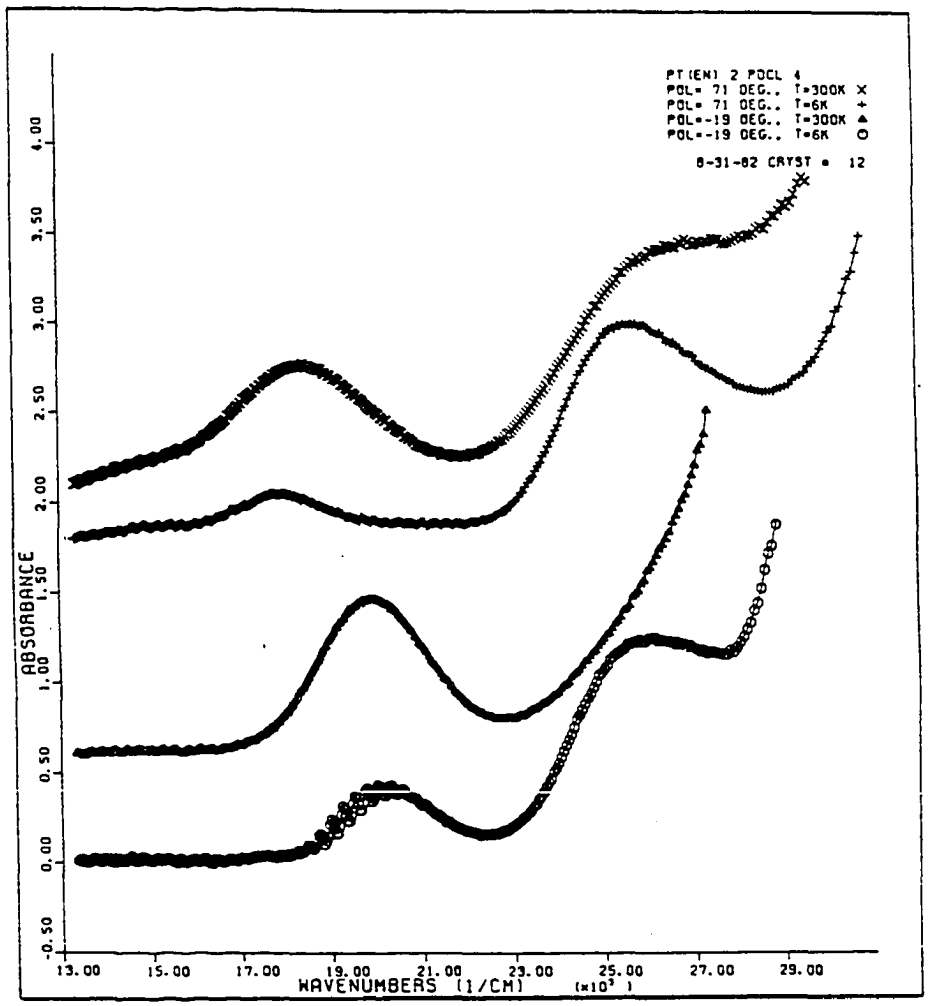

Figure 10. Polarized absorption spectra for $Pt(en)_2PdCl_4$

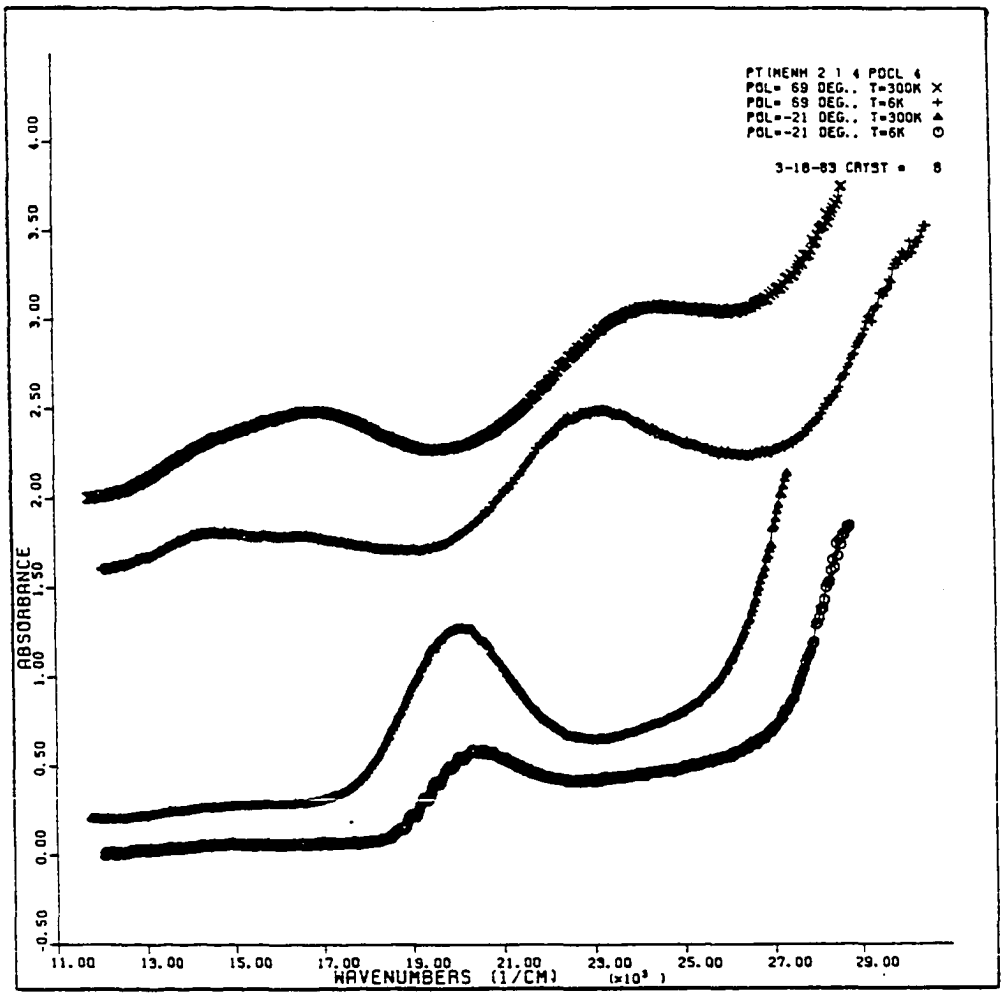

Figure 11. Polarized absorption spectra for $Pt(CH_3NH_2)_4PdCl_4$

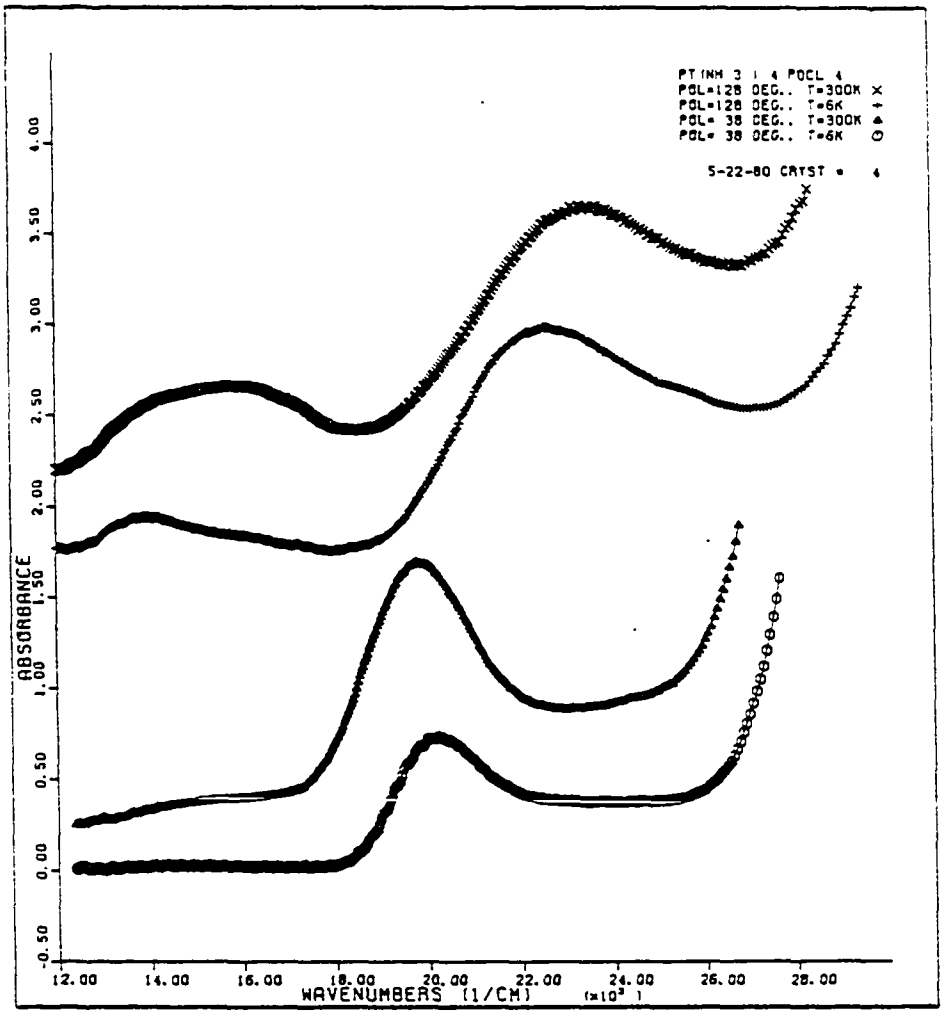

Figure 12. Polarized absorption spectra for $Pt(NH_3)_4PdCl_4$

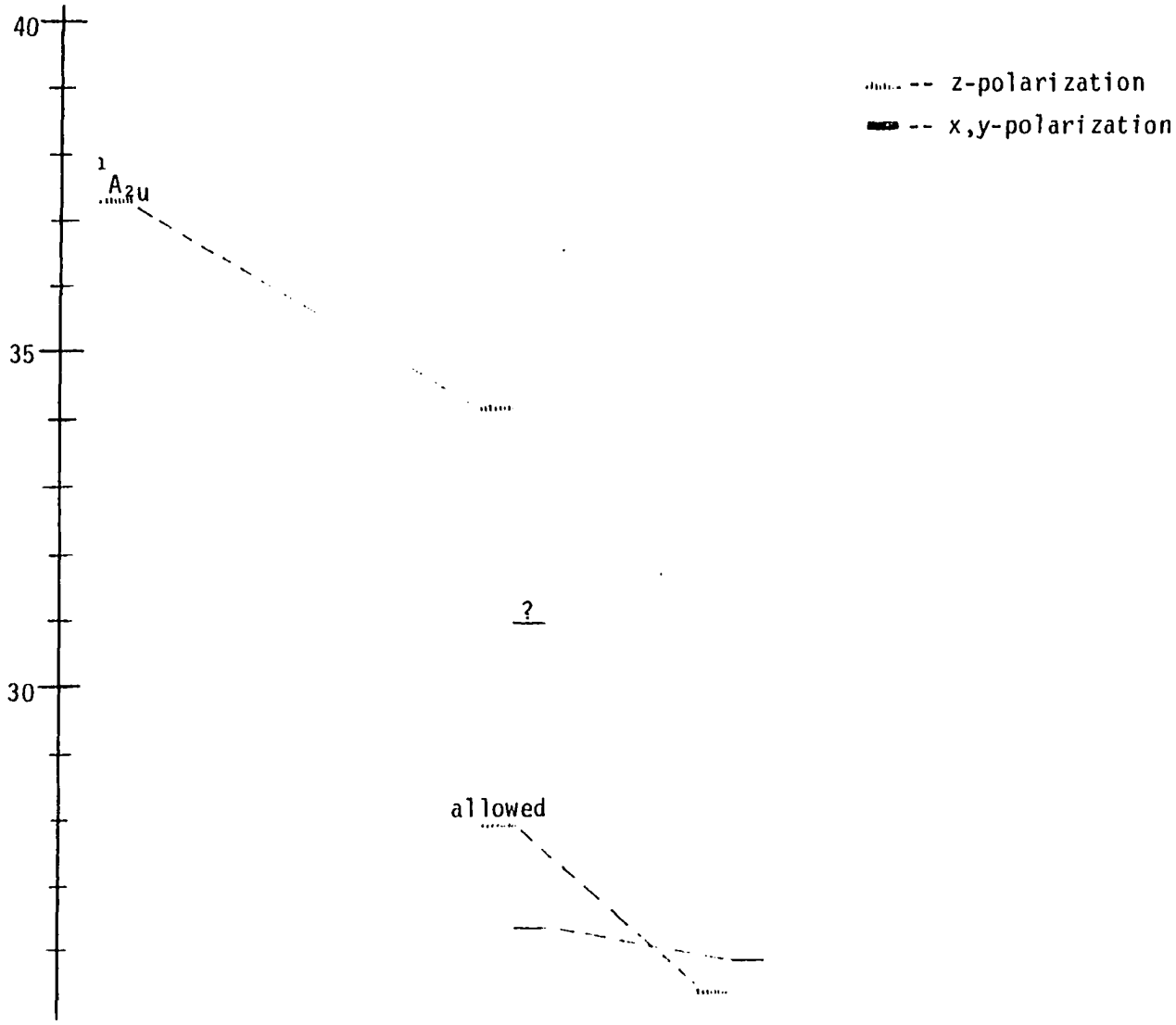
40
35
30
$^1A_{2u}$
?
allowed
-- z-polarization
-- x,y-polarization

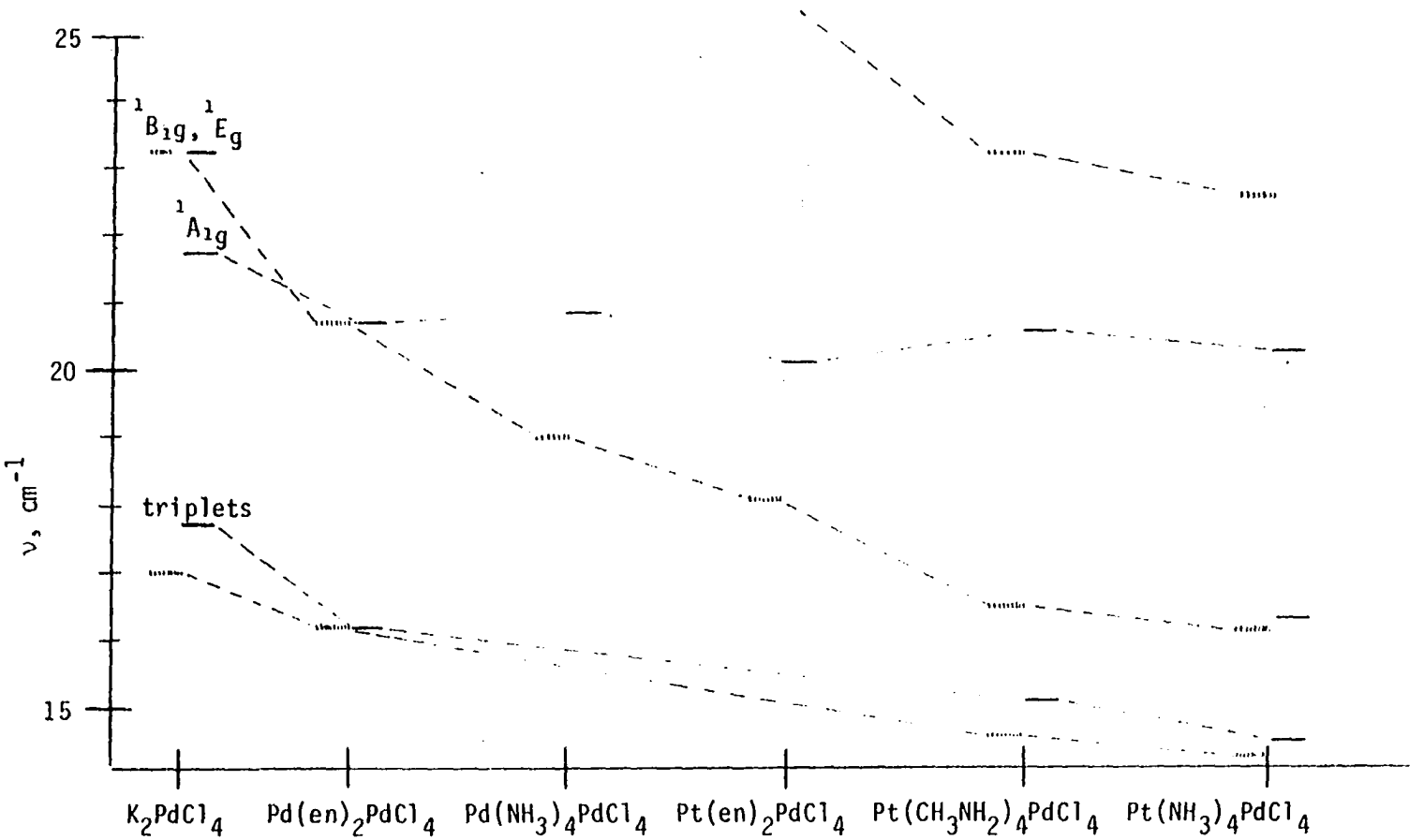

Figure 13. Shifts of absorptions across the $PdCl_4^{2-}$ series

The small size of the shift for the $^1A_{2g}$ transition is a consequence of the fact that the $d_{x^2-y^2}$ and d_{xy} orbitals are both concentrated in the plane perpendicular to the cation d_{z^2} orbital; even very close approach of the d_{z^2} orbital facilitates little difference in any overlap of the orbitals.

The peaks in the Magnus-type salts corresponding to the $^1E_g \leftarrow {}^1A_{1g}$ ($d_{x^2-y^2} \leftarrow d_{xz,yz}$) transition at 23,000 cm^{-1} in both x,y- and z-polarizations for K_2PdCl_4 were not as readily identified as was the $^1A_{2g}$ state. There is evidence, however, in the form of low-energy spin-forbidden transitions, that suggests that the ^1E_g state shifts by about 3000 cm^{-1} from K_2PdCl_4 to $Pt(NH_3)_4PdCl_4$, where it is a component of the primarily $^1A_{2g}$ peak at 20,200 cm^{-1}. Three of the salts, $Pd(en)_2PdCl_4$, $Pt(CH_3NH_2)_4PdCl_4$, and $Pt(NH_3)_4PdCl_4$ definitely show low-intensity transitions in the 14,200 - 16,100 cm^{-1} region for both x,y- and z-polarizations. While the other two salts in the series, $Pt(en)_2PdCl_4$ and $Pd(NH_3)_4PdCl_4$ do not show distinguishable peaks in this region, the z-polarized spectra of these salts do exhibit rising absorptions from 14,000 cm^{-1} - 16,000 cm^{-1} that suggests the presence of a weak, presumably spin-forbidden transition.

Such weak, spin-forbidden bands appearing at 17,000 cm^{-1} (z) and 17,700 cm^{-1} (x,y) in K_2PdCl_4 were assigned by Martin and coworkers to the $^3A_{2g}$ and ^3E_g states. The relatively small differences in the $^1A_{2g}$ and ^1E_g transition energies in the $PdCl_4^{2-}$ series (which in turn give rise to small differences in the triplet energies), coupled with

the relatively low intensities of the triplet ← singlet transitions, may account for the lack of resolved $^3A_{2g}$ and ^3E_g components at low temperatures.

Making the assignment of $^3A_{2g}$ and ^3E_g to the low-energy bands in the Magnus-type salts, we find that the shifts of these low-energy peaks, from K_2PdCl_4 to $Pt(NH_3)_4PdCl_4$, are 3300 cm^{-1} for x,y- and 2800 cm^{-1} for z-polarization. Since the shift for $^1A_{2g}$ is known to be much smaller that 2800 - 3300 cm^{-1} over the series, we can infer that the shift of the triplet bands corresponds to a similar shift for ^1E_g. As it happens, the peak maximum of the x,y-polarized absorption in $Pt(NH_3)_4PdCl_4$ at 20,200 cm^{-1} is 3000 cm^{-1} to the red of the peak assigned to ^1E_g in K_2PdCl_4.

Identical behavior is observed for the shifts of the low-energy transitions in each of the other three series studied (see the following sections), thereby supporting the assignments of the ^3E_g and ^1E_g transitions made for the $PdCl_4^{2-}$ series.

With the assignment for ^1E_g, $^1A_{2g}$, ^3E_g, and $^3A_{2g}$ made, only one d-d vibronic transition, $B_{1g} \leftarrow A_{1g}$, remains to be assigned. The $B_{1g} \leftarrow A_{1g}$ transition, corresponding to $d_{x^2-y^2}^* \leftarrow d_{z^2}$, is vibronically allowed in both x,y- and z-polarizations. This transition should also show the greatest shift in energy as d(M-M) is decreased. The only observed vibronic band in the series which has not yet been assigned is a moderately weak, z-polarized absorption which shifts from 23,200 cm^{-1} in K_2PdCl_4 to 16,100 cm^{-1} in $Pt(NH_3)_4PdCl_4$, possesses several

features which support its assignment to the $^1B_{1g} \leftarrow {}^1A_{1g}$ transition. We should not be overly concerned about the lack of an observed $^3B_{1g}$ band; the triplet bands are weak and often difficult to detect.

The magnitude of the peak intensities of the remaining vibronic transition indicates that the transition at 23,200 cm^{-1} in K_2PdCl_4 is the same as the one at 16,100 cm^{-1} in $Pt(NH_3)_4PdCl_4$. The presence of ^1E_g at 23,200 cm^{-1} in K_2PdCl_4 is well-established by the observation of an A-term in that region in the MCD spectrum (21). However, the MCD results do not rule out the possibility of $^1B_{1g}$ occurring at the same energy. Indeed, it is possible that $^1B_{1g}$ provides the major contribution to the absorption at 23,200 cm^{-1} in K_2PdCl_4. If so, the magnitude of the K_2PdCl_4 intensities will be primarily characteristic of $^1B_{1g}$, rather than ^1E_g.

In each salt, the extinction coefficients for the z-polarized peaks are much smaller than the values for the $^1A_{2g}$ and ^1E_g (x,y) peaks. Of course, this is not conclusive proof that the z-polarized peaks arise from the same transition, but the excitation mechanism is expected to produce similar intensities for each $PdCl_4^{2-}$ ion, regardless of the cation used, according to the premise set forth by Day et al., and others (14,28) that the low-intensity transitions in the Magnus-type salts are simply the vibronically allowed d-d transitions of the anion that are perturbed by crystal effects due to the close approach of the cation.

By measuring the polarized spectra at both 6K and room tem-

perature, we were able to obtain ratios of the peak intensities at the two temperatures. Although the "estimated" extinction coefficients were used to calculate the ratios, the ratios were checked by comparison with ratios calculated from the room temperature and 6K absorbance values for individual crystals. The check used no crystal thickness values, so that the large error due to the thickness measurement would not affect the calculated ratios. Perhaps somewhat surprising was the good agreement shown by the two methods of calculations: none of the pairs of ratios differed by more than 10 percent.

It should be noted that $Pt(CH_3NH_2)_4PdCl_4$ formed a special case to the above procedure. Because two peaks, at 16,500 cm^{-1} and 14,500 cm^{-1}, overlapped to form the large feature at low-energy in z, the feature was subjected to Gaussian analysis (see Figures 14 and 15), and the oscillator strengths of the two components at both 6K and 300K were calculated from the equation

$$f = 4.6 \times 10^{-9} \varepsilon_{max} \nu^{\frac{1}{2}} \qquad (12)$$

which gives the approximate oscillator strength of a Gaussian absorption feature for which the extinction coefficicent at the peak maximum and the width of the peak at half-maximum height are known (13). The temperature dependence ratios were then calculated from the oscillator strengths at 6K and room temperature (normally 300K).

Table 9 shows the calculated ratios, $\varepsilon_6/\varepsilon_{300}$, for several peaks observed in each compound of the series. With the exception of $Pd(NH_3)_4PdCl_4$, the peaks in x,y assigned to $^1A_{2g}$ showed a temperature

Figure 14. Gaussian decomposition of the low-energy bands in $Pt(CH_3NH_2)_4PdCl_4$ at 300K

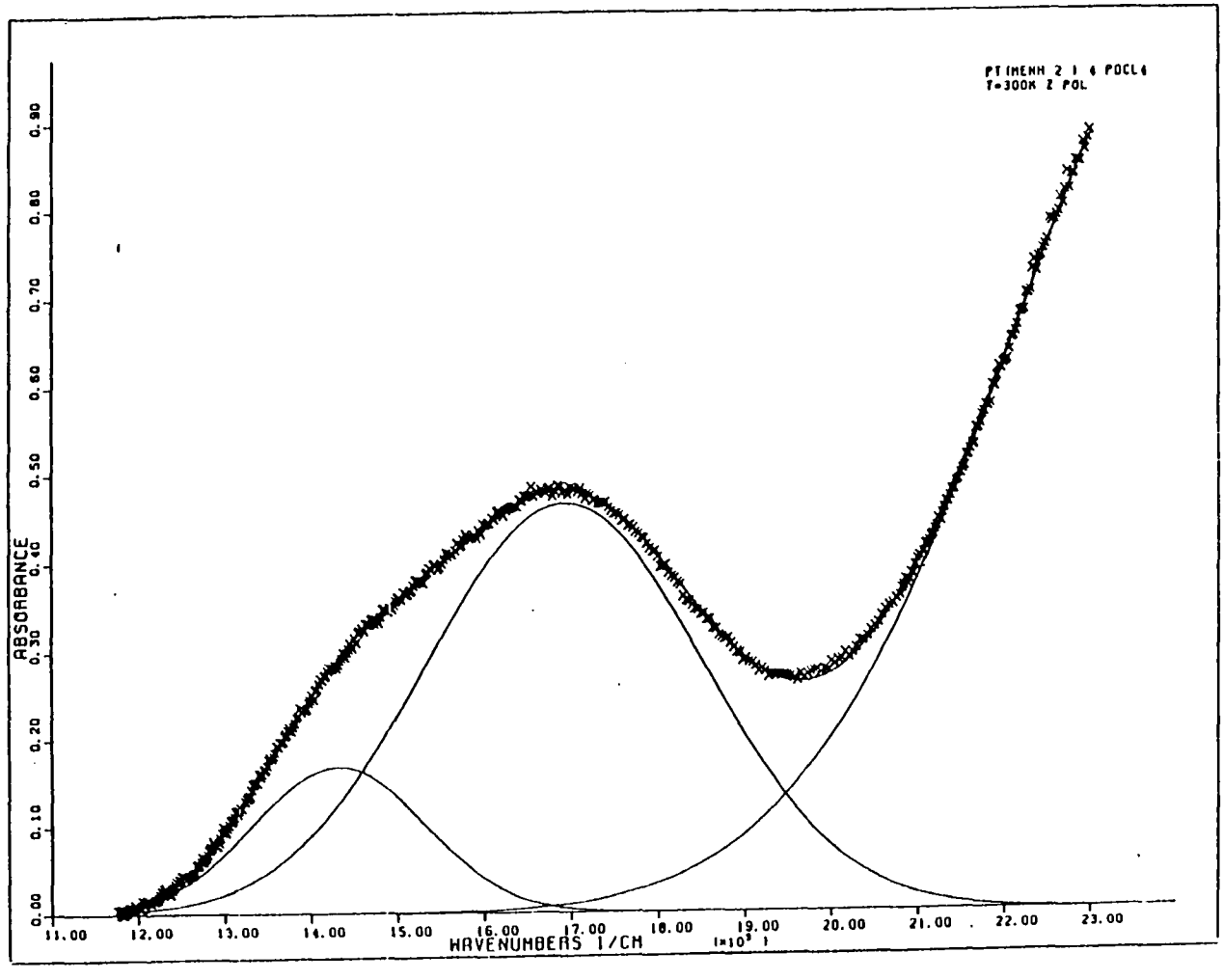
PT(NH3)4(PCL4)
T=300K Z POL
ABSORBANCE
0.00
0.10
0.20
0.30
0.40
0.50
0.60
0.70
0.80
0.90
11.00
12.00
13.00
14.00
15.00
16.00
17.00
18.00
19.00
20.00
21.00
22.00
23.00
WAVENUMBERS 1/CM
I=10³ I

Figure 15. Gaussian decomposition of the low-energy bands in $Pt(CH_3NH_2)_4PdCl_4$ at 6K

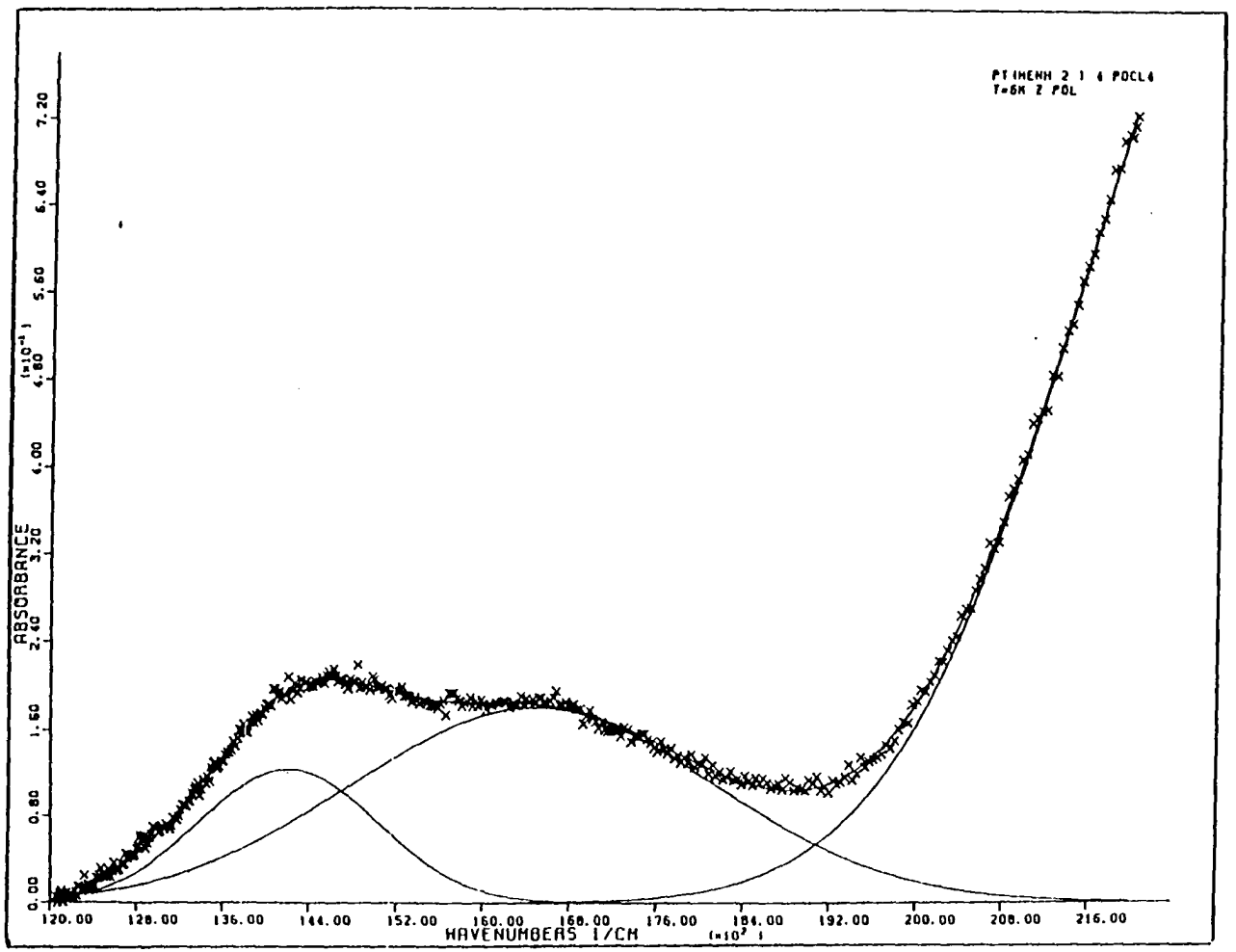
PT(HEN)H 2 1 4 POCL4
T=6K Z POL
ABSORBANCE
0.00
0.80
1.60
2.40
3.20
4.00
4.80
5.60
6.40
7.20
(*10^-1)
120.00
128.00
136.00
144.00
152.00
160.00
168.00
176.00
184.00
192.00
200.00
208.00
216.00
WAVENUMBERS 1/CM
(*10^2)

Table 9. Temperature behavior for selected peaks in the $PdCl_4^{2-}$ series

Compound	Peak location[a]	Polarization	ϵ_{300}[b]	ϵ_6[c]	$\epsilon_6/\epsilon_{300}$	Assignment
K_2PdCl_4[d]	17000	z	5	1	0.20	triplets
	23200	z	80	36	0.45	^1E_g
	21700	x,y	245	118	0.482	$^1A_{2g}$
	23200	x,y	80	30	0.375	^1E_g
$Pd(en)_2PdCl_4$	16075	z	10.3	5.2	0.505	triplets
	20900	z	154	61.6	0.400	$^1B_{1g}$, ^1E_g
	20600	x,y	202	107	0.530	$^1A_{2g}$, ^1E_g
$Pd(NH_3)_4PdCl_4$	19600	z	114	57.9	0.508	$^1B_{1g}$, ^1E_g
	20400	x,y	174	110	0.632	$^1A_{2g}$, ^1E_g
$Pt(en)_2PdCl_4$	18000	z	110	44.1	0.401	$^1B_{1g}$, ^1E_g

	20000	x,y	154	76.9	0.500	$^1A_{2g}$, ^1E_g
	26000	z	225	196	0.871	allowed
$Pt(CH_3NH_2)_4PdCl_4$	14250	z	-	-	0.605[e]	triplet
	16500	z	-	-	0.404[e]	$^1B_{1g}$
	23250	z	280	216	0.771	allowed
	20500	x,y	255	138	0.541	$^1A_{2g}$, ^1E_g
$Pt(NH_3)_4PdCl_4$	20200	x,y	233	122	0.524	$^1A_{2g}$, ^1E_g
	23000	z	230	200	0.870	allowed

[a]Location of peak maxima, in cm^{-1}.

[b]Extinction coefficient at 300K, $cm^{-1}M^{-1}$.

[c]Extinction coefficient at 6K, $cm^{-1}M^{-1}$.

[d]Reference 36.

[e]Calculated from oscillator strengths obtained graphically from Gaussian decomposition of the bands.

dependence ratio $\varepsilon_6/\varepsilon_{300}$ of 0.482 to 0.541. The z-polarized $^1B_{1g}$ peaks, on the other hand, always had a lower ratio, from 0.400 to 0.45, with ratios for the $^1B_{1g}$ peaks averaging about 80 percent of the ratios for $^1A_{2g}$. Even $Pd(NH_3)_4PdCl_4$ showed the 80 percent average value, despite the fact that $\varepsilon_6/\varepsilon_{300}$ were high for both transitions.

The consistency of the $\varepsilon_6/\varepsilon_{300}$ ratios throughout the series indicates that the peak occurring at 23,200 cm^{-1} in K_2PdCl_4 does indeed have as its origin the peak at 16,100 cm^{-1} in $Pt(NH_3)_4PdCl_4$. Hence, the peak at 23,200 cm^{-1} for K_2PdCl_4 may be assigned to both $^1B_{1g}$ and ^1E_g.

Furthermore, the ratios agree qualitatively with the ratios calculated from the theoretical expression for the temperature dependence of vibronic transitions (13):

$$f(300K) = f(0K)\coth(h\nu_i/2kT) \qquad (1)$$

where ν_i is the frequency of the exciting vibration, and f(300K), f(0K) are the oscillator strengths at 300K and 0K, respectively.

As shown in Appendix A, the z-polarization of $^1B_{1g}$ arises from the b_{2u} vibration, which is primarily bending. The ^1E_g x,y- polarization arises from both b_{2u} and a_{2u} bending vibrations. The $^1A_{2g}$ and $^1B_{1g}$ x,y-polarization, and the ^1E_g z-polarization are vibronically allowed by the e_u stretching and bending vibrations. The vibration frequencies for a_{2u}, e_u stretch, and e_u bend in the ground state are 170 cm^{-1}, 325 cm^{-1}, and 191 cm^{-1} respectively (36). Since the b_{2u} vibration is neither IR nor Raman active, no value for b_{2u} is known,

but since b_{2u} is a bending vibration, it is expected to have a frequency similar to the other bending vibration, and lower than the stretching vibrations.

From the vibration frequency data, ratios of f(0K)/f(300K) were calculated for all the singlet transitions. ^1E_g (z) should have a dependence similar to that for $^1A_{2g}$, since both are excited by the e_u stretching and bending vibrations. $^1B_{1g}$, on the other hand, should have a smaller temperature dependence ratio than $^1A_{2g}$, since $^1B_{1g}$ (z) gains its intensity by way of the lower-frequency, pure bending b_{2u} vibration. These calculations therefore support the assignment of the 23,200 cm^{-1} - 16,100 cm^{-1} z-polarized peak in the series to $^1B_{1g}$, rather than ^1E_g.

The distribution of intensities between the x,y- and z-polarizations of the peaks assigned to $^1B_{1g}$ is in qualitative agreement with molecular orbital calculations of the oscillator strengths of the transitions in the $PdCl_4^{2-}$ ion by Erny and Moncuit (43). The oscillator strengths at 0K calculated by these authors for the $^1B_{1g}$ state were 7.0×10^{-6} for x,y- and 1.4×10^{-4} for z-polarizations. Thus, the z-polarized peak would be 20 times as intense as the x,y-polarized peak which, with the sensitivity of our spectrophotometer, could appear as an essentially cleanly z-polarized transition. Erny and Moncuit also predict that ^1E_g (z) will be fairly weak, $f(0K) = 1.3 \times 10^{-4}$, or only about 15 percent as much intensity as the combined ^1E_g and $^1A_{2g}$ transitions in x,y. Hence, the ^1E_g (z) absorptions may be hidden in the

high-energy tail of the $^1B_{1g}$ transition in z for K_2PdCl_4, $Pd(en)_2PdCl_4$, $Pd(NH_3)_4PdCl_4$, and $Pt(en)_2PdCl_4$; and in the low-energy tail of the fairly intense allowed transitions at about 22,500 cm^{-1} in $Pt(CH_3NH_2)_4$-$PdCl_4$ and $Pt(NH_3)_4PdCl_4$.

Unfortunately, the Magnus-type salts seem to give only qualitative agreement with Erny and Moncuit's calculations. Estimates of the ratio of oscillator strengths of the z-polarized peak in each salt were determined graphically. Values of 0.661 for $Pd(en)_2PdCl_4$, 0.633 for $Pd(NH_3)_4PdCl_4$, 0.504 for $Pt(en)_2PdCl_4$, and 0.369 for $Pt(Ch_3NH_2)_4$-$PdCl_4$ (peak at 16,100 cm^{-1} only) do not compare very well with 0.314 obtained from Erny and Moncuit's values of $5.7 \times 10^{-4} + 2.9 \times 10^{-4}$ for $^1A_{2g}$ and ^1E_g (x,y) and $1.3 \times 10^{-4} + 1.4 \times 10^{-4}$ for ^1E_g (z) and $^1B_{1g}$ (z).

The disagreements may be due to the intrusion of the absorption tail of the high-energy transitions into the region of the z-polarized bands. Especially in $Pd(en)_2PdCl_4$ and $Pd(NH_3)_4PdCl_4$, the tail adds significantly to the estimated oscillator strengths of the z-polarized features at about 20,000 cm^{-1}, and in doing so, will tend to inflate the ratio to a higher value than would otherwise be obtained.

Finally, the shift associated with the $^1B_{1g}$ (z) peak is 7100 cm^{-1} across the series. This is much larger than the shifts observed for ^1E_g and $^1A_{2g}$, just as we expected from the orientation of the orbitals involved in the three d-d transitions. Therefore, we not only have substantial evidence that the d_z2 and $d_{xz,yz}$ electrons have about the

same transition energies in K_2PtCl_4, but also that the major influence on these transition energies is in the form of electronic repulsions from the filled orbitals on the ions, which raise the energy of the $d_{xz,yz}$ orbitals, and especially the d_z2 orbitals, closer to the energy of the $d_{x^2-y^2}$* antibonding orbital.

The behavior of the d-d bands for the $PdBr_4^{2-}$ series is quite similar to that observed for the $PdCl_4^{2-}$ series. Table 5 listed the shifts observed for each of the d-d transitions within the series. Figures 16-20 show representative spectra for each salt in the series, and Figure 21 displays in graph form the shifts in the transitions, as determined by our assignments.

The x,y-polarized bands possessing vibrational structure in the 20,200 cm^{-1} - 19,200 cm^{-1} region have been assigned to the $^1A_{2g}$ state on the basis of their polarization in x,y. These bands appear at lower energies than the $^1A_{2g}$ bands in the $PdCl_4^{2-}$ salts because of the smaller crystal-field splittings associated with the bromide ligand (44). The $^1A_{2g}$ peaks in the $PdBr_4^{2-}$ salts also tend to shift less than their counterparts in the $PdCl_4^{2-}$ series as the metal-metal spacing decreases. This is because the bromide ligands adjust d(M-M) to larger distances in the $PdBr_4^{2-}$ salts compared to the $PdCl_4^{2-}$ salts: d(M-M) is approximately 0.10 A larger in the $PdBr_4^{2-}$ salts than in the $PdCl_4^{2-}$ salts. The d-orbital splittings are smaller in the $PdBr_4^{2-}$ spectra because the bromide ligands have a poorer capacity for σ and π bonding with the metal. The small orbital energy splittings, combined with the

Figure 16. Polarized absorption spectra for $Pd(en)_2PdBr_4$

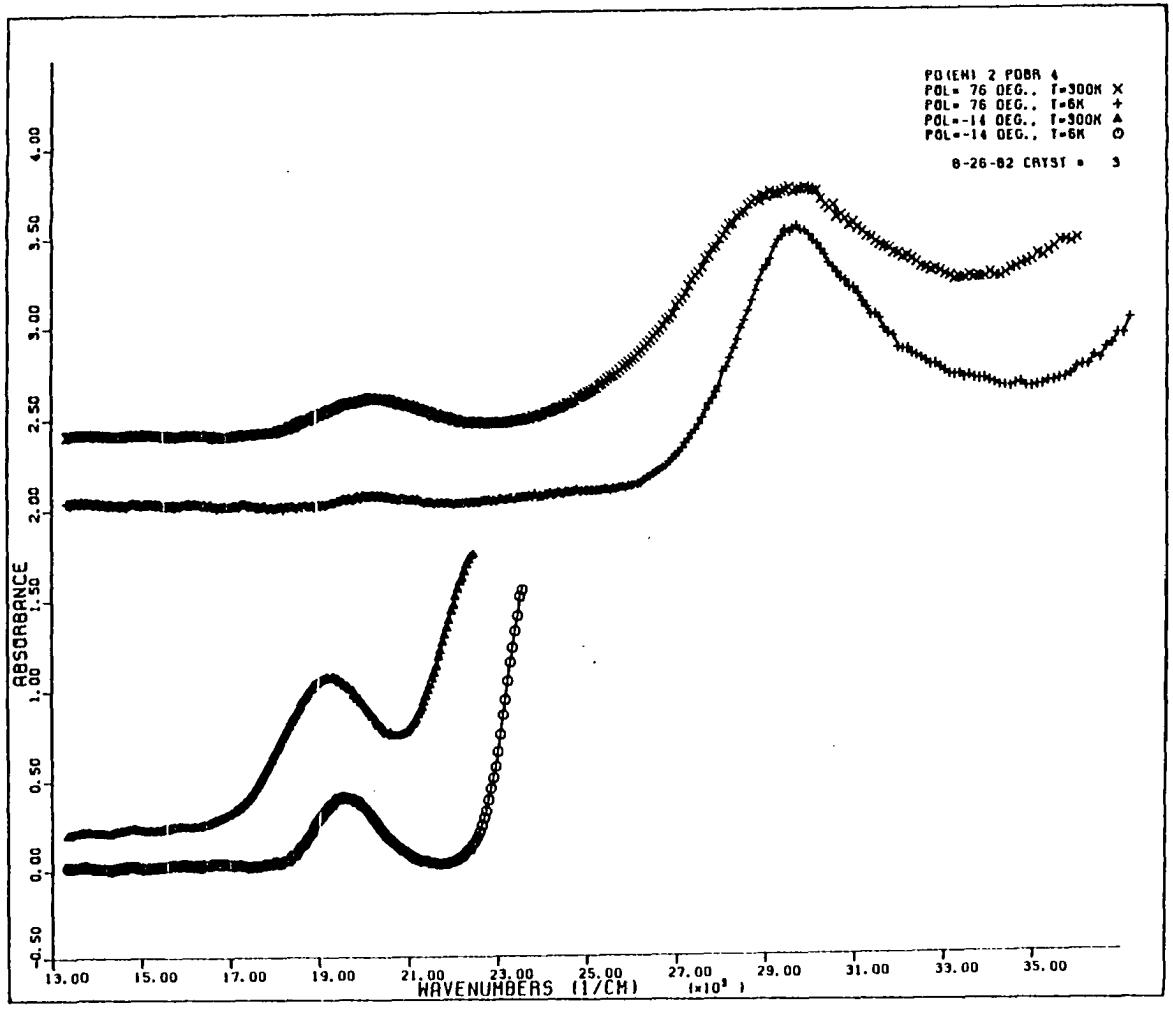
PD(EN) 2 PDBR 4
POL= 76 DEG., T=300K X
POL= 76 DEG., T=6K +
POL=-14 DEG., T=300K ▲
POL=-14 DEG., T=6K O
8-26-82 CRYST # 3
ABSORBANCE
4.00
3.50
3.00
2.50
2.00
1.50
1.00
0.50
0.00
-0.50
13.00
15.00
17.00
19.00
21.00
23.00
25.00
27.00
29.00
31.00
33.00
35.00
WAVENUMBERS (1/CM) (x10³)

Figure 17. Polarized absorption spectra for $Pd(NH_3)_4PdBr_4$

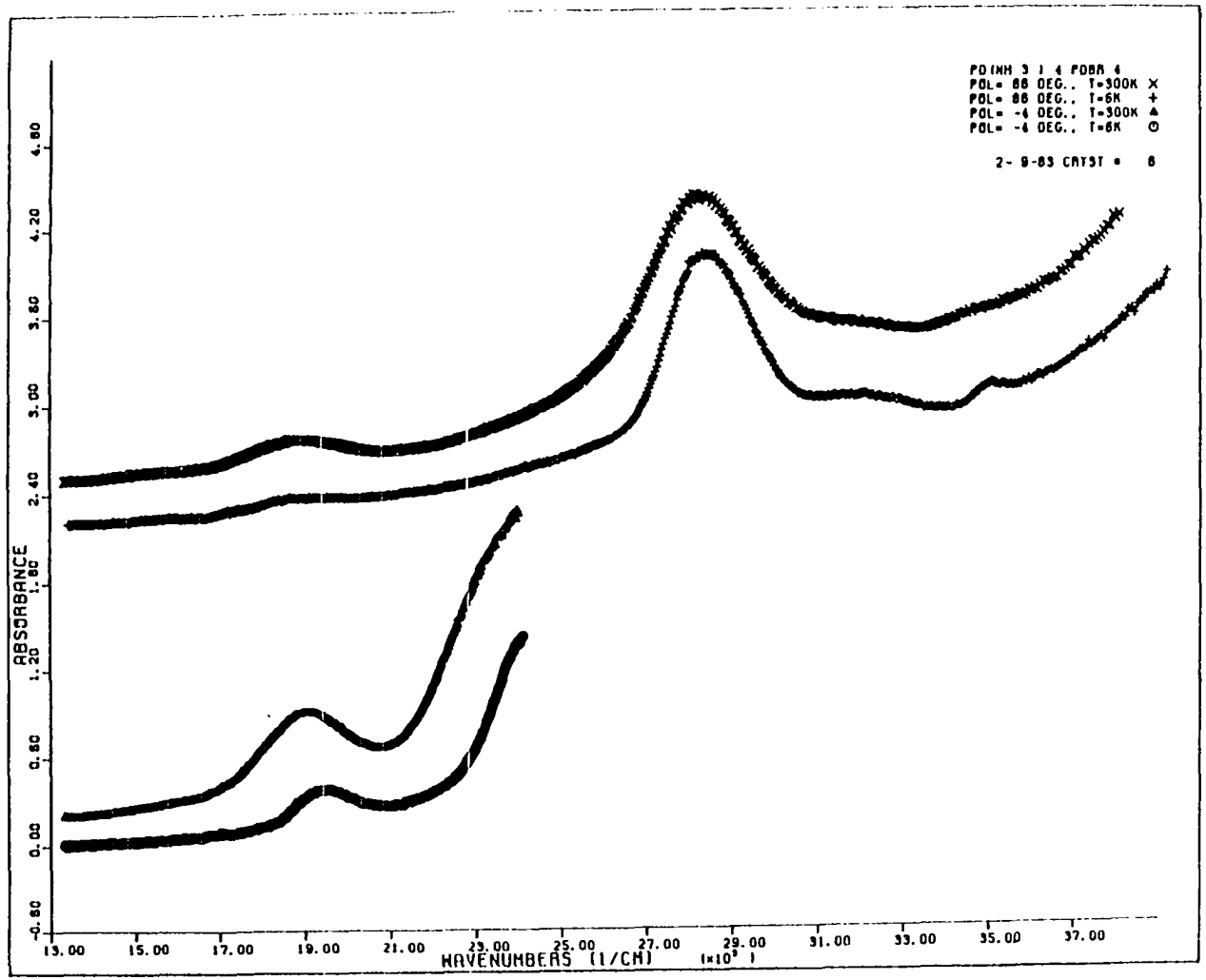
POINH 3 1 4 POBR 4
POL= 86 DEG., T=300K
POL= 86 DEG., T=6K
POL= -4 DEG., T=300K
POL= -4 DEG., T=6K
2- 8-83 CRYST # 8
ABSORBANCE
4.80
4.20
3.60
3.00
2.40
1.80
1.20
0.60
0.00
-0.60
13.00
15.00
17.00
19.00
21.00
23.00
25.00
27.00
29.00
31.00
33.00
35.00
37.00
WAVENUMBERS (1/CM)
(*10³)

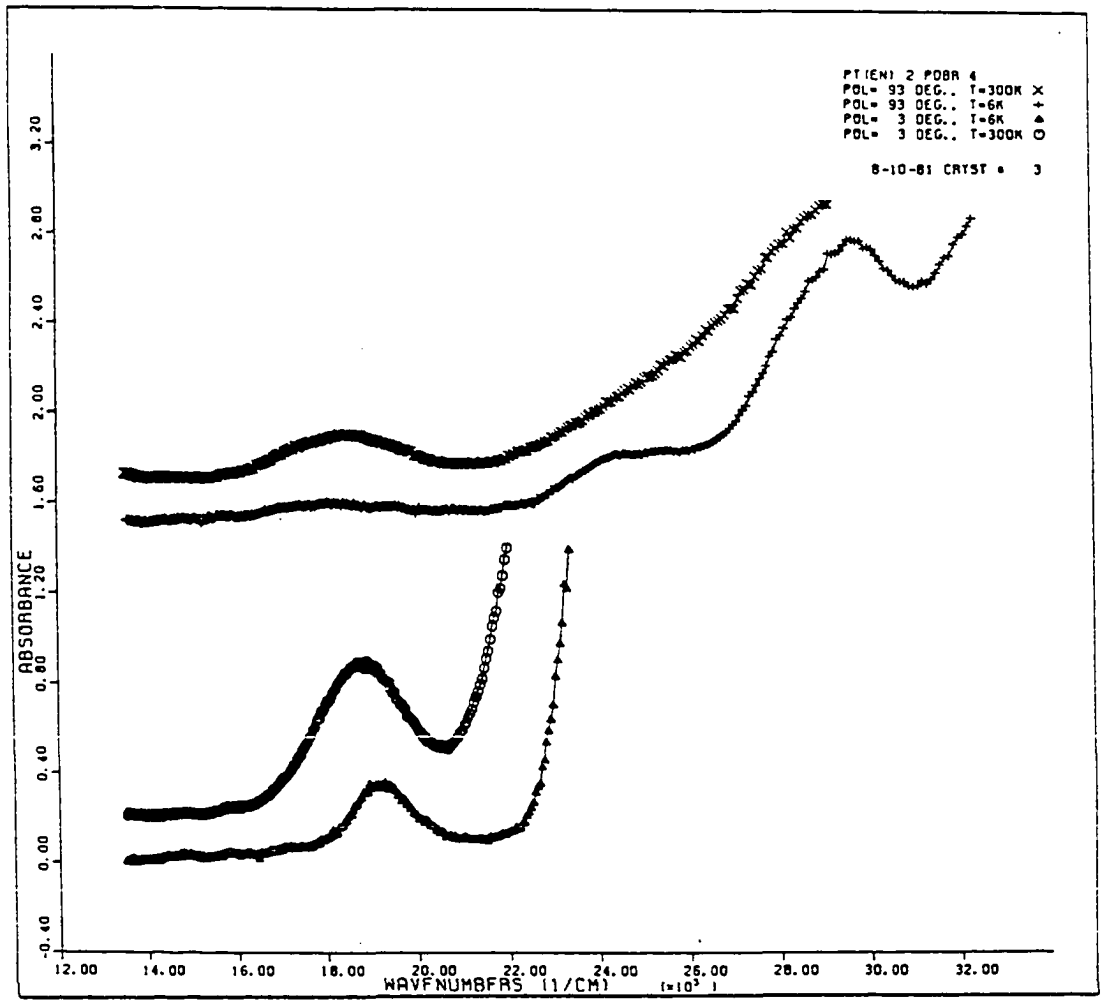

Figure 18. Polarized absorption spectra for $Pt(en)_2PdBr_4$

Figure 19. Polarized absorption spectra for $Pt(CH_3NH_2)_4PdBr_4$

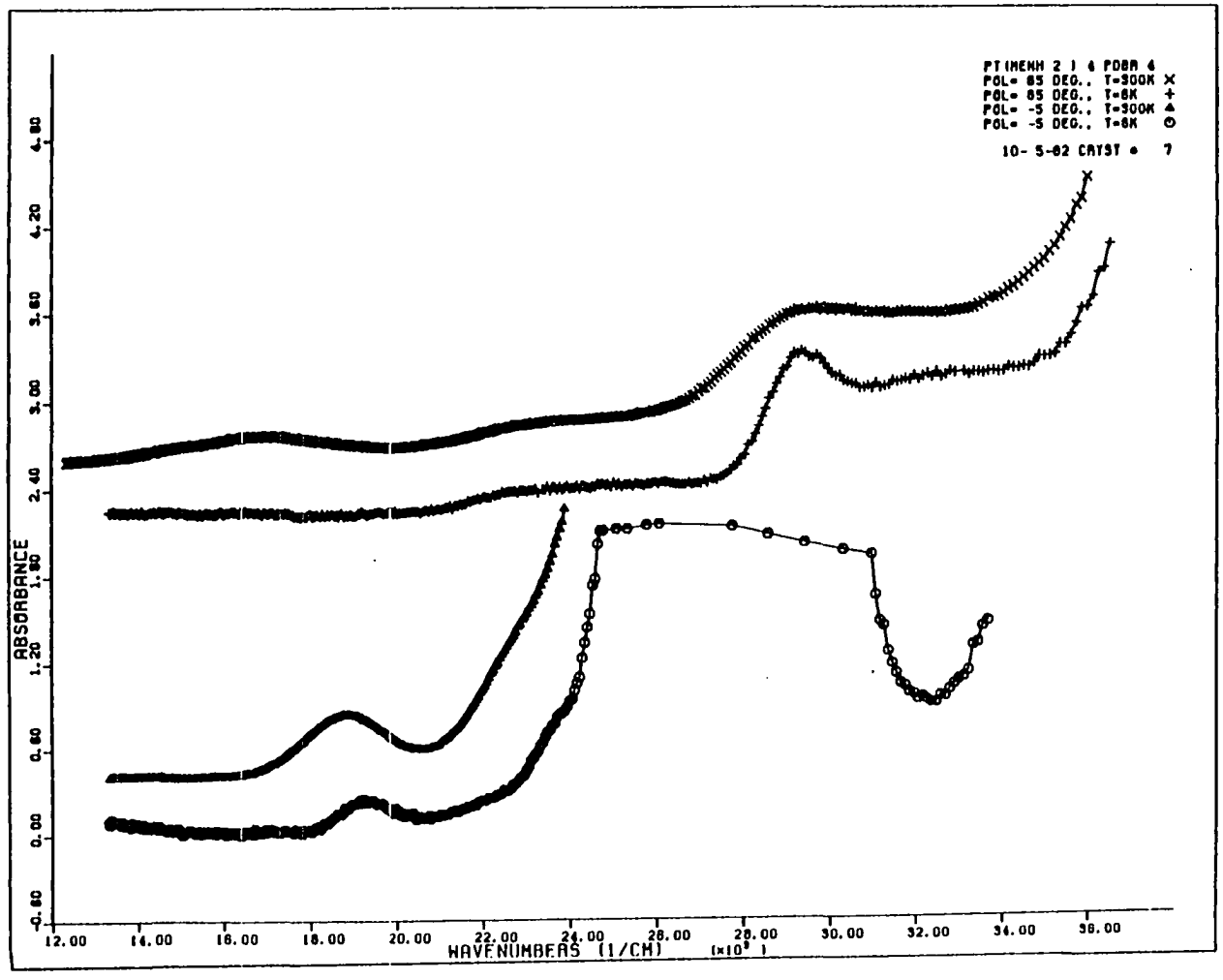
PT(MEHH 2) & PDBR 4
POL= 85 DEG., T=300K X
POL= 85 DEG., T=8K +
POL= -5 DEG., T=300K ▲
POL= -5 DEG., T=8K ⊙
10- 5-82 CRYST # 7
ABSORBANCE
4.80
4.20
3.60
3.00
2.40
1.80
1.20
0.60
0.00
-0.60
12.00
14.00
16.00
18.00
20.00
22.00
24.00
26.00
28.00
30.00
32.00
34.00
36.00
WAVENUMBERS (1/CM)
(×10³)

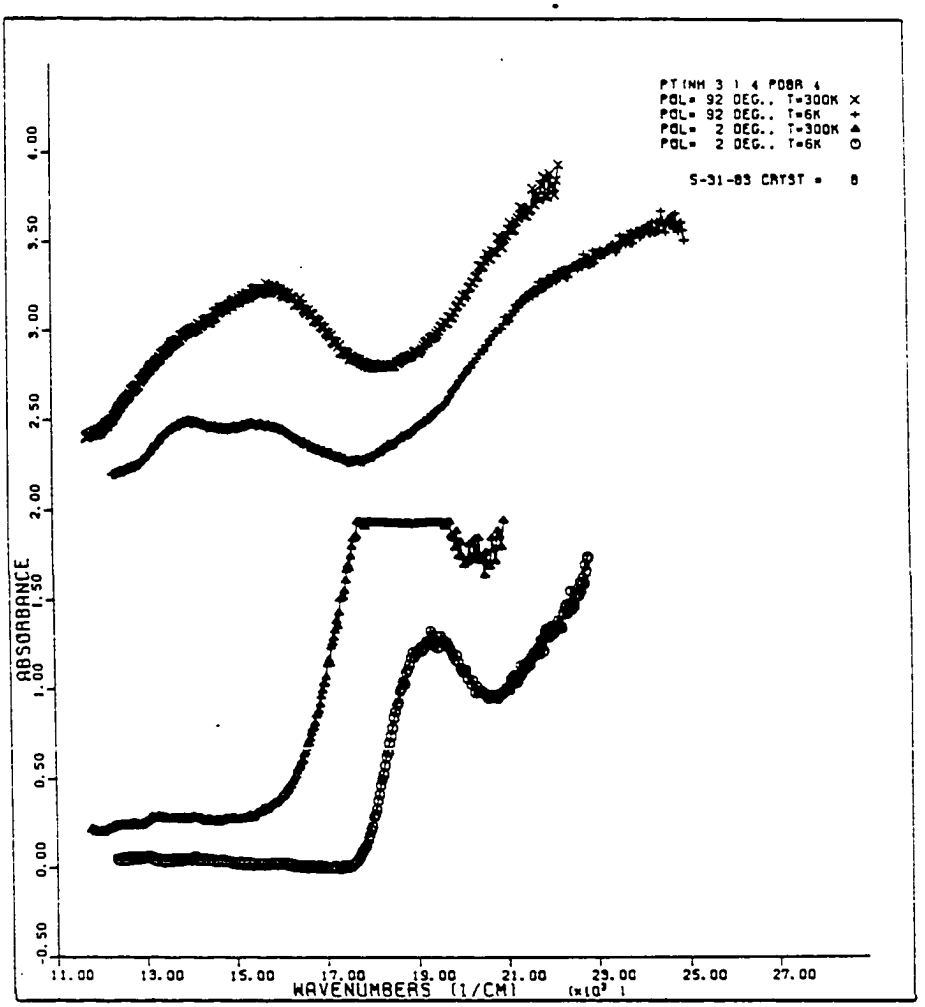

Figure 20. Polarized absorption spectra for $Pt(NH_3)_4PdBr_4$

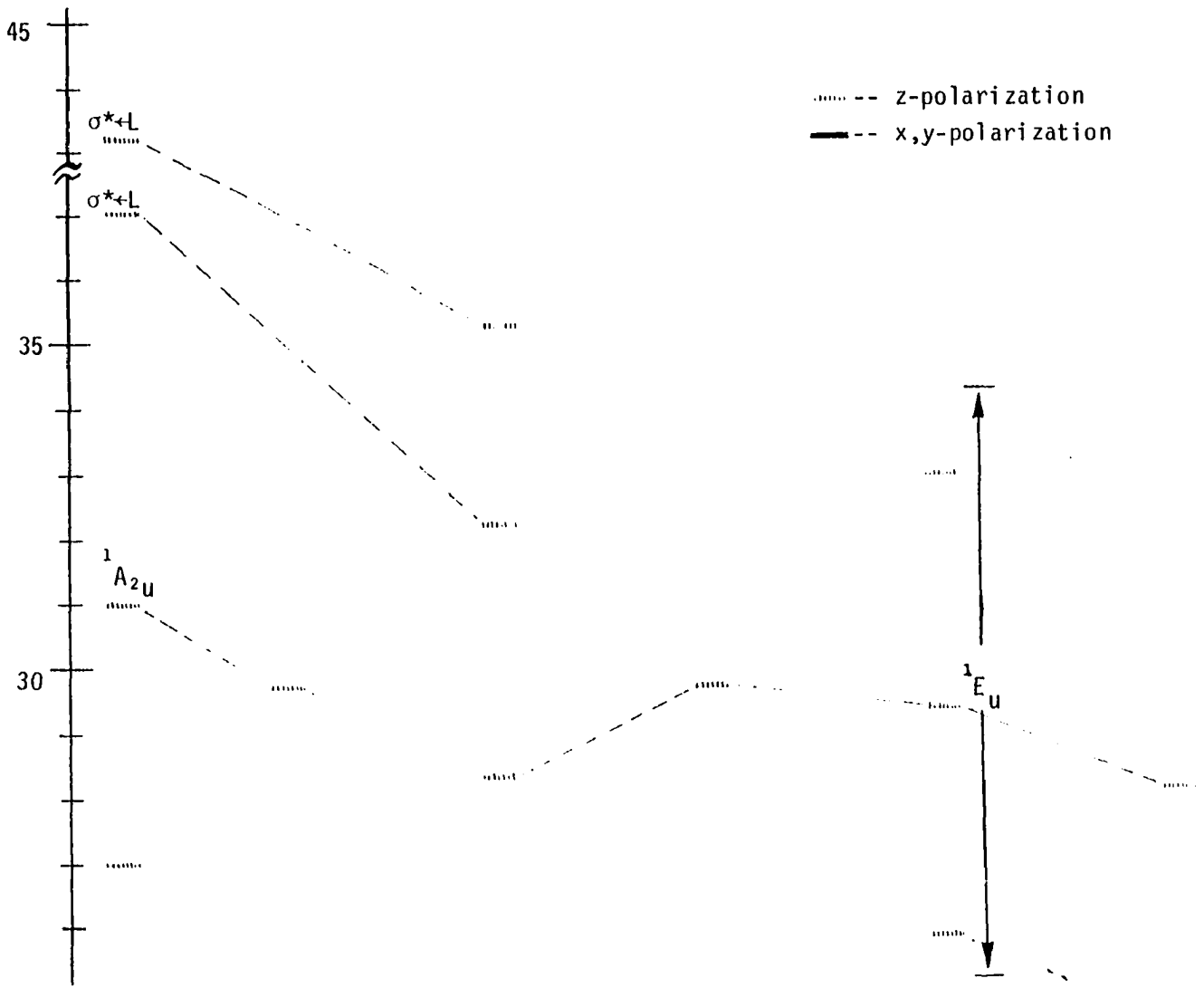
45
35
30
σ*←L
σ*←L
$^1A_{2u}$
^1E_u
-- z-polarization
-- x,y-polarization

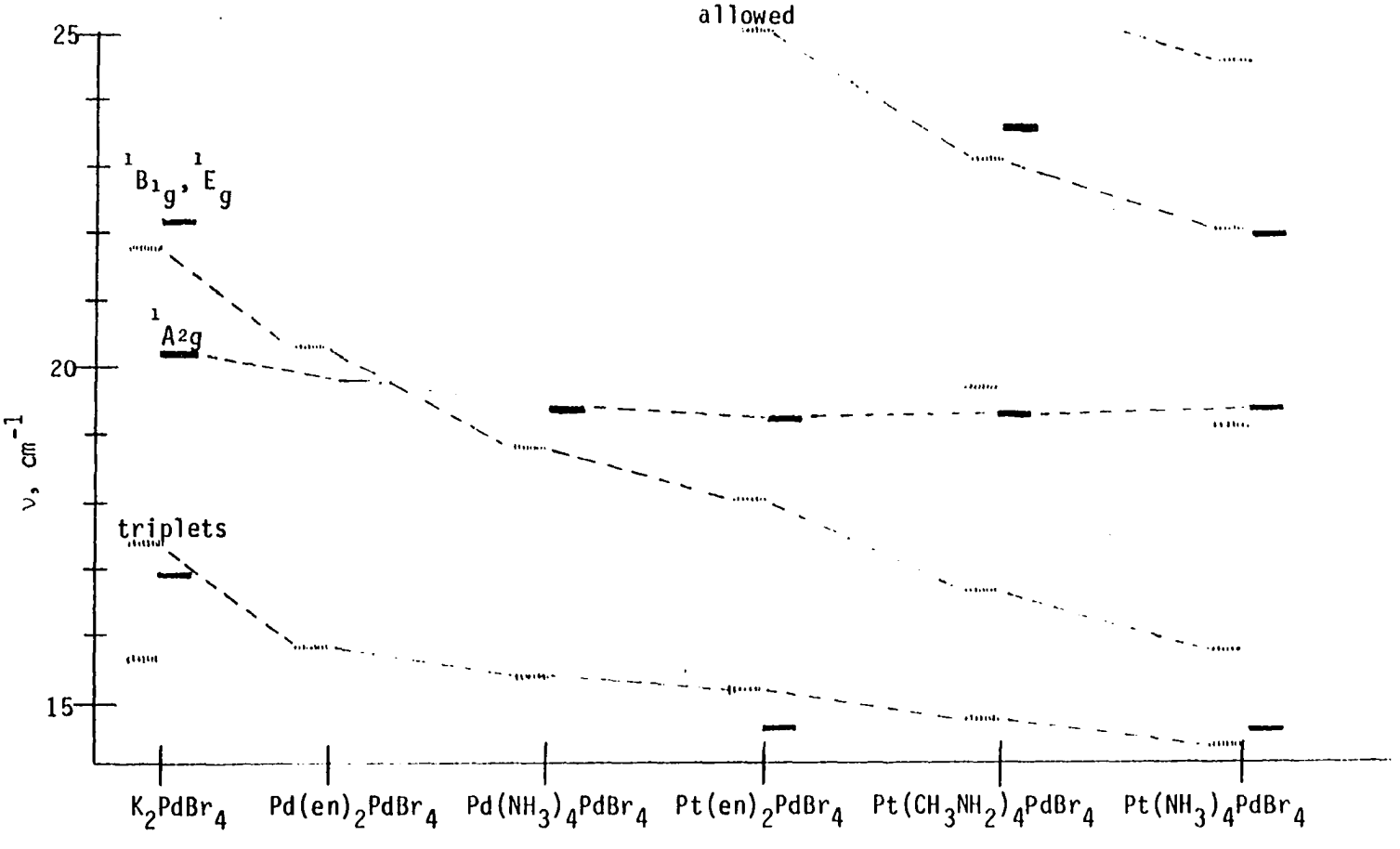

Figure 21. Shifts of absorptions across the $PdBr_4^{2-}$ series

larger d(M-M) where bromide is present tends to produce similar low transition energies and small shifts in all other d-d bands as well.

Triplet states are observed for all compounds in the series, from 17,400 cm^{-1} to 14,100 cm^{-1}. The peaks are weak and mainly z-polarized. By analogy with K_2PdBr_4 (36), they were assigned to both ^3E_g and $^3A_{2g}$ states.

Shifts for the triplet states of 3300 cm^{-1} (z) and 2500 cm^{-1} (x,y) were consistent with shifts of 2730 cm^{-1} (z) and 2750 cm^{-1} (x,y) necessary to place ^1E_g with the $^1A_{2g}$ band at 19,350 cm^{-1} (x,y) in $Pt(NH_3)_4PdBr_4$. Other support for the assignment of ^1E_g to the $^1A_{2g}$ region appears as a weak peak in z at 19,600 cm^{-1} for $Pt(CH_3NH_2)_4PdBr_4$, and as a weak shoulder, also z-polarized, at the same energy in $Pt(NH_3)_4PdBr_4$. Furthermore, the z-polarized bands at 18,000 to 18,700 cm^{-1} for both $Pd(NH_3)_4PdBr_4$ and $Pt(en)_2PdBr_4$ are definitely asymmetric, with an elongated tail appearing on the high-energy side of the peak at exactly the same energy for which the $^1A_{2g}$ band appears in x,y. Loss of polarization cannot be responsible for these features: the low-energy side of the peak in z extends to the red of the band in x,y, yet the x,y peak rises cleanly from a flat baseline in that region. The arrow above the z-polarized spectrum in Figure 22 indicates the high-energy tail in which ^1E_g appears. We conclude, then, that the weak z-polarized component contains the ^1E_g z-polarized band shifted down to the $^1A_{2g}$ absorption region.

Figure 22. Polarized absorption spectra of $Pd(NH_3)_4PdBr_4$ at 6K, showing the location of the ^1E_g band

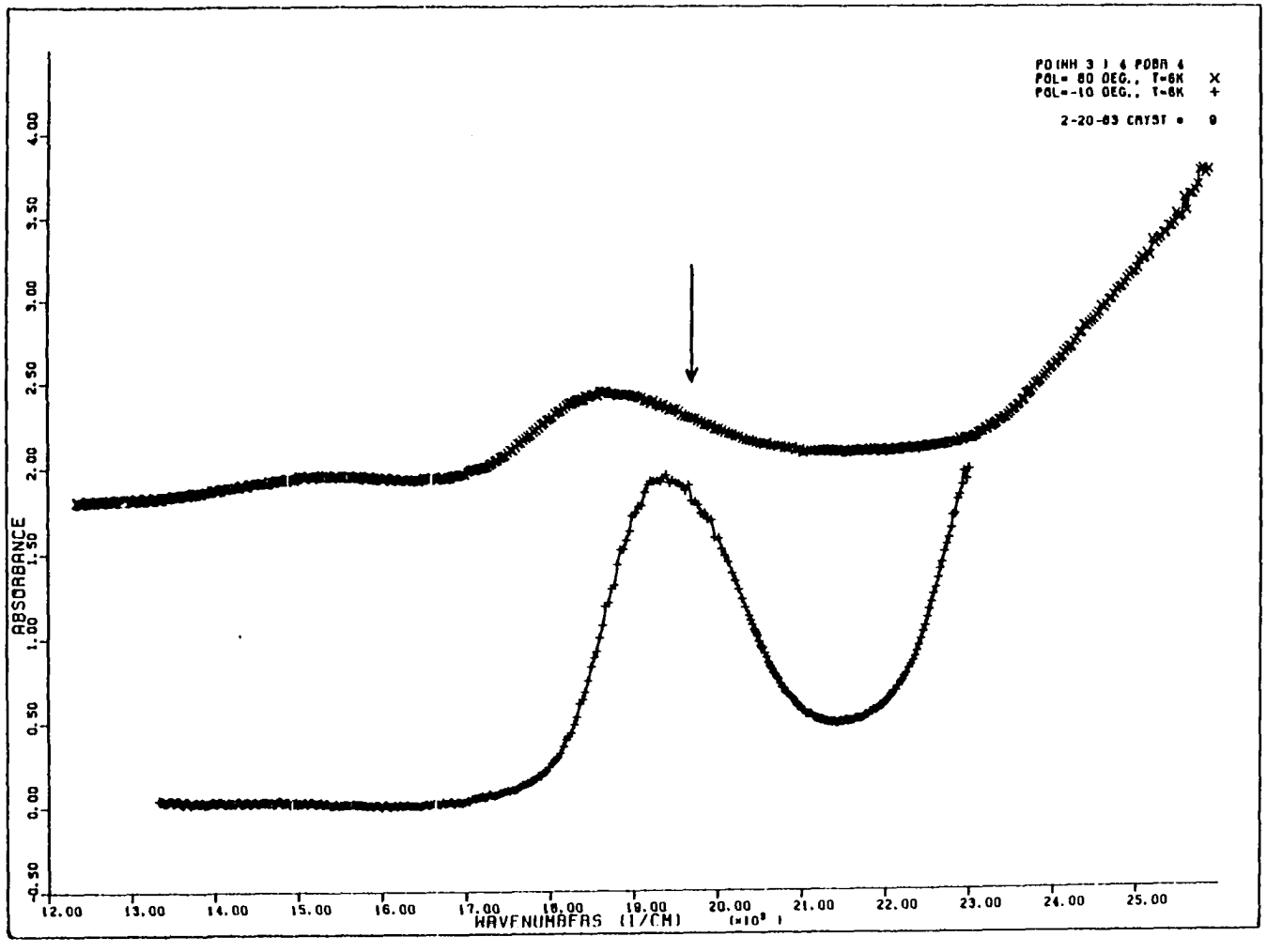
POINH 3) 4 POBA 4
POL= 80 DEG., T=6K X
POL=-10 DEG., T=6K +
2-20-83 CRYST • 8
ABSORBANCE
4.00
3.50
3.00
2.50
2.00
1.50
1.00
0.50
0.00
-0.50
12.00
13.00
14.00
15.00
16.00
17.00
18.00
19.00
20.00
21.00
22.00
23.00
24.00
25.00
WAVENUMBERS (1/CM) (*10³)

The primarily z-polarized band assigned to $^1B_{1g}$ is associated with the ^1E_g band at about 22,000 cm^{-1} in K_2PdBr_4 by analogy with the ^1E_g bands in the $PdCl_4^{2-}$ series associated with the ^1E_g peak at 23,200 cm^{-1} in K_2PdCl_4. The magnitude of the peak intensities, temperature behavior, and polarization are all remarkably similar to the data obtained for the $PdCl_4^{2-}$ series. Table 10 shows the peak intensities and temperature behavior ratios, $\varepsilon_6/\varepsilon_{300}$ for the $PdBr_4^{2-}$ salts. As with the $PdCl_4^{2-}$ series, every z-polarized peak is much lower in intensity than the $^1A_{2g}/^1E_g$ peak, and the intensity of $^1A_{2g}/^1E_g$ changes less with temperature than does the z-polarized $^1B_{1g}$ (and ^1E_g) band.

Indeed, comparison of $\varepsilon_6/\varepsilon_{300}$ for the $PdBr_4^{2-}$ salts with $\varepsilon_6/\varepsilon_{300}$ for the $PdCl_4^{2-}$ salts shows that the temperature ratios tend to be smallest for the $PdBr_4^{2-}$ salts. This behavior is quite consistent with the temperature behavior expected from theory: the exciting vibration frequencies for $PdBr_4^{2-}$ are lower than those for $PdCl_4^{2-}$, so smaller ratios for $PdBr_4^{2-}$ are calculated from equation 1.

The overall energy shift for the $^1B_{1g}$ band in $PdBr_4^{2-}$ is 6030 cm^{-1}, from K_2PdBr_4 to $Pt(NH_3)_4PdBr_4$, which is consistent with the 7100 cm^{-1} shift observed over the $PdCl_4^{2-}$ series. The shift is expected to be smaller for $PdBr_4^{2-}$ because the bromides prohibit metal-metal spacings as small as those seen with the smaller chloride ligands.

Table 10. Temperature behavior for selected peaks in the $PdBr_4^{2-}$ series

Compound	Peak location[a]	Polarization	ε_{300}[b]	ε_6[c]	$\varepsilon_6/\varepsilon_{300}$	Assignment
K_2PdBr_4[d]	21730	z	80	33	0.413	^1E_g
	30900	z	475	550	1.16	$^1A_{2u}$
	20200	x,y	420	177	0.44	$^1A_{2g}$
	22100	x,y	-	31	-	^1E_g
$Pd(en)_2PdBr_4$	20200	z	82.8	29.0	0.350	$^1B_{1g}$, ^1E_g
	29600	z	560	640	1.14	allowed
	19300	x,y	360	166	0.461	$^1A_{2g}$, ^1E_g
$Pd(NH_3)_4PdBr_4$	18900	z	101	46.3	0.458	$^1B_{1g}$, ^1E_g
	28500	z	713	675	0.947	allowed
	19350	x,y	226	134	0.593	$^1A_{2g}$, ^1E_g
$Pt(en)_2PdBr_4$	18000	z	151	43	0.282	$^1B_{1g}$, ^1E_g
	29600	z	745	725	0.973	allowed

	19200	x,y	334	164	0.491	$^1A_{2g}$, ^1E_g
$Pt(CH_3NH_2)_4PdBr_4$	16500	z	-	-	-	$^1B_{1g}$
	29300	z	704	741	1.05	allowed
	19250	x,y	322	189	0.569	$^1A_{2g}$, ^1E_g
$Pt(NH_3)_4PdBr_4$	28000	z	599	735	1.23	allowed
	19350	x,y	144	80.2	0.557	$^1A_{2g}$, ^1E_g

[a]Location of peak maxima, in cm^{-1}.

[b]Extinction coefficient at 300K, in $cm^{-1}M^{-1}$.

[c]Extinction coefficient at 6K, in $cm^{-1}M^{-1}$.

[d]All values and assignments from Reference 36.

Several vibronic transitions are observed for the $PtCl_4^{2-}$ series. Table 6 presented a summary of the absorptions. Figures 23 through 27 show the spectra for the five salts, and Figure 28 shows the degree of shifting that occurs over the series as d(M-M) changes. In general, the spittings of the d-orbital energies are larger in the $PtCl_4^{2-}$ salts than in the $PdCl_4^{2-}$salts because the greater radial extension of the platinum d-orbitals permits more orbital overlap, which results in stronger σ and π bonds.

The $^1A_{2g}$ band lies in the 26,300 cm^{-1} - 25,200 cm^{-1} region, and is readily identified by its characteristic vibrational structure and small shift over the series, analogous to the $^1A_{2g}$ peaks in the $PdCl_4^{2-}$ salts. Although the $^1A_{2g}$ band is obviously x,y-polarized in K_2PtCl_4, the polarization of $^1A_{2g}$ cannot be used to assign the state in the Magnus-type salts: the encroachment of a high-intensity allowed band into the d-d region in the z-polarized spectra put the absorption in z at the $^1A_{2g}$ band off scale in $Pd(en)_2PtCl_4$, $Pt(CH_3NH_2)_4PtCl_4$, and $Pt(NH_3)_4PtCl_4$. In $Pd(NH_3)_4PtCl_4$ and $Pt(en)_2PtCl_4$, the x,y- and z-polarized bands assigned to ^1E_g have shifted into the region occupied by $^1A_{2g}$, causing a peak to appear at the same region in z. Nevertheless, there is little doubt that the $^1A_{2g}$ bands are correctly assigned.

The assignment of ^1E_g is more difficult. The appearance of an A-term at 30,300 cm^{-1} in the MCD spectrum of aqueous $PtCl_4^{2-}$ establishes the x,y- and z-polarized bands at 29,300 - 29,800 cm^{-1} in K_2PtCl_4 as the ^1E_g band (21). In the Magnus-type salts, however, no isolated

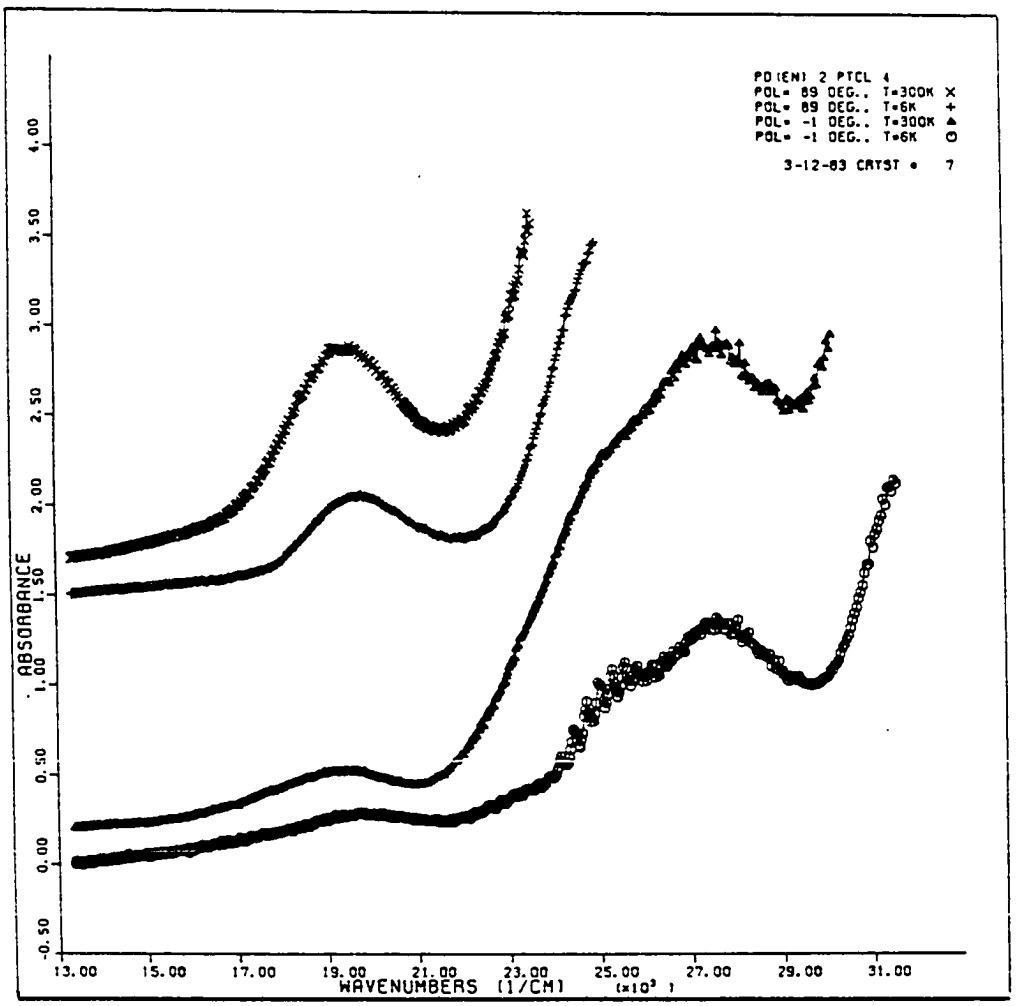

Figure 23. Polarized absorption spectra for $Pd(en)_2PtCl_4$

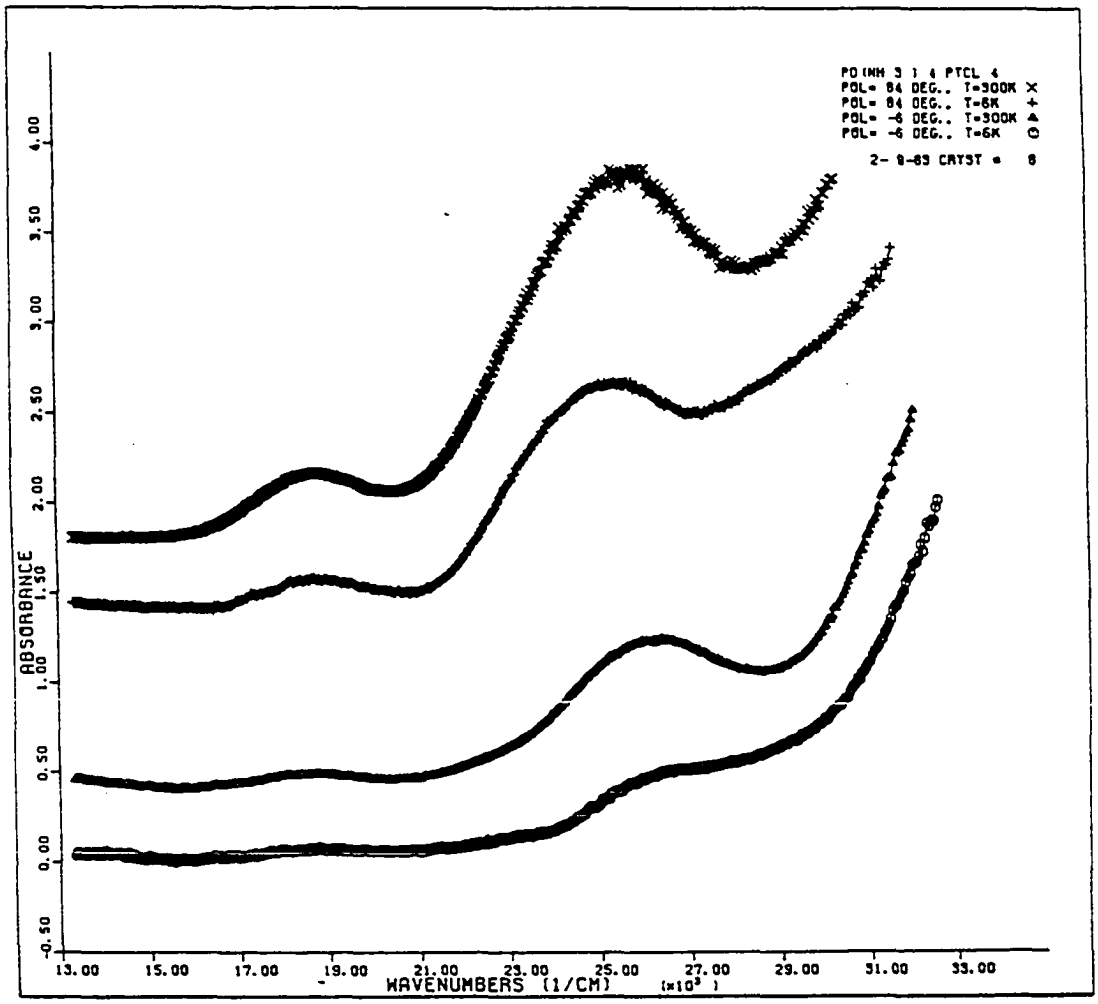

Figure 24. Polarized absorption spectra for $Pd(NH_3)_4PtCl_4$

Figure 25. Polarized absorption spectra for $Pt(en)_2PtCl_4$

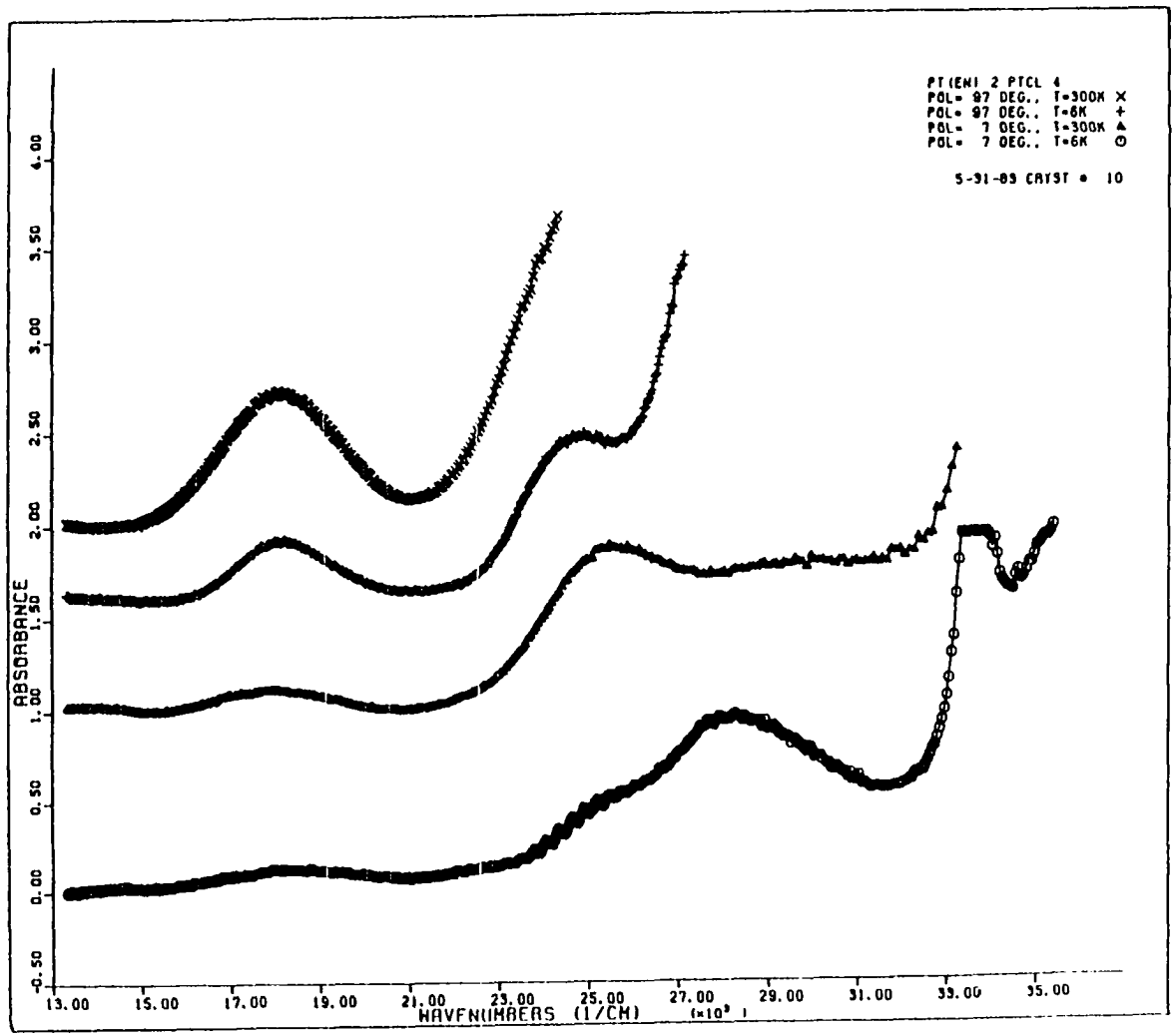
PT(EN) 2 PTCL 4
POL= 97 DEG., T=300K X
POL= 97 DEG., T=6K +
POL= 7 DEG., T=300K ▲
POL= 7 DEG., T=6K ⊙
5-31-89 CRYST # 10
ABSORBANCE
4.00
3.50
3.00
2.50
2.00
1.50
1.00
0.50
0.00
-0.50
13.00
15.00
17.00
19.00
21.00
23.00
25.00
27.00
29.00
31.00
33.00
35.00
WAVENUMBERS (1/CM) (*10³)

Figure 26. Polarized absorption spectra for $Pt(CH_3NH_2)_4PtCl_4$

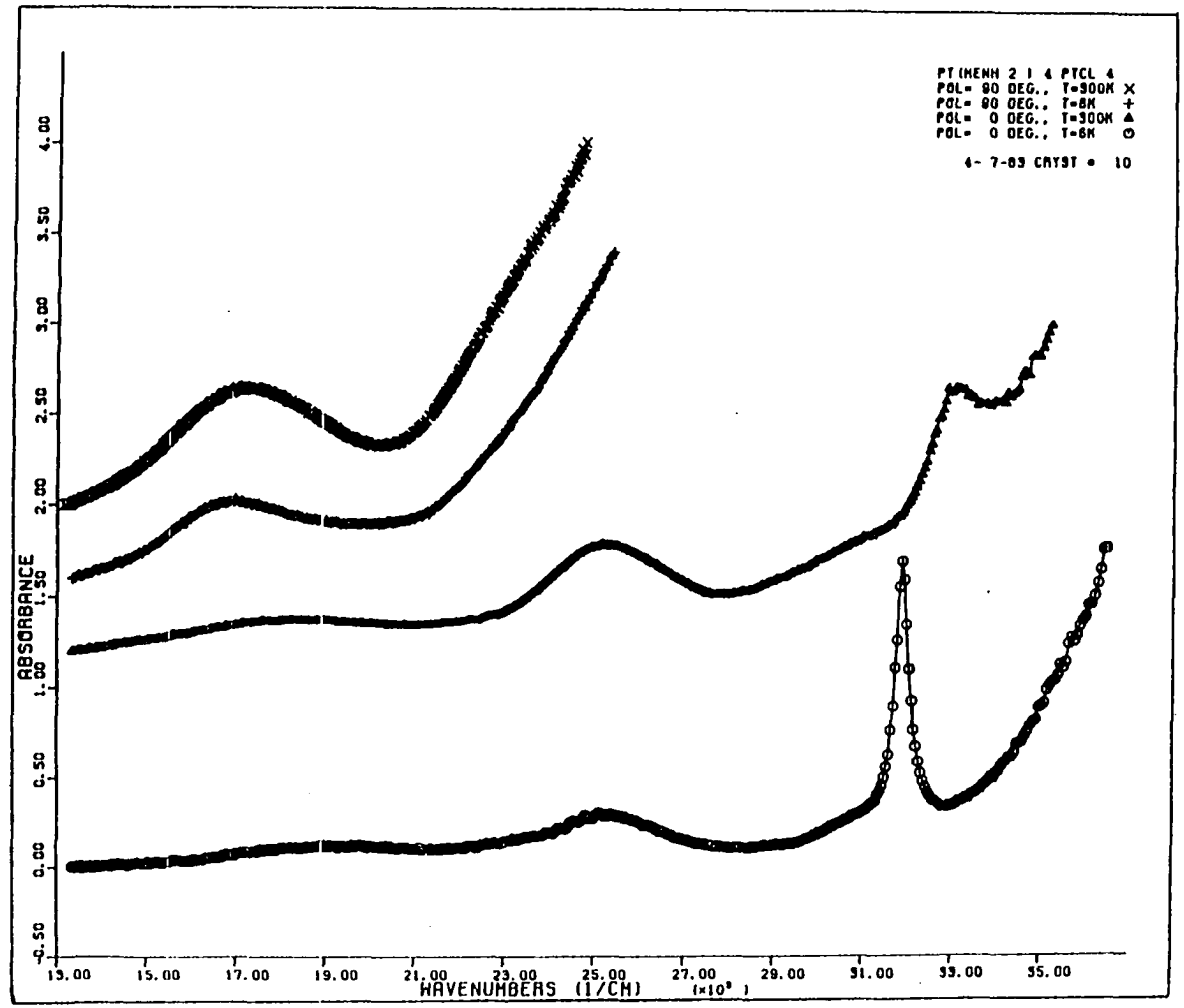
PT(NENH 2) 4 PTCL 4
POL= 90 DEG., T=300K X
POL= 90 DEG., T=8K +
POL= 0 DEG., T=300K ▲
POL= 0 DEG., T=8K ⊙
4- 7-83 CRYST # 10
ABSORBANCE
4.00
3.50
3.00
2.50
2.00
1.50
1.00
0.50
0.00
-0.50
15.00
17.00
19.00
21.00
23.00
25.00
27.00
29.00
31.00
33.00
35.00
WAVENUMBERS (1/CM) (x10³)

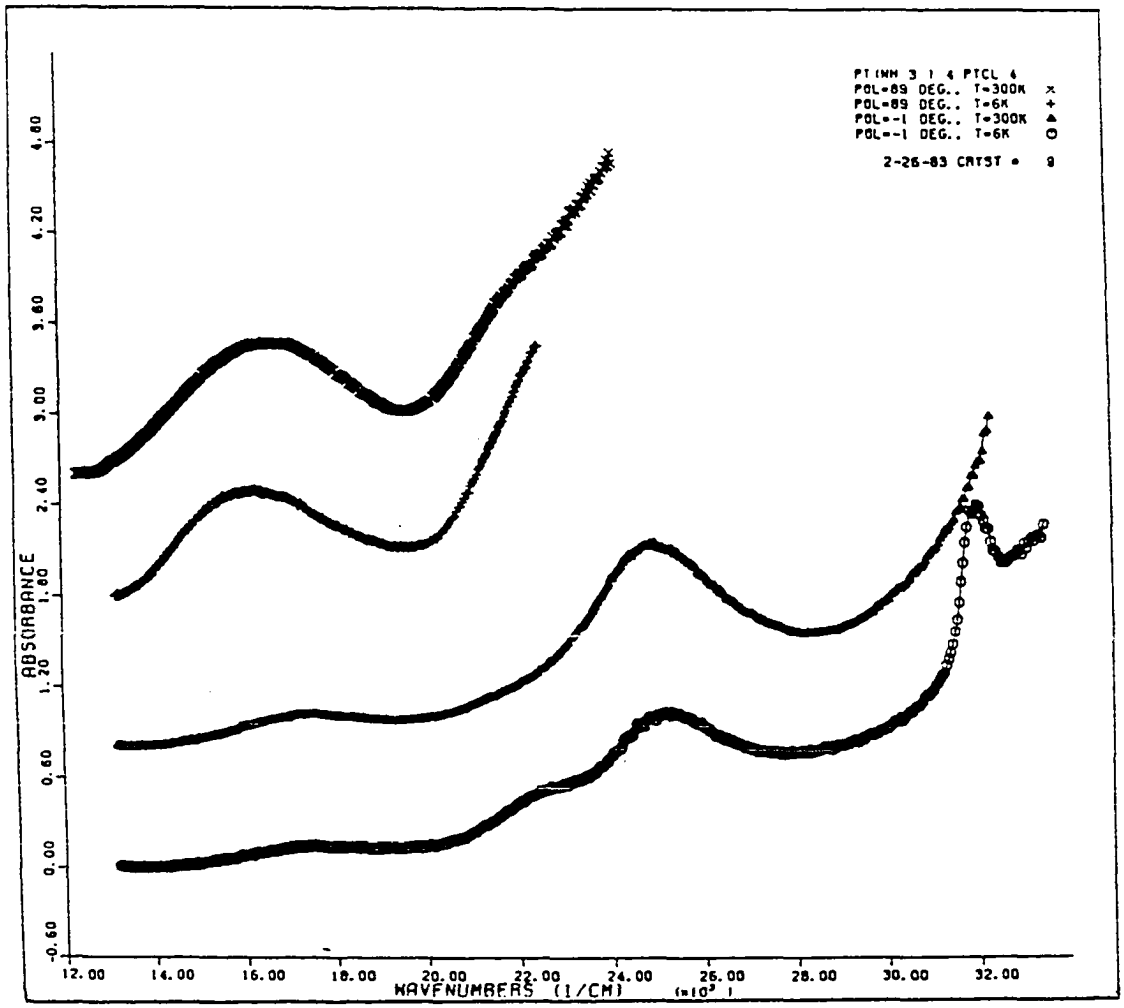

Figure 27. Polarized absorption spectra for $Pt(NH_3)_4PtCl_4$

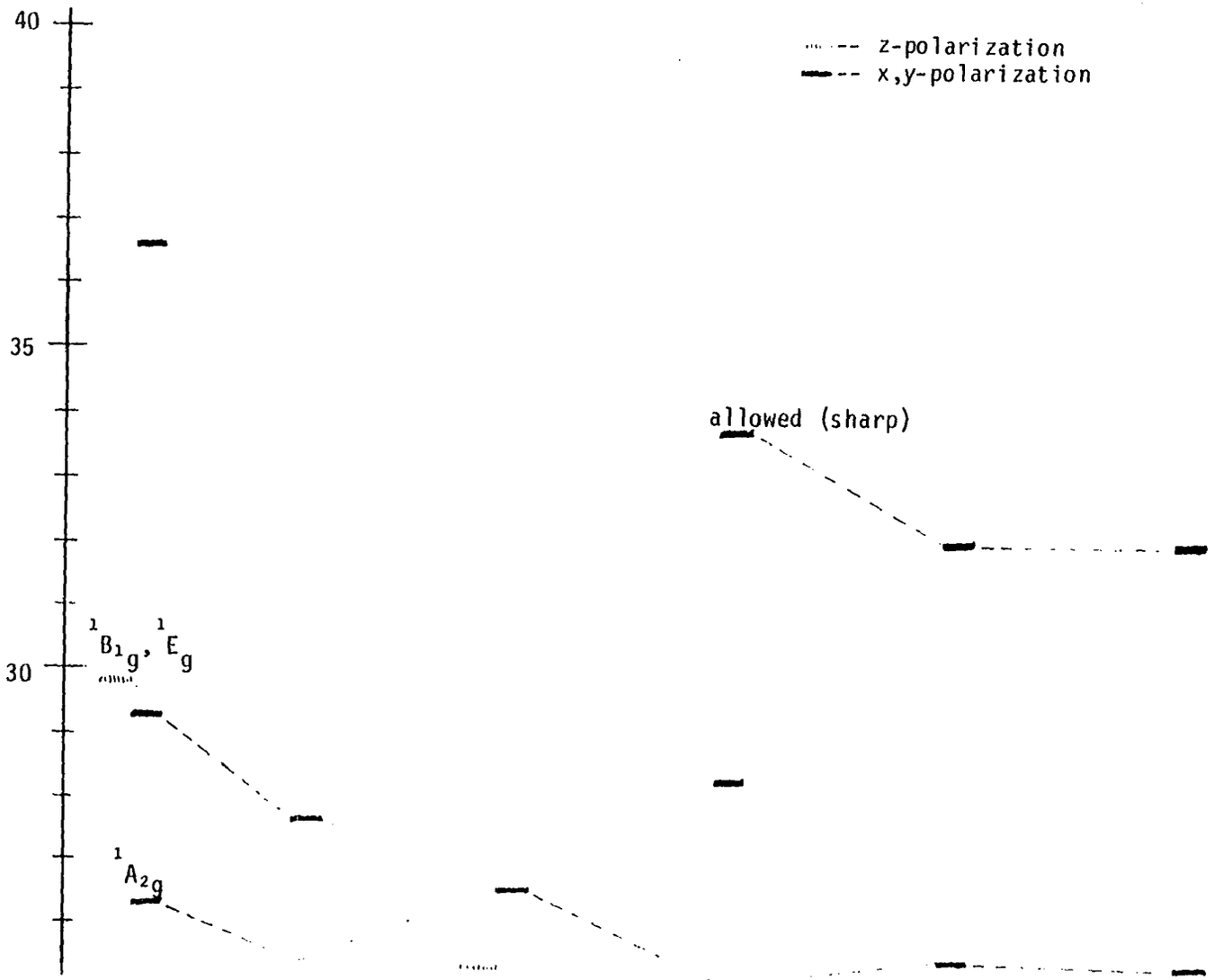
40
35
30
z-polarization
x,y-polarization
allowed (sharp)
$^1B_{1g}$, ^1E_g
$^1A_{2g}$

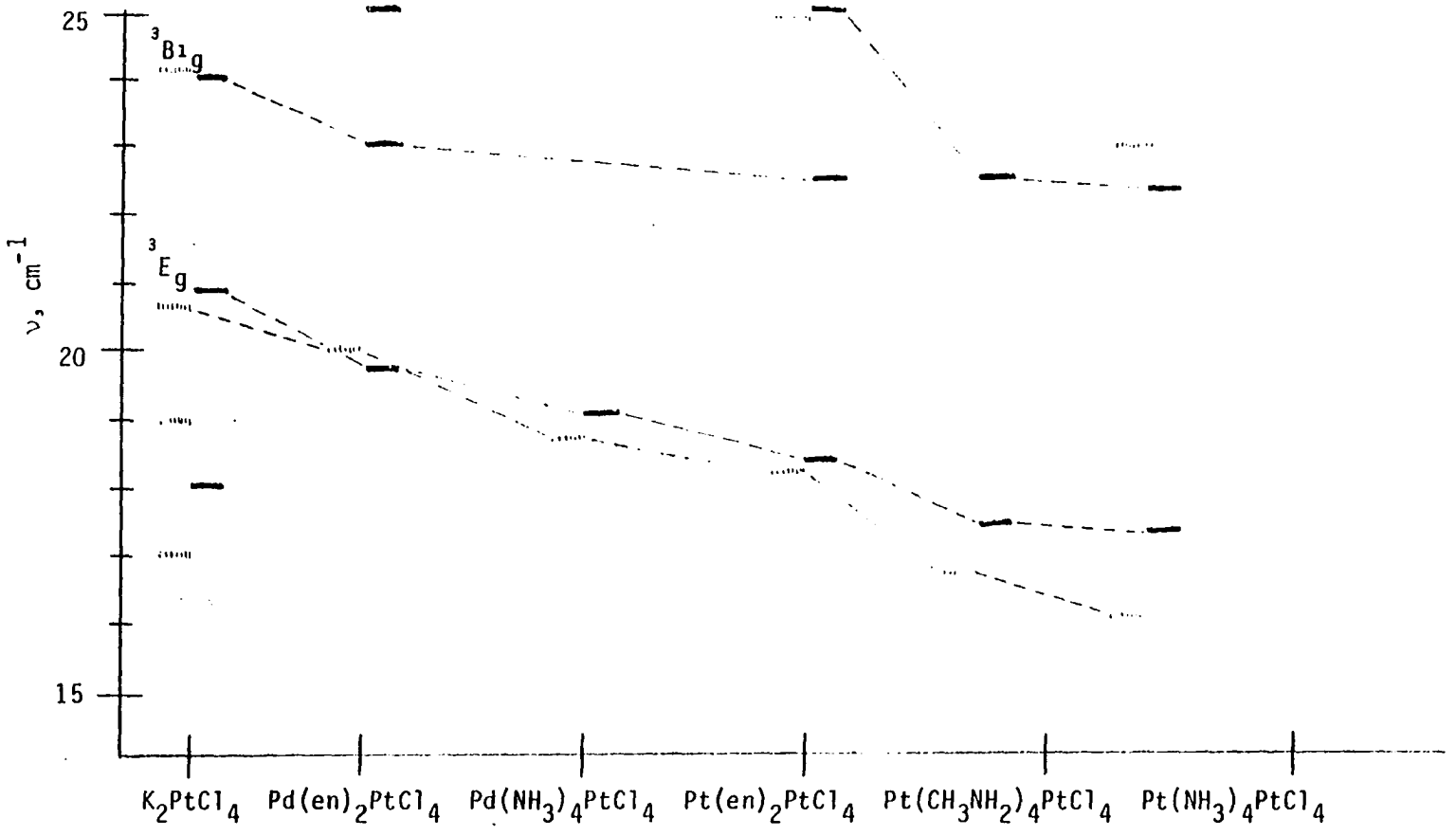

Figure 28. Shifts of absorptions across the $PtCl_4^{2-}$ series

band in both x,y and z is seen that can readily be attributed to ^1E_g. Instead, ^1E_g is assigned by inference from the shift of the low-energh ^3E_g bands, which appear for all of the salts in the $PtCl_4^{2-}$ series.

The low-energy, presumably spin-forbidden bands from 20,900 cm^{-1} to 16,100 cm^{-1} are assigned to ^3E_g by analogy to K_2PtCl_4: the bands at 20,600 cm^{-1} - 20,900 cm^{-1} are the most intense low-energy bands in K_2PtCl_4, with the z-polarized absorption more intense than the x,y-polarized absorption. The low-energy bands in the Magnus-type salts are also fairly intense, with z-polarization much more intense that x,y. The bands in K_2PtCl_4 are themselves assigned to ^3E_g because they lie at higher energy than another weak transition, just as ^1E_g lies above $^1A_{2g}$ (19).

The energy shifts of ^3E_g over the $PtCl_4^{2-}$ series are 3500 cm^{-1} (x,y) and 4500 cm^{-1} (z). If ^1E_g in MGS lies at the same energy as $^1A_{2g}$, ^1E_g must have shifted 4100 cm^{-1} from its energy in K_2PtCl_4. Such a shift is obviously in good agreement with the shifts observed for ^3E_g. We therefore favor assignment of ^1E_g to the band at 25,200 cm^{-1} (x,y) in MGS.

The observed shifts for the other salts are largely consistent with the assignment for ^1E_g. $Pd(en)_2PtCl_4$ shows an x,y-polarized band at 27,600 cm^{-1}, although the expected z-polarized peak is off scale, apparently due to the presence of an intense allowed band that has red-shifted into the visible region in z. $Pd(NH_3)_4PtCl_4$ shows a z-polarized band at 25,600 cm^{-1}, with a broadened band at 26,000 cm^{-1}

in x,y arising from both $^1A_{2g}$ and ^1E_g. A similar situation is observed in $Pt(en)_2PtCl_4$, with x,y- and z-polarized bands at 24,900 cm^{-1} and 25,000 cm^{-1} respectively. That the ^1E_g state is not observed at lower energies than $^1A_{2g}$ in $Pt(CH_3NH_2)_4PtCl_4$ and $Pt(NH_3)_4PtCl_4$ is somewhat surprising, since d(M-M) is 0.17 A less in $Pt(CH_3NH_2)_4PtCl_4$ and MGS than in $Pt(en)_2PtCl_4$. The presence of $^1A_{2g}$ may serve to obscure the exact location of ^1E_g within the band, however, especially since ^1E_g is expected to be rather less intense than $^1A_{2g}$ (45).

The only reasonable alternative to the above scheme was assignment of ^1E_g to the weak z- and x,y-polarized shoulders at about 22,500 cm^{-1} in MGS and 23,000 cm^{-1} in $Pt(CH_3NH_2)_4PtCl_4$. This possibility was rather inviting, since we did expect ^1E_g to continue shifting to still lower values as d(M-M) decreased from 3.41 A in $Pt(en)_2PtCl_4$ to 3.24 A in $Pt(CH_3NH_2)_4PtCl_4$ and MGS. However, assignment of ^1E_g to this band results in a shift from K_2PtCl_4 of 6800 cm^{-1}, much larger than the shift expected on the basis of the ^3E_g shifts.

Unfortunately, no isolated d-d vibronic bands are observed which readily suggest assignment to the $^1B_{1g}$ state. The spectra possess some features, however, which lend credence to the assignment of $^1B_{1g}$ to the weak shoulders at 22,500 cm^{-1} to 23,000 cm^{-1} in MGS and $Pt(CH_3NH_2)_4PtCl_4$.

If the band at 22,500 cm^{-1} in MGS is $^1B_{1g}$, it probably shifted from the absorption containing ^1E_g at 29,300 cm^{-1} (x,y) and 29,800 cm^{-1} (z) in K_2PtCl_4, for a shift of about 6800 cm^{-1} across the $PtCl_4^{2-}$ series. Such a shift is quite reasonable if ^1E_g shifts by 4100 cm^{-1} over the

series, as was proposed above. On the other hand, the $^1B_{1g}$ shift in the $PdCl_4^{2-}$ series is about 7100 cm^{-1}. The larger splitting of the d-orbital energies in $PtCl_4^{2-}$, and the greater perturbing effect of the cation on platinum's larger d-orbitals requires a larger shift in the $^1B_{1g}$ energy in the platinum salts, thus seeming to rule out the scheme for $^1B_{1g}$ proposed here. However, if we omit the shifts from the potassium salts in both series, and consider only the shifts for the Magnus-type salts themselves, we find that $^1B_{1g}$ shifts by 4550 cm^{-1} from $Pd(en)_2PdCl_4$ to $Pt(NH_3)_4PdCl_4$, and by 5200 cm^{-1} from $Pd(en)_2PtCl_4$ to $Pt(NH_3)_4PtCl_4$.

Although the omission of shifts from the potassium salts in each series does give the expected relationship for $^1B_{1g}$ shifts across the two series, a rationalization of the shifts from the potassium salts is required, especially since the difference in d(M-M) from K_2PtCl_4 to $Pd(en)_2PtCl_4$ is 0.73 A, while the d(M-M) difference K_2PdCl_4 to $Pd(en)_2PdCl_4$ is only 0.67 A, which in itself suggests a larger shift for the $PtCl_4^{2-}$ salts.

The environments around the $PdCl_4^{2-}$ and $PtCl_4^{2-}$ ions provide a possible explanation for the shifts. In the potassium salts, each anion is sandwiched between two other anions in the stacking plane. In the $Pd(en)_2^{2+}$ salts, the anions are presumed to be sandwiched between the positively-charged $Pd(en)_2^{2+}$ ions. Now, the d-orbitals of a negatively-charged complex ion should be rather larger than those in a complex cation. As a result, the $PdCl_4^{2-}$ and $PtCl_4^{2-}$ ions in the potassium salt should experience more electron-electron repulsion than they would

experience in the $Pd(en)_2^{2+}$ salts, if d(M-M) were equal for all compounds. The increased repulsion would, of course, likely result in a destabilization of the $d_{xz,yz}$ and d_z2 orbitals.

The d-orbitals on $PtCl_4^{2-}$ should experience greater destabilization than the d-orbitals in $PdCl_4^{2-}$ experience since the Pt d-orbitals extend farthest from the nucleus. For the same reason, $PtCl_4^{2-}$ ions will cause greater destabilization in the neighboring ions than will the $PdCl_4^{2-}$ ions. Of course, the $Pd(en)_2^{2+}$ ions will cause the least destabilization of all, since their d-orbitals are located on a positively-charged Pd ion.

The upshot of the argument is this: the d_z2 and $d_{xz,yz}$ orbitals will be destabilized to a significant degree in K_2PtCl_4, even though d(Pt-Pt) is large, at 4.14 A (46). Much less destabilization should be experienced in K_2PdCl_4, since d(Pd-Pd) is almost equal to d(Pt-Pt), at 4.11 A (40,46). The transition energies of $^1B_{1g} \leftarrow {}^1A_{1g}$ ($d_{x^2-y^2}{}^* \leftarrow d_z2$) and $^1E_g \leftarrow {}^1A_{1g}$ ($d_{x^2-y^2}{}^* \leftarrow d_{xz,yz}$) may therefore already be somewhat red-shifted from the value for an unperturbed ion in the K_2PtCl_4 crystal spectra, and essentially unchanged from the unperturbed ion values in the K_2PdCl_4 crystal spectra. Replacing K^+ by $Pd(en)_2^{2+}$ effectively removes the red-shift caused by the anion-anion interactions, although the large drop in d(M-M) still results in a net red-shift for the $^1B_{1g}$ and ^1E_g absorptions. The shift of $^1B_{1g}$ and ^1E_g going from K_2PtCl_4 to $Pd(en)_2PtCl_4$ reflect only a part of the shifts from the unperturbed $PtCl_4^{2-}$ ion, while the shifts of $^1B_{1g}$

and ^1E_g going from K_2PdCl_4 to $Pd(en)_2PdCl_4$ reflect the total shifts from the unperturbed $PdCl_4^{2-}$ ion.

The Magnus-type salts provide no direct spectroscopic evidence to support this mechanism. However, comparison of the aqueous and crystal spectra of K_2PdCl_4 at 300K with the spectra of K_2PtCl_4 shows that the ^1E_g (and, by our assignment, $^1B_{1g}$) peak at 22, 440 cm^{-1} (aqueous spectrum) in K_2PdCl_4 actually blue-shifts by about 500 cm^{-1} in the crystal spectrum, indicating negligible d_z2 (or $d_{xz,yz}$) destabilization. The $^1E_g/^1B_{1g}$ peak in K_2PtCl_4, on the other hand, red-shifts from 30,300 cm^{-1} in the aqueous spectrum to 29,300 cm^{-1} (z) and 28,700 cm^{-1} (x,y) in the crystal spectra, about 1000 - 1600 cm^{-1}. This shift suggests a significant perturbation of d_z2, and possibly $d_{xz,yz}$, in K_2PtCl_4.

Invoking the anion-anion interactions yields a reasonable explanation for the discrepancies in the $^1B_{1g}$ shifts over the $PdCl_4^{2-}$ and $PtCl_4^{2-}$ series. The same arguments can be used on the $PdBr_4^{2-}$ and $PtBr_4^{2-}$ series as well. In considering the shifts of other transitions across any of the series, however, these arguments are not necessary: to include them results in no change in the relationships of the shifts. The shift of 5200 cm^{-1} from $Pd(en)_2PtCl_4$ to $Pt(NH_3)_4$-$PtCl_4$ for $^1B_{1g}$ is in good accord with the shifts across the same series of about 2400 cm^{-1} for ^1E_g (x,y), and about zero for $^1A_{2g}$. The shift of 2350 cm^{-1} (x,y) agrees very well with the shift for ^1E_g, although the 3850 cm^{-1} shift in z is rather higher than anticipated. The ^3E_g (z)

shift is not necessarily a cause for alarm, however, since the actual shift of ^1E_g in z is unknown, due to the encroachment of strong absorption into the ^1E_g region in both $Pd(en)_2PtCl_4$ and MGS, which obscures the ^1E_g (z) bands in both crystals' spectra. Figure 28 provides a graphic summary of these shifts.

The evidence collected from the $PtCl_4^{2-}$ series spectra is not conclusive proof that $^1B_{1g}$ shifts from about 29,300 cm^{-1} in K_2PtCl_4 to 22,500 cm^{-1} in MGS. Two other schemes also have merit.

A shift of ^1E_g from 29,300 cm^{-1} to 22,500 cm^{-1}, and a shift of $^1B_{1g}$ from 29,300 cm^{-1} to 16,100 cm^{-1} (z) over the full $PtCl_4^{2-}$ series is one alternative scheme that received consideration. This scheme is attractive because it continues the shift of ^1E_g beyond its position in $Pt(en)_2PtCl_4$ as d(M-M) is decreased to its value in MGS. The scheme also accounts for the relatively high intensity of the 16,100 cm^{-1} (z) peak in MGS, by placing $^1B_{1g}$ there. However, a shift of 13,100 cm^{-1} does seem large for $^1B_{1g}$, even in the $PtCl_4^{2-}$ series. Also, a peak corresponding to $^1B_{1g}$ intermediate between $^1A_{2g}$ and the triplets might be expected in $Pt(en)_2PtCl_4$; only the very weak peak at 22,500 cm^{-1} is observed. Moreover, the ^1E_g shifts would no longer agree with the ^3E_g shifts. Finally, the inclusion of $^1B_{1g}$ in the triplet region would be expected to produce marked changes in the band's intensity and temperature dependence. The $^1B_{1g}$ state is excited by the b_{2u} vibration, which gives $\varepsilon_6/\varepsilon_{300}$ of only 0.387, as calculated by equation (1). The observed temperature dependence remains constant

at around 0.5 across the entire series, including K_2PtCl_4, as shown in Table 11. The increase in intensity has been attributed to an "intensity borrowing" mechanism, whereby the triplets "borrow" intensity from a nearby allowed transition (28). In view of the high spin-orbit coupling associated with platinum, and the closeness of a high-intensity band in z which could facilitate intensity borrowing, the borrowing explanation seems adequate to account for the intensity of the z-polarized, low-energy peaks in MGS.

The other alternative considered places ^1E_g with $^1A_{2g}$, but shifts $^1B_{1g}$ from 36,500 cm^{-1} in K_2PtCl_4 to the valley around 28,000 cm^{-1} in MGS. The $^1B_{1g}$ shift of 8500 cm^{-1} here is quite reasonable, and the presence of significant absorption at 28,000 cm^{-1} makes the assignment possible. Furthermore, intensity data on the weak band at 22,500 cm^{-1} in MGS obtained from Gaussian fits of the room-temperature and 6K spectra give $\varepsilon_6/\varepsilon_{300} = 2.4$, not at all consistent with the behavior of vibronic transitions. We tend to believe that the intensity data for the room-temperature (x,y) spectrum is low because of broadening of the stronger bands in the spectrum. The temperature dependence might indicate an allowed transition, however, in which case the band may be a spin-forbidden LMCT, such as $^3E_u \leftarrow {}^1A_{1g}$ ($d_{x^2-y^2}{}^* \leftarrow e_u$ L-π). In any case, assignment of the band to a vibronic transition is not required, and ^1E_g can remain with $^1A_{2g}$ at 25,200 cm^{-1} while $^1B_{1g}$ remains at higher energy.

Perhaps the major problem with this scheme lies with the $PdCl_4^{2-}$ series. Rush et al. have shown (36) that K_2PdCl_4 can have no singlet

Table 11. Temperature behavior for selected peaks in the $PtCl_4^{2-}$ series

Compound	Peak location[a]	Polarization	ε_{300}[b]	ε_6[c]	$\varepsilon_6/\varepsilon_{300}$	Assignment
K_2PtCl_4[d]	20600	z	20	10	0.500	triplets
	29500	z	101	55	0.545	^1E_g
	26300	x,y	62	28	0.452	$^1A_{2g}$
	29200	x,y	74	37	0.500	^1E_g
$Pd(en)_2PtCl_4$	19500	z	70.1	36.2	0.516	triplets
	25000	x,y	127	64.3	0.508	$^1A_{2g}$
	27500	x,y	145	84	0.579	$^1B_{1g}$, ^1E_g
$Pd(NH_3)_4PtCl_4$	18700	z	58.6	27.7	0.473	triplets
	25200	z	320	203	0.613	$^1B_{1g}$, ^1E_g
	26400	x,y	135	81.4	0.603	$^1A_{2g}$, ^1E_g
$Pt(en)_2PtCl_4$	18200	z	98.1	43.6	0.444	triplets
	25000	x,y	118	61.3	0.520	$^1A_{2g}$, ^1E_g

$Pt(CH_3NH_2)_4PtCl_4$	16700	z	124	67.4	0.543	triplets
	25400	x,y	177	108	0.610	$^1A_{2g}$, ^1E_g
$Pt(NH_3)_4PtCl_4$	16100	z	124	61	0.492	triplets
	25200	x,y	184	140.3	0.763	$^1A_{2g}$, ^1E_g

[a]Location of peak maxima, in cm^{-1}.

[b]Extinction coefficient at 300K, $cm^{-1}M^{-1}$.

[c]Extinction coefficient at 6K, $cm^{-1}M^{-1}$.

[d]All values and assignments from Reference 33.

bands between 23,200 cm^{-1} and the $^1A_{2u}$ band at 37,500 cm^{-1}. Consequently, $^1B_{1g}$ must be at 37,500 cm^{-1} if it is not with ^1E_g at 23,200 cm^{-1}, or else be too weak to detect.

It would be difficult indeed to account for $^1B_{1g}$ in K_2PtCl_4 at 36,500 cm^{-1}, about 8000 cm^{-1} above ^1E_g, when $^1B_{1g}$ and ^1E_g are at the same energy in K_2PdCl_4. It would be equally difficult to account for the smaller $^1B_{1g}$ transition energy (36,500 cm^{-1}) in K_2PtCl_4 if $^1B_{1g}$ were placed at 37,500 cm^{-1} in K_2PdCl_4. Apparently, $^1B_{1g}$ must be at 23,200 cm^{-1} in K_2PdCl_4 and 29,300 cm^{-1} in K_2PtCl_4 in order to maintain reasonable relationships of the shifts and energies of both series.

Finally, we should note that a weak band featuring vibrational structure is observed in the 22,500 cm^{-1} - 23,000 cm^{-1} region of the x,y-polarized spectra for $Pd(en)_2PtCl_4$ and $Pt(en)_2PtCl_4$. A similar band in K_2PtCl_4 has been assigned by Martin et al. (19) to $^3B_{1g}$ because its transition energy lies below the singlet ← singlet energies, and because the band has low intensity characteristic of triplet ← singlet transitions. We assign the bands in $Pd(en)_2PtCl_4$ and $Pt(en)_2PtCl_4$ to $^3B_{1g}$ for the same reasons. While the weak transitions in both of these salts are close in energy, they form the spin-forbidden counterpart to $^1B_{1g}$, the transition that changes most over the series, according to our postulates for the behavior of the orbitals. The small differences in the triplet energies may not be so alarming if we realize that the only difference in the two compounds is the metal in the cations.

The vibronic bands observed in the $PtBr_4^{2-}$ series are reminiscent of the d-d bands in the $PtCl_4^{2-}$ series, in much the same way that the $PdBr_4^{2-}$ series spectra were reminiscent of those for the $PdCl_4^{2-}$ series. Table 7 listed the observed absorptions and their intensities. Figures 29 through 34 show the representative spectra for each compound, and Figure 35 provides a graphic summary of the shifts. In general, the weaker crystal-field effects of Br^- puts the transitions at lower energies in the $PtBr_4^{2-}$ salts, compared to the $PtCl_4^{2-}$ salts.

The strictly x,y-polarized peaks appearing between 23,600 cm^{-1} and 25,000 cm^{-1} across the series were, of course, assigned to $^1A_{2g} \leftarrow {}^1A_{1g}$. The observation of vibrational structure for the peaks of all compounds except $Pt(NH_3)_4PtBr_4$ and $Pd(NH_3)_4PtBr_4$ support the assignment, as do the small shifts from the $^1A_{2g}$ energy in K_2PtBr_4 observed over the series. All the $^1A_{2g}$ bands except that for $Pd(NH_3)_4PtBr_4$ lie between 24,400 cm^{-1} and 23,600 cm^{-1}. Undoubtedly, the $Pd(NH_3)_4$-$PtBr_4$ peak is at higher energy (25,000 cm^{-1}) because the band contains other transitions in addition to $^1A_{2g}$ which tend to obscure the exact location of the $^1A_{2g}$ peak maximum.

The ^1E_g band is located above the $^1A_{2g}$ band in both x,y- and z-polarizations for $Pd(en)_2PtBr_4$, by analogy with the assignments (47) for the very similar K_2PtBr_4 spectra. By inference from the shifts of the weak bands assigned to ^3E_g in the 15,500 cm^{-1} - 19,200 cm^{-1} region, ^1E_g is believed to lie at 23,600 cm^{-1} with $^1A_{2g}$ in $Pt(NH_3)_4$-$PtBr_4$. The shift over the series is 3200 cm^{-1} (x,y) and 3400 cm^{-1} (z).

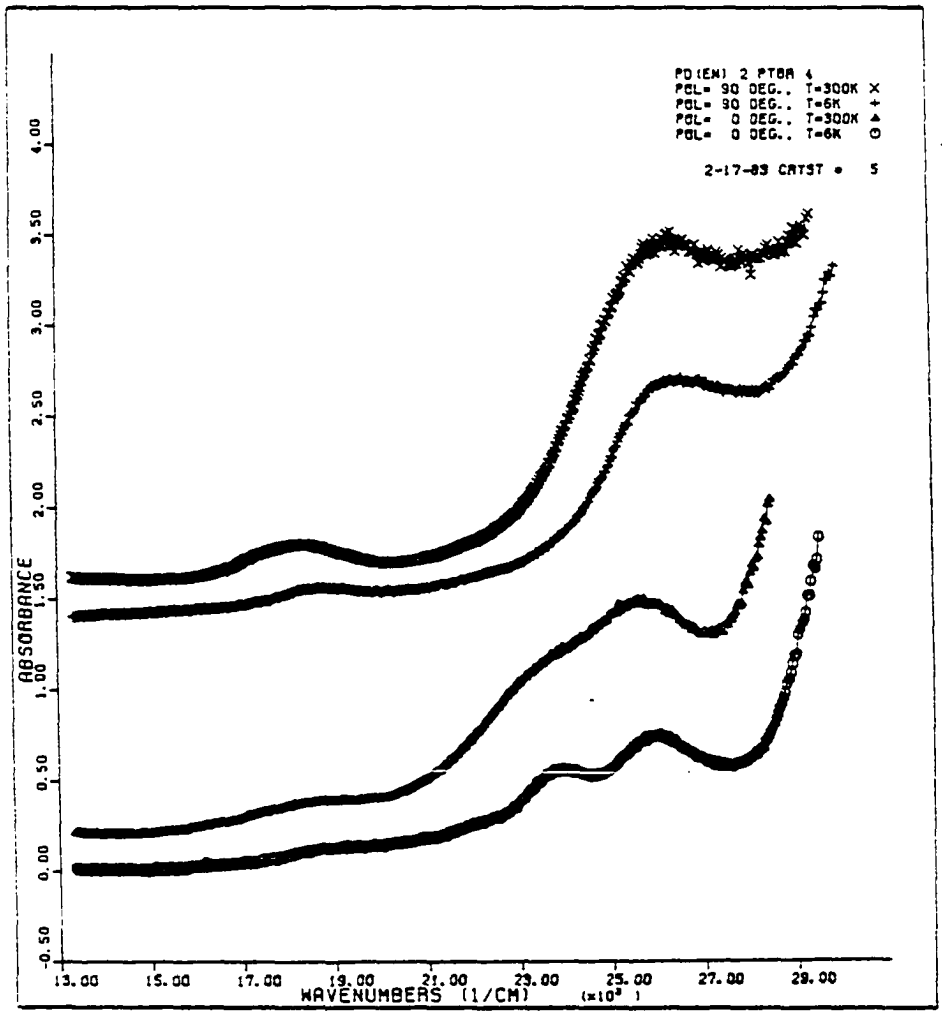

Figure 29. Polarized absorption spectra for $Pd(en)_2PtBr_4$

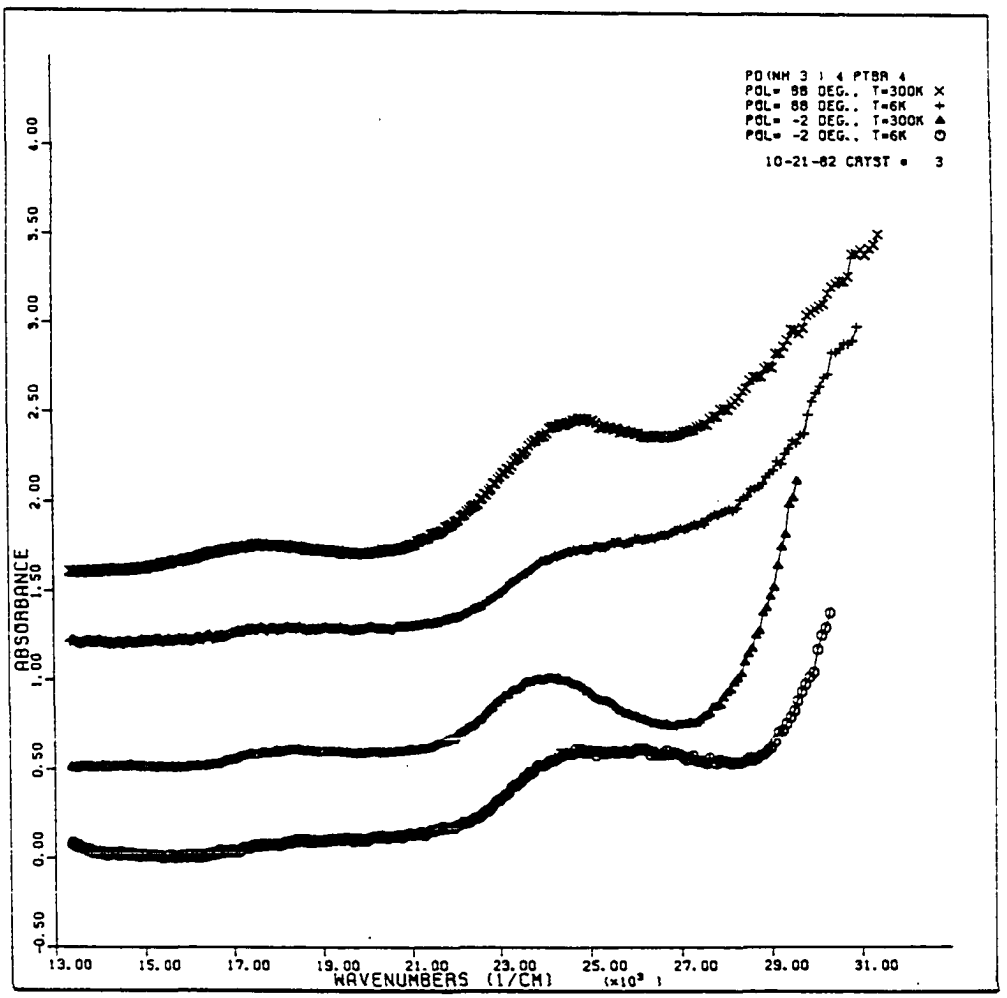

Figure 30. Polarized absorption spectra for $Pd(NH_3)_4PtBr_4$

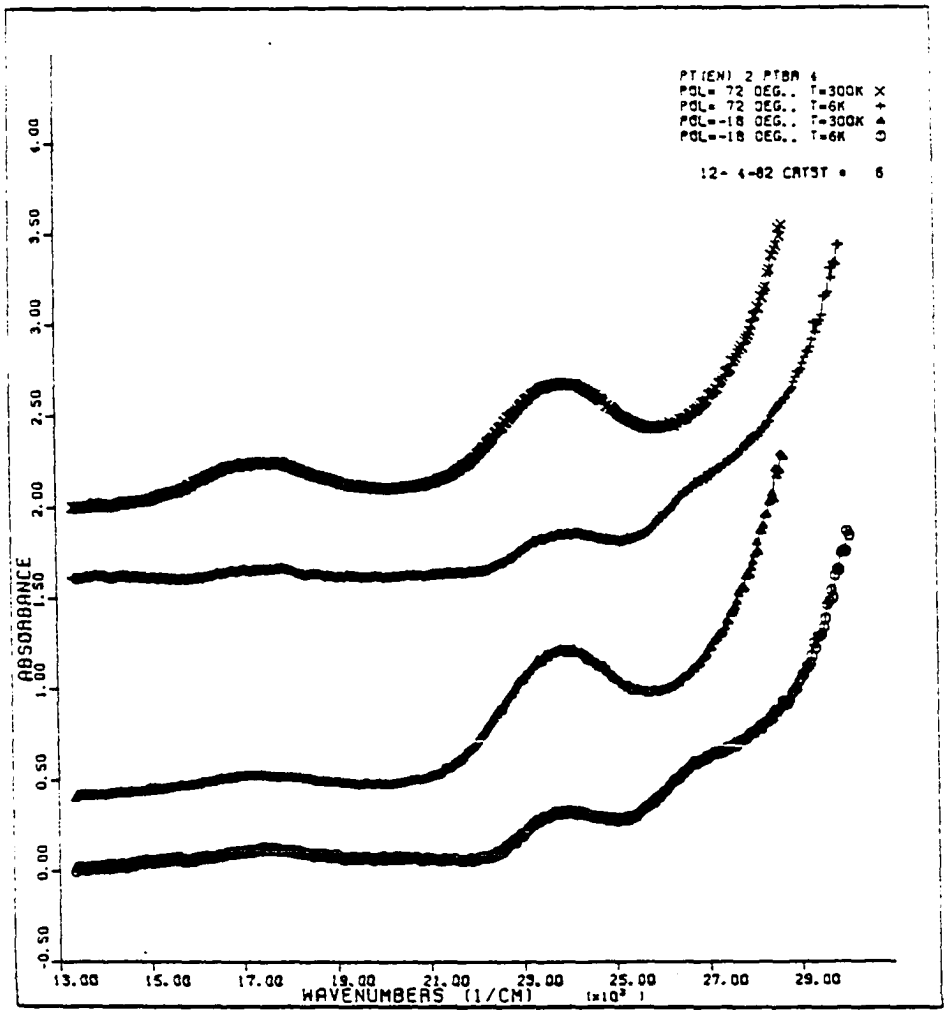

Figure 31. Polarized absorption spectra for $Pt(en)_2PtBr_4$

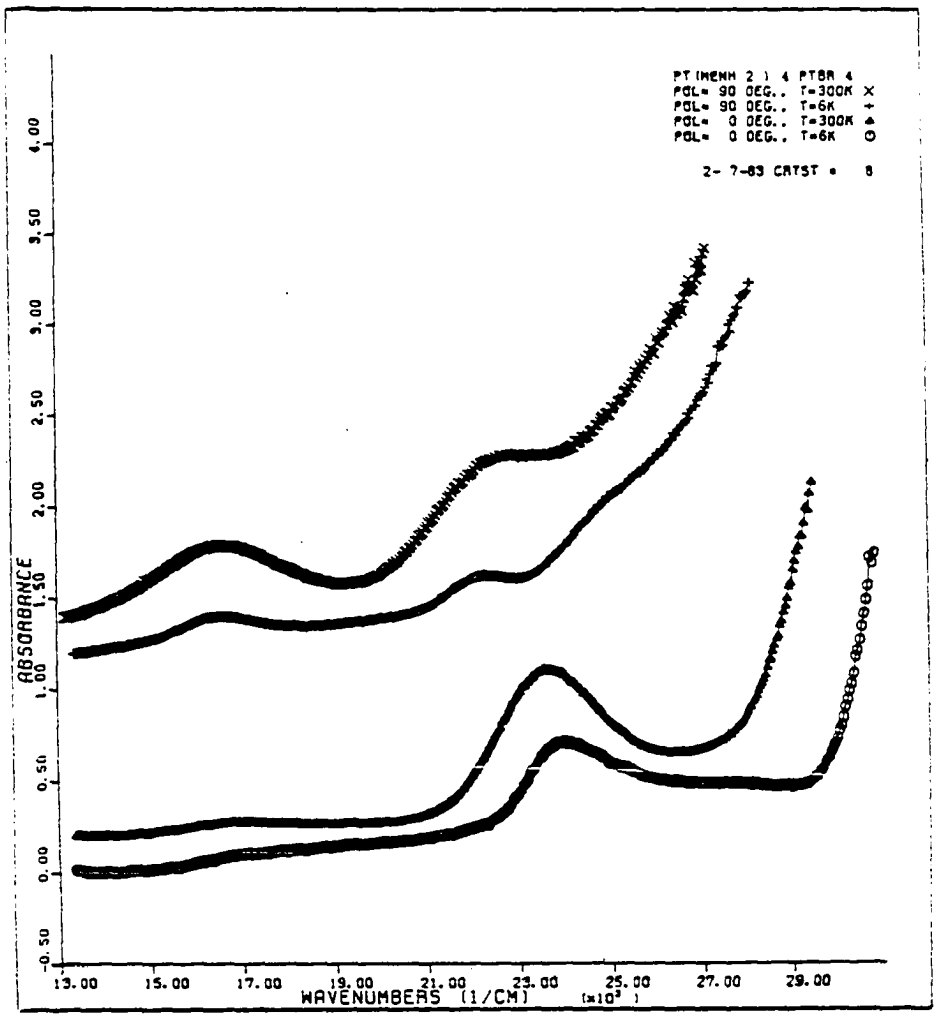

Figure 32. Polarized absorption spectra for $Pt(CH_3NH_2)_4PtBr_4$, emphasizing high-energy transitions

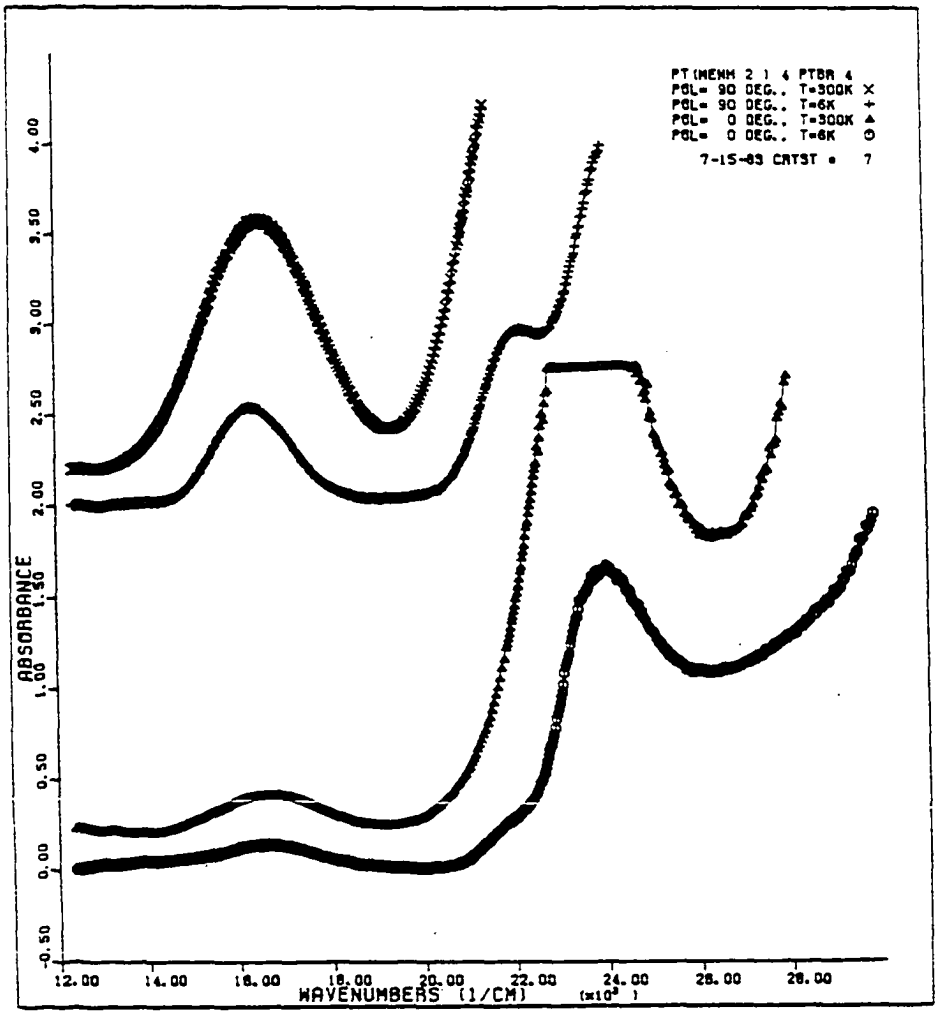

Figure 33. Polarized absorption spectra for $Pt(CH_3NH_2)_4PtBr_4$, emphasizing low-energy transitions

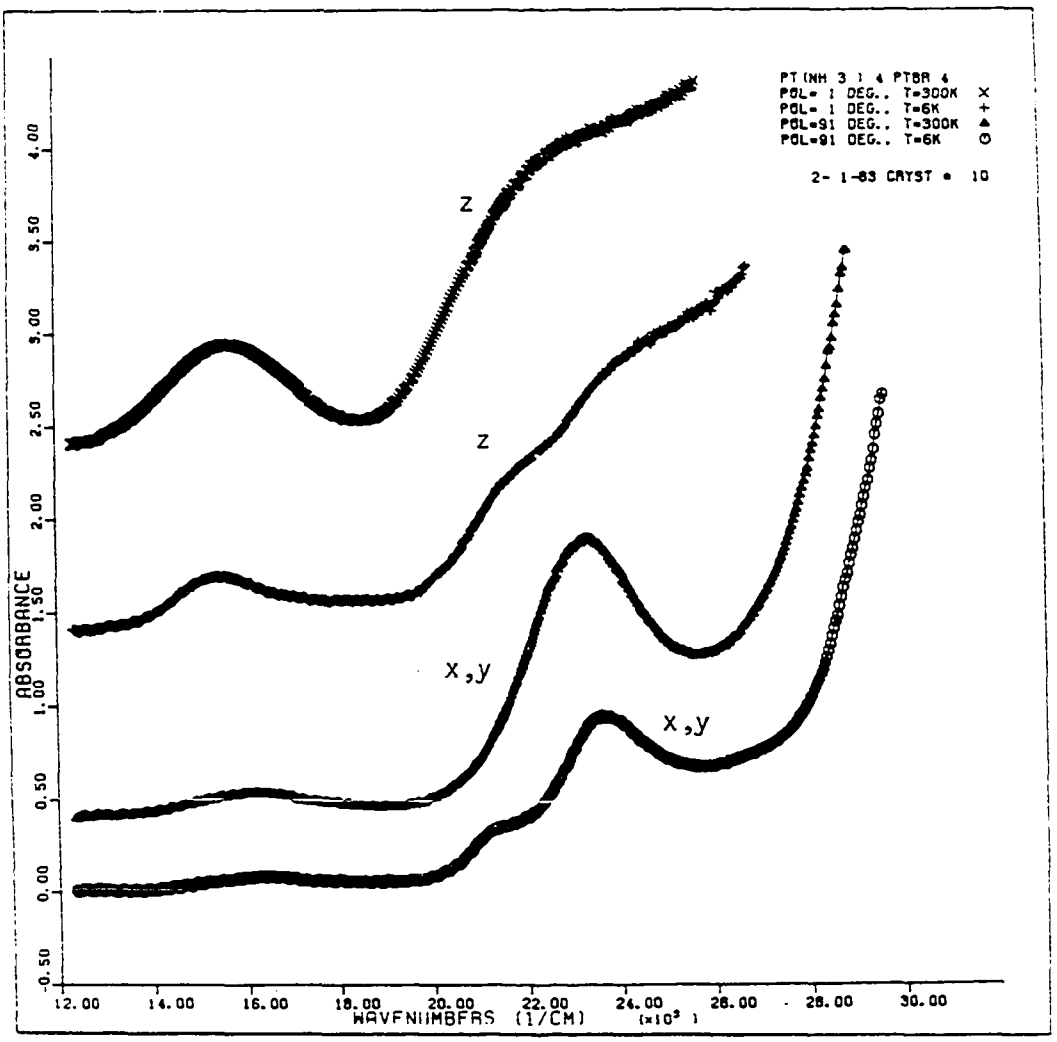

Figure 34. Polarized absorption spectra for $Pt(NH_3)_4PtBr_4$. Note that the polarization angles do not follow the convention given on page 49

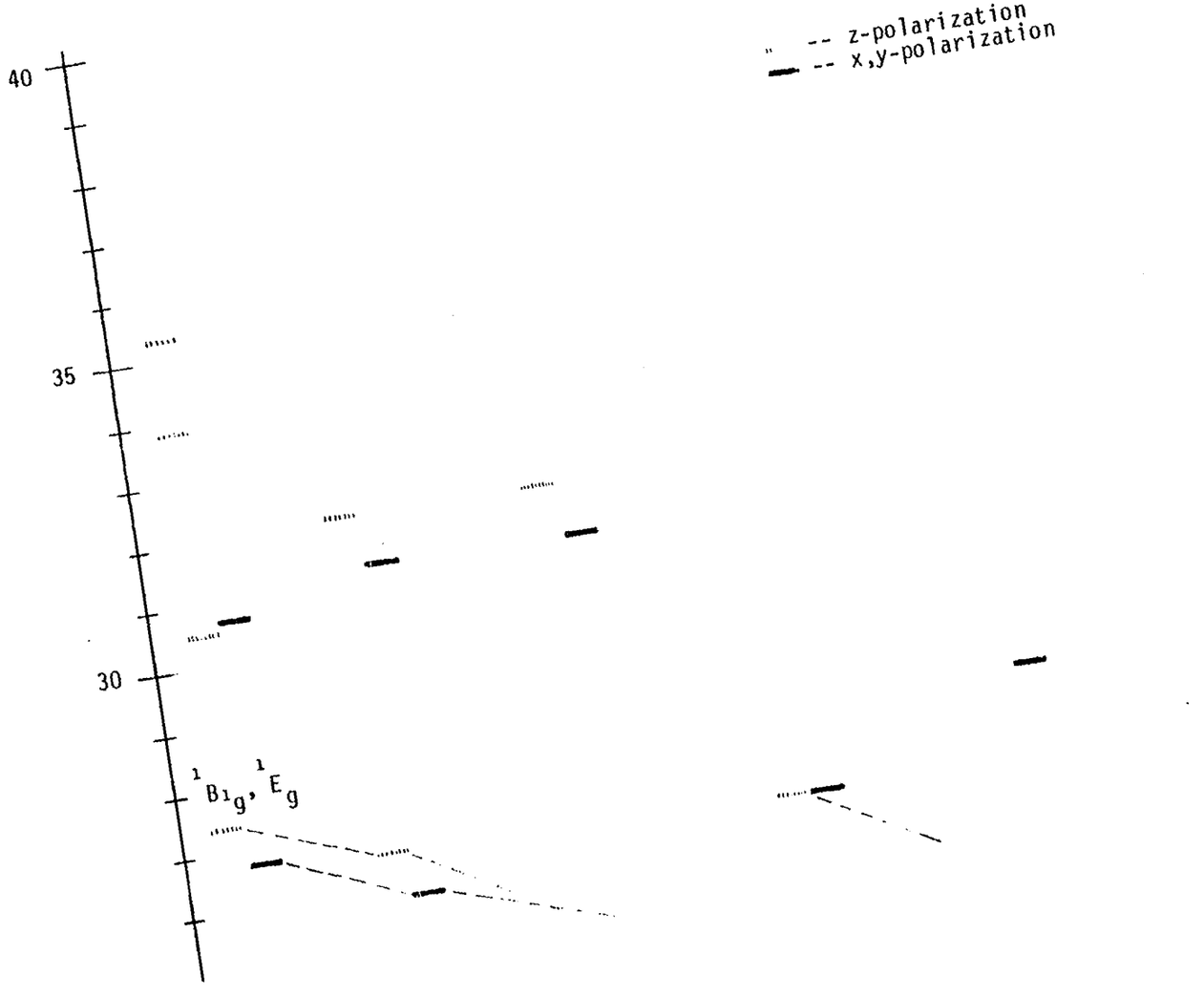
-- z-polarization
-- x,y-polarization
40
35
30
$^1B_{1g}, ^1E_g$

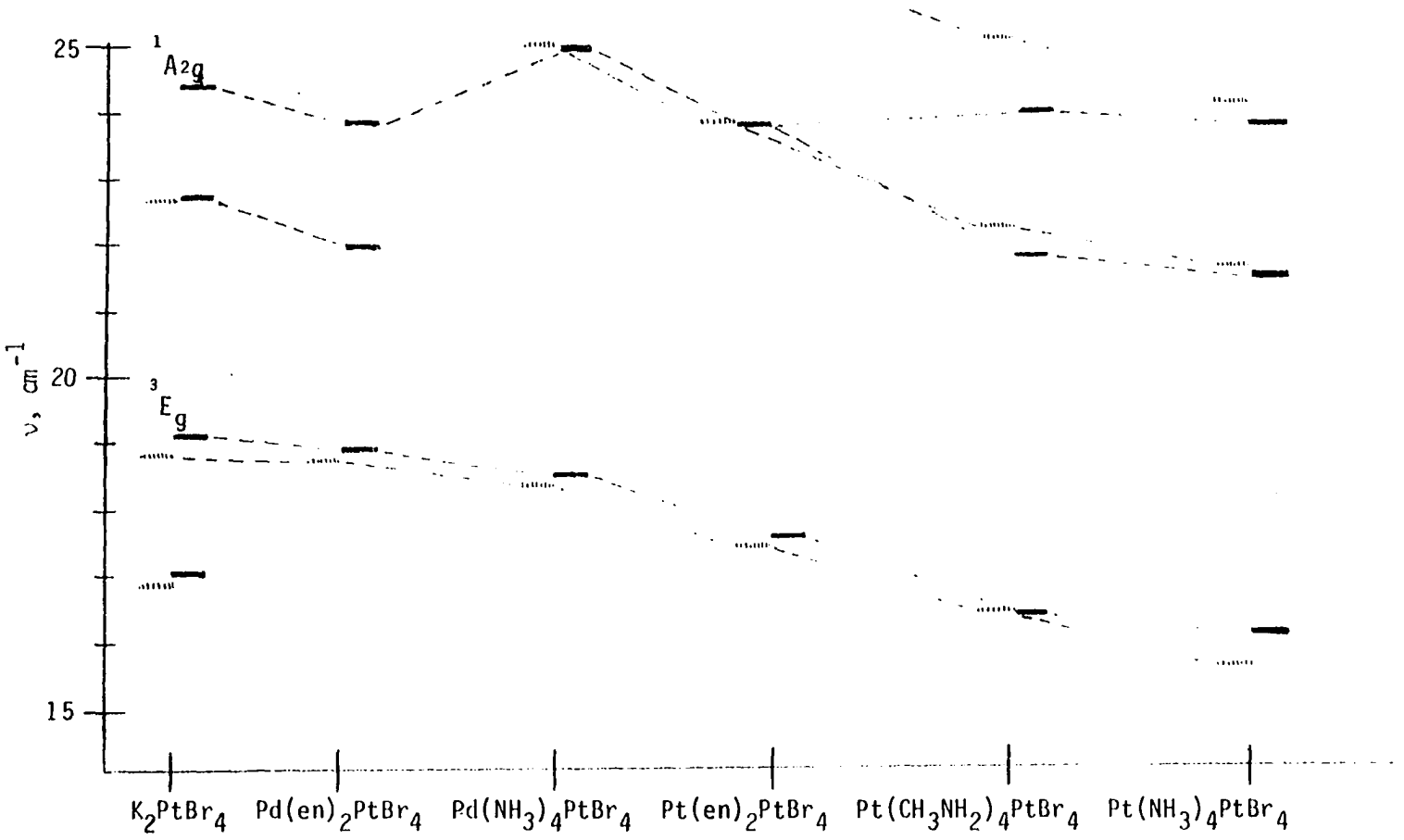

Figure 35. Shifts of absorptions across the $PtBr_4^{2-}$ series

This is about 900 cm^{-1} less than the corresponding shift in the $PtCl_4^{2-}$ series, just as expected from the greater d(M-M) in the $PtBr_4^{2-}$ series.

The $^1B_{1g}$ state is assigned to the z-polarized peaks that shift 5800 cm^{-1}, from 27,400 cm^{-1} (z) in K_2PtBr_4 to 21,600 cm^{-1} (z) in $Pt(NH_3)_4PtBr_4$. This shift compares well with the 6800 cm^{-1} shift observed for $^1B_{1g}$ in the $PtCl_4^{2-}$ series. Over the Magnus-type series only, the shift is 5100 cm^{-1}, in good agreement with the shift for $^1B_{1g}$ in the $PtCl_4^{2-}$ Magnus-type series of 5200 cm^{-1}.

The intense allowed bands which dominate the z-polarized spectra in the $PtCl_4^{2-}$ salts and in $Pt(NH_3)_4PtBr_4$ remain far enough into the ultraviolet region to permit estimates of $\varepsilon_6/\varepsilon_{300}$ to be made for the z-polarized peaks in every salt except $Pt(NH_3)_4PtBr_4$. The temperature dependence ratio, $\varepsilon_6/\varepsilon_{300}$ of each salt is larger for the z-polarized peak than it is for the x,y-polarized $^1A_{2g}/^1E_g$ band, as Table 12 indicates. The ratio for the $Pt(en)_2PtBr_4$ and $Pt(CH_3NH_2)_4PtBr_4$ bands deserve special note: although the z-polarized bands have rather different $\varepsilon_6/\varepsilon_{300}$ values (0.245 and 0.389, respectively), comparison with the $^1A_{2g}/^1E_g$ band in each salt shows that $\varepsilon_6/\varepsilon_{300}$ for the z-polarized band in $Pt(en)_2PtBr_4$ is smaller than $\varepsilon_6/\varepsilon_{300}$ for $^1A_{2g}/^1E_g$ by nearly the same proportion that $\varepsilon_6/\varepsilon_{300}$ (z) is smaller than $\varepsilon_6/\varepsilon_{300}$ in $Pt(CH_3NH_2)_4PtBr_4$, i.e., by about 40 percent. The ratios for the other salts are only qualitatively consistent with the ratios for $Pt(en)_2PtBr_4$ and $Pt(CH_3NH_2)_4PtBr_4$, perhaps because the broad peaks often overlap, making intensity measurements difficult. Also, $Pd(NH_3)_4PtBr_4$ and

Table 12. Temperature behavior for selected peaks in the $PtBr_4^{2-}$ series

Compound	Peak location[a]	Polarization	ε_{300}[b]	ε_6[c]	$\varepsilon_6/\varepsilon_{300}$	Assignment
K_2PtBr_4[d]	18800	z	20	12	0.600	triplets
	27400	z	125	44	0.352	^1E_g
	24400	x,y	130	46	0.354	$^1A_{2g}$
	26800	x,y	175	73	0.417	^1E_g
$Pd(en)_2PtBr_4$	18700	z	46.2	38.5	0.833	triplets
	26700	z	487	326	0.669	^1E_g , $^1B_{1g}$
	23850	x,y	254	141	0.555	$^1A_{2g}$
	25900	x,y	326	190	0.583	^1E_g , $^1B_{1g}$
$Pd(NH_3)_4PtBr_4$	18250	z	28.2	16.9	0.599	triplets
	25000	z	160	98	0.613	^1E_g , $^1B_{1g}$
	25000	x,y	93.9	113	1.20	$^1A_{2g}$, ^1E_g
$Pt(en)_2PtBr_4$	17400	z	75.0	18.0	0.24	triplets

	23800	z	204	78	0.382	^1E_g , $^1B_{1g}$
	23800	x,y	246	99	0.402	$^1A_{2g}$, ^1E_g
$Pt(CH_3NH_2)_4PtBr_4$	16340	z	64.8	27.4	0.423	triplets
	22170	z	156	60.7	0.389	$^1B_{1g}$
	23920	x,y	167	110	0.659	$^1A_{2g}$, ^1E_g
$Pt(NH_3)_4PtBr_4$	15500	z	107	60.4	0.564	triplets
	16000	x,y	27.3	19.5	0.714	triplets
	23600	x,y	292	185	0.634	$^1A_{2g}$, ^1E_g

[a]Location of peak maxima, in cm^{-1}.

[b]Extinction coefficient at 300K, in $cm^{-1}M^{-1}$.

[c]Extinction coefficient at 6K, in $cm^{-1}M^{-1}$.

[d]All values and assignments from Reference 47.

$Pd(en)_2PtBr_4$ were the most difficult crystals to synthesize of all the Magnus-type salts. All crystals of these two salts for which spectra were recorded were extremely small. As a result, the spectra tended to be rather less reproducible than those of the other salts, with baseline drift believed to be the most important problem. Moreover, significant differences in the exciting vibrational frequencies for the transitions from compound to compound may also give rise to temperature dependence ratios that differ over the $PtBr_4^{2-}$ series. Evidence for such differences in the exciting vibrational frequencies exists, and is discussed in the section on Vibrational Structure.

In any case, the z-polarized bands appear to be more sensitive to temperature than $^1A_{2g}/^1E_g$. We therefore assign to $^1B_{1g}$ the z-polarized absorptions from 26,700 cm^{-1} to 21,600 cm^{-1}.

Although the x,y-component of $^1B_{1g}$ is hidden in the $^1A_{2g}$ and ^1E_g absorptions over most of the series, a weak, x,y-polarized shoulder, observed at 21,740 cm^{-1} for $Pt(CH_3NH_2)_4PtBr_4$ and 21,400 cm^{-1} for $Pt(NH_3)_4PtBr_4$, is assigned to $^1B_{1g}$ (x,y). Moncuit predicts (43,45) that that $^1B_{1g}$ (x,y) will be much less intense than $^1B_{1g}$ (z) for $PtCl_4^{2-}$ and $PdCl_4^{2-}$; the intensities observed here for the two polarizations are certainly in agreement with Moncuit's calculated oscillator strengths, in view of the similar behavior expected for the chloride and bromide series.

Allowed Transitions

The allowed transitions, which generally occur at higher energies than the observed d-d vibronic bands, are distinguished from the vibronic bands by the temperature dependence of their intensities. As discussed in the Introduction, the allowed bands appear to gain peak-height as the temperature decreases, while the vibronic bands lose intensity under the same conditions. Tables 4 through 7, which summarize the locations and extinction coefficients of the d-d peaks, provide the same data for the allowed bands in each series. Graphical summaries of the shifts of these bands are presented in Figures 13, 21, 28, and 35.

Allowed bands are observed for every compound in the $PdCl_4^{2-}$ series except $Pd(en)_2PdCl_4$. In that compound, intense absorption appears in both polarizations as a rapidly-rising tail which becomes too intense to measure at 28,000 cm^{-1}.

The intense absorption at high-energy in $Pd(en)_2PdCl_4$ has partially withdrawn off-scale to higher energies in the $Pd(NH_3)_4PdCl_4$ spectra. As a consequence, thin crystals permit detection of a z-polarized band at 34,250 cm^{-1}. This band is assigned to the transition $^1A_{2u} \leftarrow {}^1A_{1g}$ (b_{2u} L-$\pi \leftarrow b_{1g}$ d_{xy} or b_{1g} $d_{xy} \leftarrow b_{2u}$ L-π), by analogy with a similar band at 37,400 cm^{-1} in the 15K spectra of K_2PdCl_4 assigned to the same state by Rush et al. (36). The x,y-polarized spectrum in this region is off-scale, making it impossible to determine the band at 34,250 cm^{-1} is strictly z-polarized, as $^1A_{2u}$ requires. However, with

ε = 388 cm^{-1} M^{-1} for the K_2PdCl_4 peak, and ε = 466 cm^{-1} M^{-1} for the $Pd(NH_3)_4PdCl_4$ band, the assignment seems to be a reasonable one.

A shoulder of questionable authenticity is observed at about 31,000 cm^{-1} in the room-temperature x,y spectrum of $Pd(NH_3)_4PdCl_4$. This transition might be $^3E_u \leftarrow {}^1A_{1g}$ ($d_{x^2-y^2}{}^* \leftarrow e_u$ L-π), or it could simply be a distortion of the baseline in the region.

Appearing at 28,000 cm^{-1} to 22,500 cm^{-1} in $Pd(NH_3)_4PdCl_4$, $Pt(en)_2PdCl_4$, $Pt(CH_3NH_2)_4PdCl_4$, and $Pt(NH_3)_4PdCl_4$ are some rather unusual transitions. The bands are broad, with extinction coefficients on the order of 200 cm^{-1} M^{-1} in z-polarization. The x,y-polarized components appear weaker, and as distinct shoulders and peaks in $Pt(en)_2PdCl_4$ and $Pd(NH_3)_4PdCl_4$. In $Pt(CH_3NH_2)_4PdCl_4$ and $Pt(NH_3)_4PdCl_4$, the absorption appear only as elevated valleys around 24,000 cm^{-1} - 26,000 cm^{-1}.

The bands do not correspond to either of the two singlet-singlet ligand-to-metal charge transfer bands observed in K_2PdCl_4 (36). The extinction coefficient of the $^1E_u \leftarrow {}^1A_{1g}$ ($d_{x^2-y^2}{}^* \leftarrow e_u$ L-π) transition in the aqueous K_2PdCl_4 spectrum is 9330 cm^{-1} M^{-1}, which is much too high to permit assignment of the bands in the Magnus-type salts to ^1E_u. Furthermore, the shift observed for these bands is much larger than any expected shift in ^1E_u. Figure 36 shows the ligand e_u orbitals lying in the $PdCl_4^{2-}$ plane. Any shift in the e_u orbital energies which occurs as d(M-M) changes will be small, and of the same order as the shift in $d_{x^2-y^2}{}^*$ energy, resulting in negligible change

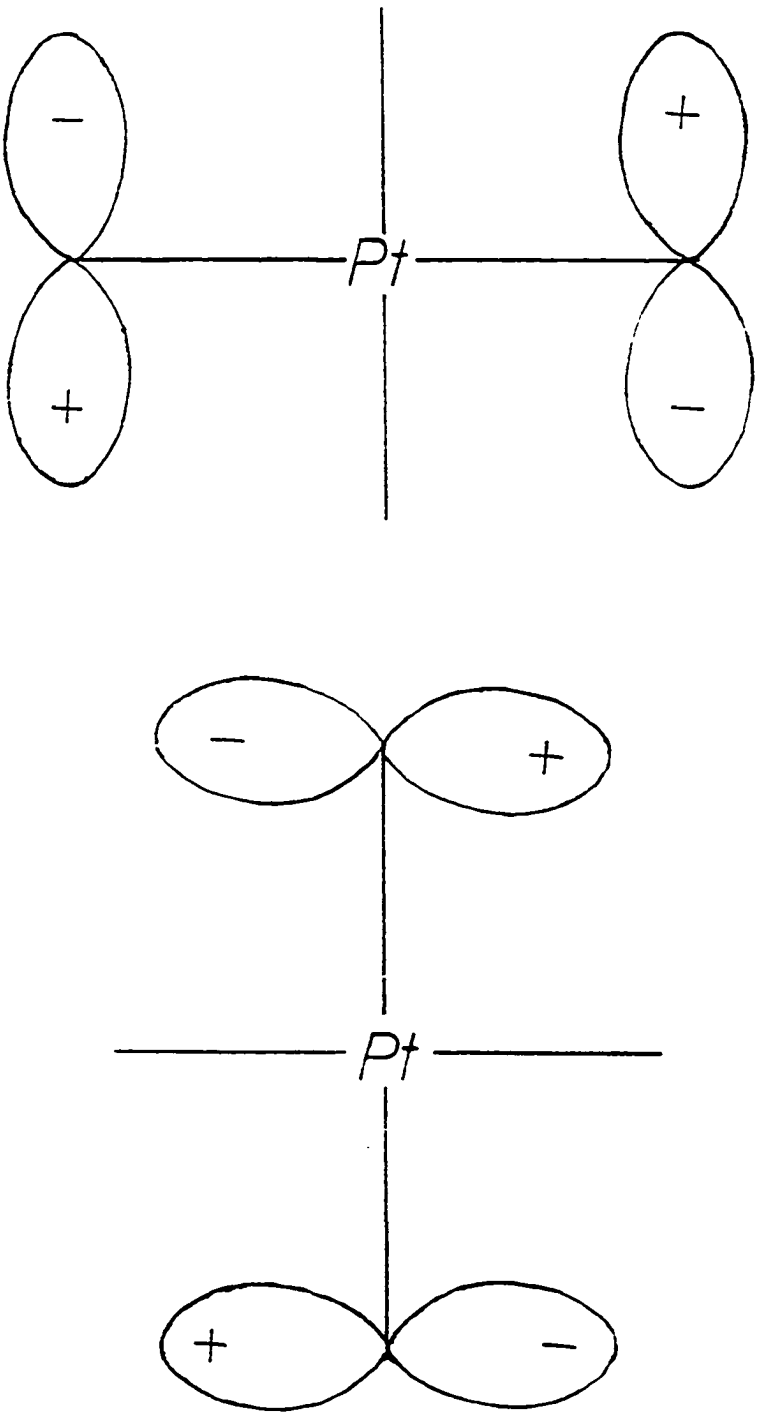

Figure 36. The e_u ligand orbitals

in the $^1E_u \leftarrow {}^1A_{1g}$ transition energy, similar to the situation for the $^1A_{2g} \leftarrow {}^1A_{1g}$ ($d_{x^2-y^2}{}^* \leftarrow d_{xy}$) transition. The observed shifts for the bands from $Pt(en)_2PdCl_4$ to $Pt(NH_3)_4PdCl_4$ is over 3100 cm^{-1}, while the shift for the $^1B_{1g}$ state is only 1900 cm^{-1} over the same series. Clearly, the transition energies of the allowed bands are too sensitive to be accounted for by the $^1E_u \leftarrow {}^1A_{1g}$ transition.

The $^1A_{2u} \leftarrow {}^1A_{1g}$ ($b_{1g}\ \sigma^* \leftarrow b_{2u}$ L-π) transition has already been noted at 34,250 cm^{-1} in $Pd(NH_3)_4PdCl_4$. The shifts for this transition over the series is expected to be greater than that for ^1E_u, but less than that for $^1B_{1g}$, on the basis of the orientation of the orbitals with respect to the metal-metal axis. Figure 37 pictures the b_{2u} L-π orbitals aligned parallel to the z-axis, so their energies will be perturbed significantly by close anion-cation spacing, in much the same manner that the metal d_z2 orbital will be perturbed. However, the energy shift will not be as great for the ligands as for d_z2 due to the smaller radial extension of the ligand p-orbitals in the direction of the cation. By this reasoning, the shift of 3100 cm^{-1} for the series from $Pt(en)_2PdCl_4$ to $Pt(NH_3)_4PdCl_4$ appears too large to be associated with the $^1A_{2u}$ state, unless the shift of $^1B_{1g}$ is actually much larger than the 1900 cm^{-1} observed according to our assignment for $^1B_{1g}$.

The arguments against the assignment of these bands to ^1E_u or $^1A_{2u}$ apply equally well to the possible spin-forbidden, dipole-allowed ligand-to-metal transitions $^3E_u \leftarrow {}^1A_{1g}$ and $^3A_{2u} \leftarrow {}^1A_{1g}$. The much lower intensities expected for these transitions make them somewhat

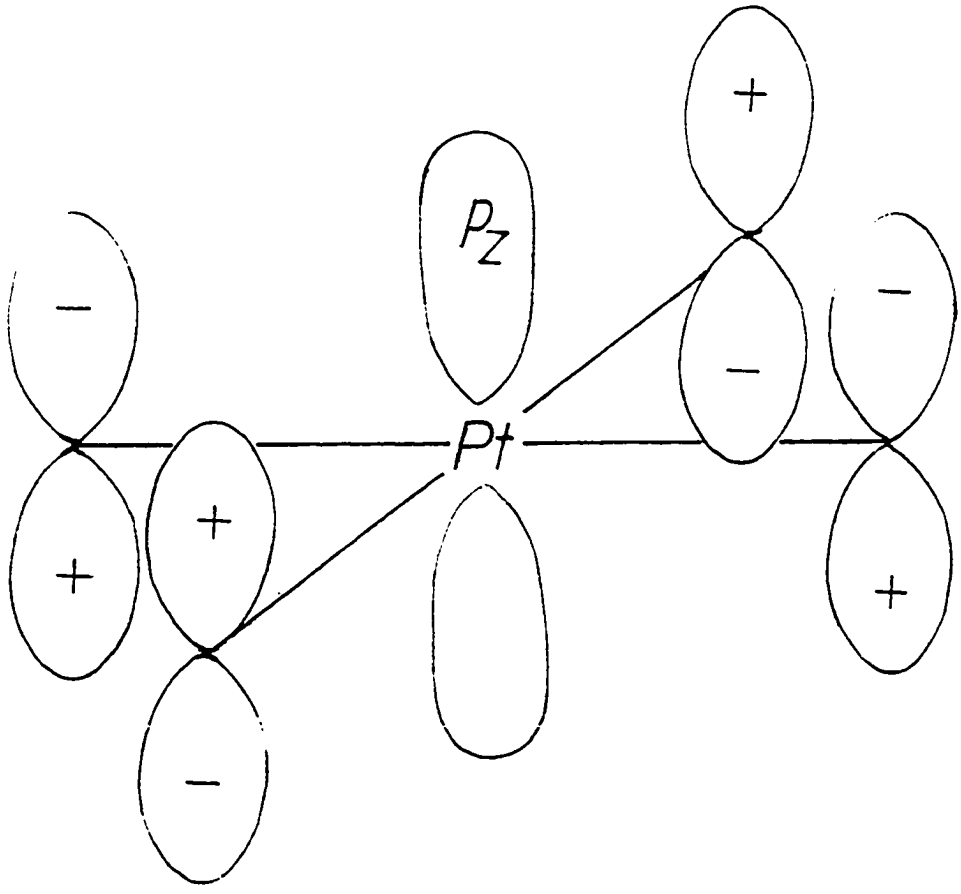

Figure 37. The b_{2u} ligand orbitals

more attractive candidates for assignment than ^1E_u and $^1A_{2u}$ are, however.

The symmetry-forbidden charge-transfer transition, $^1B_{2g} \leftarrow {}^1A_{1g}$ has received attention from Erny and Moncuit (43) and Elding and Olsson (24). This transition is assigned by both groups to the moderately intense (ε = 490 cm^{-1} M^{-1}, 36) peak at 30,900 cm^{-1} in the $PdCl_4^{2-}$ solution spectrum. The intensity and location of this peak compels us to consider this transition for assignment to the allowed bands in the Magnus-type salts.

Several problems with this prospective assignment are immediately noted. One concern is that the band at 30,100 cm^{-1} may not arise from a $PdCl_4^{2-}$ transition at all. Harrison et al. (27) have observed a shoulder at about 29,000 cm^{-1} in the crystal spectrum of $PdCl_4^{2-}$ in a Cs_2HfCl_6 matrix at 2K. Others (48,49) have also observed bands in the 27,400 cm^{-1} to 29,300 cm^{-1} region, but these bands are all very weak. Rush et al. (36) have reported finding no band in the single-crystal spectra of K_2PdCl_4, although they do observe a band in the solution spectrum at 30,100 cm^{-1}. They concluded that the observed band was a charge-transfer band belonging to $Pd_2Cl_6^{2-}$, which might have formed as an impurity in solution. Such a band is known to exist in that region for $Pd_2Cl_6^{2-}$. Elding and Olsson, however, report that the band is higher in intensity for those complexes in the series $PdCl_n(H_2O)_{4-n}^{-n}$ for which $^1B_{2g}$ is allowed by symmetry (24), suggesting that the band in $PdCl_4^{2-}$ does arise from $^1B_{2g} \leftarrow {}^1A_{1g}$. Erny and Moncuit's molecular orbital calculations also place $^1B_{2g} \leftarrow {}^1A_{1g}$ in the region (43).

Whether or not the band at 30,000 cm^{-1} in $PdCl_4^{2-}$ is $^1B_{2g} \leftarrow {}^1A_{1g}$, the polarization associated with the band is primarily x,y. The polarizations of the bands in the Magnus salts are primarily z, which again raises doubts about assignment of the bands in the Magnus-type salts to $^1B_{2g}$.

Perhaps the most important argument against the assignment comes from the temperature dependence of the intensities. It is fairly clear that the bands in the Magnus-type salts are allowed; the bands tend to grow more narrow and to retain their intensities as temperature is decreased. The $^1B_{2g} \leftarrow {}^1A_{1g}$ transition, on the other hand, is actually vibronic (though not d-d), since it is excited by an e_u vibration. Consequently, $^1B_{2g} \leftarrow {}^1A_{1g}$ cannot be assigned to the allowed bands in the Magnus-type salts.

Transitions within the cation provide yet another possibility for the assignment of the allowed bands. Such transitions, however, suffer from the same shift and intensity restrictions that were imposed on the anion LMCT's. Furthermore, assignment of allowed bands as low as 22,500 cm^{-1} would likely require us to abandon our assumption that the cation d-d bands remain at energies too high to be detected here.

Finally, shifts in the transition energies of the allowed bands as temperature increases from 6K suggests that these bands might be interionic electron transfer transitions. Table 13 lists observed differences in peak maxima at 300K and 6K for each $PdCl_4^{2-}$ salt. A positive shift indicates that the band's maximum red-shifts as tempera-

Table 13. Shifts of selected bands in the $PtCl_4^{2-}$ and $PdCl_4^{2-}$ upon decreasing temperature from 300K to 6K, in cm^{-1}

Salt	triplets[a]	$^1B_{1g}$	$^1A_{2g}/^1E_g$	allowed[b]
$Pd(en)_2PtCl_4$	+400	+100	shoulder	-
$Pd(NH_3)_4PtCl_4$	+300	-400	+300	-
$Pt(en)_2PtCl_4$	+100	-400	-500	-1000
$Pt(CH_3NH_2)_4PtCl_4$	-500	-	+100	-1225
$Pt(NH_3)_4PtCl_4$	-500	-	+200	-1700
$Pd(en)_2PdCl_4$	+100	-200	+150	-
$Pd(NH_3)_4PdCl_4$	-	-500	+400	shoulder
$Pt(en)_2PdCl_4$	-	-500	+ 50	- 900
$Pt(CH_3NH_2)_4PdCl_4$	-350	-350	+450	-1250
$Pt(NH_3)_4PdCl_4$	0	+150	+450	-1000

[a]Positive value denotes a red-shift as the temperature changes

[b]The bands are those in z between 28,000 cm^{-1} and 22,500 cm^{-1} for the $PdCl_4^{2-}$ series. For the $PtCl_4^{2-}$ series, the bands are those sharp bands in x,y between 33,600 cm^{-1} and 31,900 cm^{-1}.

ture goes from 6K to 300K; a negative shifts indicates a blue-shift over the same temperature change. All bands except the allowed ones show positive or modestly negative shifts. The allowed bands, in contrast, exhibit a blue-shift about twice as large as any other band's. Now, thermal excitations of molecular vibrations and phonons can produce a red-shift for a molecular transition. The significant blue-shift that we observe for the allowed bands suggests that the transitions occur between adjacent ions, rather than within the anions.

Interionic electron transfers require substantial overlap of orbitals on the adjacent ions to gain intensity. Large orbitals and small metal-metal distances increase the transition probability by promoting orbital overlap. With the exception of $Pd(NH_3)_4PdCl_4$, which as a d(M-M) of only 3.25 A, only those compounds with platinum cations exhibit the kind of allowed bands ascribed here to interionic electron transfers. Presumably, the larger d-orbitals on platinum facilitate sufficient overlap for such transitions to occur.

An electron-transfer transition is possible which has z-polarization (50), consistent with the predominantly z-polarized bands observed in the $PdCl_4^{2-}$ salts. This transition excites an electron out of the d_{xy} (b_{2g}) orbital on Pd, and into a linear combination of the $d_{x^2-y^2}$* orbitals on the two adjacent cations. If we view the angle formed by the Pt-N (or Pd-N) and Pd-Cl bonds as being exactly 45 degrees (perfectly staggered bonds), the $d_{x^2-y^2}$* orbitals would combine to give b_{2g} and b_{1u} linear combinations in D_{4h}, with the $PdCl_4^{2-}$ ion at the

center. The transition $A_{2u} \leftarrow A_{1g}$ (b_{1u} $[M(NH_3)_4^{2+}] \leftarrow b_{2g}$ $[PdCl_4^{2-}]$) would be dipole-allowed in z-polarization. Neither the crystal structure for MGS (6), nor our attempted structure for $Pt(en)_2PdCl_4$ show that the bonds in the cation are perfectly staggered with respect to the anion bonds. The linear combination should produce some allowed character, even if the bonds are not perfectly staggered, however. We therefore propose this transition for the z-polarized bands at 28,000 cm^{-1} 22,500 cm^{-1} in the $PdCl_4^{2-}$ series.

The absorption in x,y may be due to incomplete polarization of the band in z, but it is more likely that this absorption is due to an x,y-polarized interionic electron transfer. The most reasonable choice for such a transition is $E_u \leftarrow A_{1g}$ (b_{1u} $[M(NH_3)_4^{2+}] \leftarrow d_{xz,yz}$- $[PdCl_4^{2-}]$). This transition is allowed in x,y-polarization, and should occur at about the same energy as the transition in z, since the energies of the $d_{xz,yz}$ and d_{xy} orbitals differ very little, according to the assignments of the $^1A_{2g}$ and ^1E_g states in the previous section.

The region above 22,000 cm^{-1} in the $PdBr_4^{2-}$ series is dominated by allowed transitions, which are identified in the spectra by their lack of temperature dependence in the transition intensities.

The most intense transition in the region, the $^1E_u \leftarrow {}^1A_{1g}$ (b_{1g} $\sigma^* \leftarrow e_u$ L-π) state, was assigned by Rush et al. (36) to the band at 30,200 cm^{-1}, ε= 10,600 cm^{-1} M^{-1} in the aqueous $PdBr_4^{2-}$ spectrum at 300K. This band is x,y-polarized, and appears in our spectra as a rapidly rising absorption in x,y at about 22,000 cm^{-1} throughout

the series. Fortunately, an extremely thin crystal of $Pt(CH_3NH_2)_4PdBr_4$ permitted us to record the valley on the high-energy side of the transition (about 33,000 cm^{-1}), which allowed the peak maximum in the crystal spectrum to be tentatively located at about 28,000 cm^{-1}, even though the maximum of the intensity was far above the maximum absorbance range of our instruments.

Since the $^1E_u \leftarrow {}^1A_{1g}$ state is a transition from ligand p orbitals lying in the ion plane (13), as shown in Figure 36, small energy shifts are expected for the transition as d(M-M) decreases. The shift calculated from the tentative values given above is only 2200 cm^{-1}, thus supporting the assignment of the band to the $^1E_u \leftarrow {}^1A_{1g}$ state.

The moderately weak, allowed transition in the 31,000 cm^{-1} - 28,000 cm^{-1} range in z is assigned to $^1A_{2u} \leftarrow {}^1A_{1g}$ ($b_{1g}\ \sigma^* \leftarrow b_{2u}\ L-$) by analogy to the assignment made by Rush et al. (36) of the z-polarized band at 31,000 cm^{-1} in K_2PdBr_4 to this state. Support for this assignment comes from the degree and pattern of the energy shift within the series. Figure 37 indicates that $^1A_{2u}$ shifts to lower energy from K_2PdBr_4 to $Pd(NH_3)_4PdBr_4$, as expected. However, $^1A_{2u}$ in $Pt(en)_2PdBr_4$ occurs at 1400 cm^{-1} higher energy than in $Pd(NH_3)_4PdBr_4$, and at nearly the same energy as in $Pd(en)_2PdBr_4$, even though all of the d-d transitions shift to lower energies in $Pt(en)_2PdBr_4$. Again, as expected, the $^1A_{2u}$ energy decreases from $Pt(en)_2PdBr_4$ to $Pt(NH_3)_4PdBr_4$, where the $^1A_{2u}$ transition energy is almost identical to that for $Pd(NH_3)_4PdBr_4$.

Clearly, the $^1A_{2u}$ energy is being affected by the metal-metal spacing produced by the amine ligands, and not by the choice of metal in the cation. Perhaps the choice of metal in the cation is irrelevant to the ligand b_{2u} energy levels because the cation metal orbitals do not significantly extend into the region occupied by the anion b_{2u} ligand orbitals. Perturbation of the b_{2u} orbital energies will then be due to close approach of the ligand orbitals on the cations. Therefore, the $^1A_{2u}$ energy for $Pd(en)_2PdBr_4$ should about be the same as the $^1A_{2u}$ energy for $Pt(en)_2PdBr_4$, and the energy for $Pd(NH_3)_4PdBr_4$ should be about the same as that for $Pt(NH_3)_4PdBr_4$, just as observed. As was the case for the $PdCl_4^{2-}$ series, the overall shift of $^1A_{2u}$ over the $PdBr_4^{2-}$ series was smaller than that for $^1B_{1g}$, as expected.

A number of weaker allowed bands are also observed. The weak, z-polarized bands at 35,100 cm^{-1} and 32,100 cm^{-1} in $Pd(NH_3)_4PdBr_4$ have been tentatively assigned to the same $\sigma^* \leftarrow L$ transition to which the 43,200 cm^{-1} and 37,000 cm^{-1} bands in K_2PdBr_4 have been assigned (36). The assignments are based on the visual similarity of the $Pd(NH_3)_4PdBr_4$ spectrum to the K_2PdBr_4 spectrum in the high-energy region. The z-polarized absorption at 32,700 cm^{-1} in $Pt(CH_3NH_2)_4PdBr_4$ may also arise from these $\sigma^* \leftarrow L$ transitions.

The weak, z-polarized bands at 25,600 cm^{-1} and 24,500 cm^{-1} in $Pt(CH_3NH_2)_4PdBr_4$ and $Pt(NH_3)_4PdBr_4$, respectively, are assigned to the $^3E_u \leftarrow {}^1A_{1g}$ (b_{1g} $\sigma^* \leftarrow e_u$ $L\text{-}\pi$) state at 27,000 cm^{-1} in K_2PdBr_4. Like the $^1E_u \leftarrow {}^1A_{1g}$ (b_{1g} $\sigma^* \leftarrow e_u$ $L\text{-}\pi$) transition described earlier, ^3E_u

is not expected to red-shift greatly over the series. The observed shift of 2500 cm^{-1} is consistent with this assignment.

The series of shoulders, predominantly z-polarized, from 25,000 cm^{-1} in $Pt(en)_2PdBr_4$ to 22,000 cm^{-1} in $Pt(NH_3)_4PdBr_4$, could be either the ^3E_u state or one of the $\sigma^* \leftarrow L$ states severely red-shifted from its value in K_2PdBr_4. It is more likely, however, that these bands correspond to the allowed bands at 28,000 cm^{-1} - 22,500 cm^{-1} in the $PdCl_4$ series. Hence, they are assigned to the interionic transfer, $A_{2u} \leftarrow A_{1g}$ ($b_{1u}[M(NH_3)_4^{2+}] \leftarrow b_{2g}[PdBr_4^{2-}]$). If so, the bands in the $PdBr_4^{2-}$ series probably (by virtue of the shifts observed) originated at about 31,000 cm^{-1} in K_2PdBr_4, along with $^1A_{2u} \leftarrow {}^1A_{1g}$ ($\sigma^* b_{1g} \leftarrow b_{2u}$-$L$-$\pi$).

An x,y-polarized shoulder observed at about 22,000 cm^{-1} in several $Pt(en)_2PdBr_4$ crystal spectra was not very reproducible. Although the absorption might be due to a weak spin-forbidden or symmetry-forbidden transition, it is more likely due to a light leak at the high absorbance values for which the absorption was recorded. Such light leaks are attributed to surface defects at the crystal (51), and have been occasionally observed in the crystal spectra for other Magnus-type salts as well.

Certainly the most striking feature in the $PtCl_4^{2-}$ spectra are the sharp, moderately intense allowed bands at 31,900 cm^{-1} - 33,600 cm^{-1} in $Pt(en)_2PtCl_4$, $Pt(CH_3NH_2)_4PtCl_4$, and $Pt(NH_3)_4PtCl_4$. Although such sharp bands are uncommon in the spectroscopy of platinum complexes, a

precedent is known. Martin et al. (32) recorded an almost identical peak at 33,100 cm^{-1} in the b-polarized single-crystal spectrum of the molecular crystal, $Pt(en)Cl_2$.

Comparison of the sharp peak in $Pt(en)Cl_2$ with that in $Pt(en)_2PtCl_4$ provides rather convincing circumstantial evidence that the two peaks arise from the same transition. Both peaks occur in the polarization including the y-axis. The peak in $Pt(en)_2PtCl_4$ occurs at 33,650 cm^{-1} (6K), and the peak in $Pt(en)Cl_2$ occurs at 33,100 cm^{-1} (77K). Both peaks exhibit a blue-shift of about 1000 cm^{-1} on going from low temperature to room temperature. The $Pt(en)_2PtCl_4$ peak has ε= 600 cm^{-1} M^{-1} while the $Pt(en)Cl_2$ peak has ε= 600 cm^{-1} M^{-1}. The metal-metal separations are also quite similar: d(Pt-Pt) = 3.41 A for $Pt(en)_2PtCl_4$, and d(Pt-Pt) = 3.39 A for $Pt(en)Cl_2$.

Martin et al. assigned the absorption at 33,100 cm^{-1} in $Pt(en)Cl_2$ to an interionic electron transfer, on the grounds that the band was present only in the crystal spectra[1]. Furthermore, they argued that no Frenkel exciton transitions were available to account for the band. These authors proposed an assignment to $(d_{xy})_{j+1} \leftarrow (d_{xz})_j$, where the transition occurs from the d_{xz} orbital on the jth molecule, to the d_{xy} orbital on the adjacent molecule, labelled j+1. Note that the axis system used by Martin et al. differs from that used

---

[1]A weak band present in the solution spectrum was assigned to $^1B_{1g} \leftarrow {}^1A_{2g}$ ($\sigma^* b_{1g} \leftarrow dz^2\ a_{1g}$); its location at 33,100 cm-1 was explained as coincidental.

here for the D_{4h} system, so that the d_{xy} orbital on j corresponds to $d_{x^2-y^2}$ in the Magnus-type salts. This transition was the only d-d interionic transition allowed in b-polarization.

The similarity to the $Pt(en)Cl_2$ band, and especially the blue-shift experienced by the peak maxima as temperature rises, leads us to conclude that the bands in the Magnus-type salts are also interionic electron transfers, and that they correspond to the same transition as the band in $Pt(en)Cl_2$, though this transition may not be the same one proposed by Martin et al. for $Pt(en)Cl_2$.

Assigning the sharp peaks in the $PtCl_4^{2-}$ series to an interionic electron transfer confronts us with a significant difficulty, however, since the other interionic electron transfers postulated in the Magnus-type salts --the bands from 28,000 cm^{-1} to 22,500 cm^{-1} in the $PdCl_4^{2-}$ series -- were much broader than these peaks. One would not expect a great variation in the characteristic shapes of the peaks within the same class of transitions.

If an electron is excited into a σ^* orbital, the strength of the bonds in the excited state will tend to be less than the strengths in the ground state. In this situation, the Franck-Condon effect permits excitation by the totally symmetric vibration into several vibrational levels. The result is a broad electronic transition, such as those observed in the d-d region for these salts. Excitation into a nonbonding orbital, on the other hand, will have little effect on the bond strengths. Consequently, the Franck-Condon effect cannot produce

broad peaks in this case.

An excitation into the lowest unfilled nonbonding orbital is represented in the Magnus-type salts by the transition, $P_z\,[Pt(NH_3)_4^{2+}] \leftarrow d_{xz,yz}\,[PtCl_4^{2-}]$. Here, the P_z orbitals on the two $Pt(NH_3)_4^{2+}$ ions adjacent to a $PtCl_4^{2-}$ ion form a_{2u} and a_{1g} linear combinations. The a_{2u} linear combination can make the transition dipole-allowed in x,y-polarization in the D_{4h} system.

Since the sharp peaks in the Magnus-type salts are believed to be the same as the peak at 33,100 cm^{-1} in the b-y crystal spectrum of $Pt(en)Cl_2$, it is important to determine if the $P_z \leftarrow d_{xz,yz}$ transition can occur with the correct polarization in C_{2v}, the point-group which is used to describe the symmetry of $Pt(en)Cl_2$. Puckering of the ethylenediamines reduces the actual symmetry to C_2. The difference from C_{2v} is slight, however, so the transitions are considered to follow the rules for C_{2v}. Using the axis conventions of Martin et al. (32), the d_{xz} orbital becomes d_{yz} (b_1) in the $Pt(en)Cl_2$ system; d_{yz} becomes d_{xy} (a_2). The linear combinations of the P_z orbitals on adjacent $Pt(en)Cl_2$ molecules have symmetries of b_1 and a_1. The symmetry products indicate that $(b_1)_{j+1} \leftarrow (d_{xz})_j$ is allowed in x-a, and $(b_1)_{j+1} \leftarrow (d_{yz})_j$ is allowed in y-b. Transitions to the a_1 linear combination are forbidden in both x and y. This is gratifying, since the transitions to the corresponding a_{1g} linear combination in the Magnus-type salts are also symmetry-forbidden. We therefore tentatively assign the sharp bands, both in the Magnus-

type salts and $Pt(en)Cl_2$, to an interionic charge transfer of the type, $P_z\ [Pt(NH_3)_4^{2+}] \leftarrow d_{xz,yz}\ [PtCl_4^{2-}]$.

The region in the $PtCl_4^{2-}$ spectra between 26,000 cm^{-1} and 29,000 cm^{-1} show modest allowed peaks and absorbances in the valleys in x,y-polarization similar to that observed in the 28,000 cm^{-1} - 22,500 cm^{-1} region for the $PdCl_4^{2-}$ salts. These features are tentatively attributed to the interionic electron transfer, $\sigma^*\ [Pt(NH_3)_4^{2+}] \leftarrow d_{xz,yz}\ [PtCl_4^{2-}]$. This transition possesses the x,y-polarization required by the spectra. The difference of about 5000 cm^{-1} from the sharp peaks at 32,000 cm^{-1} is in accord with the difference of 6000 cm^{-1} in the $6p_z$ and $d_{x^2-y^2}{}^*$ band energies in $Pt(NH_3)_4^{2+}$, as assigned by Isci and Mason from the $Pt(NH)_4^{2+}$ solution spectra (35).

Although supporting evidence for the assignments to interionic electron transfer transitions is scarce, such transitions appear to provide a better explanation for the observed features than any of the other types of transitions considered.

The salts in the $PtBr_4^{2-}$ series display a number of absorption bands above the d-d region that can be attributed to allowed transitions.

Both $Pd(en)_2PtBr_4$ and $Pd(NH_3)_4PtBr_4$ display weak absorptions between 31,000 cm^{-1} and 32,000 cm^{-1} in both polarizations. Similar absorption has been observed at that region in the aqueous $PtBr_4^{2-}$ spectrum, and attributed to an intense ligand-to-metal charge-transfer band in $Pt_2Br_6^{2-}$, a minor species believed to be present in both $Pd(en)_2PtBr_4$ and $Pd(NH_3)_4PtBr_4$; they could be due to the $Pt_2Br_6^{2-}$

transition. However, the $Pt_2Br_6^{2-}$ ion is not likely to fit into the crystal sites, so this assignment is not favored. These bands seem to be better explained as spin-forbidden charge transfers, such as $^3E_u \leftarrow {}^1A_{1g}$ ($d_{x^2-y^2}{}^* \leftarrow e_u L\text{-}\pi$) or $^3A_{2u} \leftarrow {}^1A_{1g}$ ($d_{x^2-y^2}{}^* \leftarrow b_{2u} L\text{-}\pi$). The negligible shift of these transitions especially supports assignment to the $^3E_u \leftarrow {}^1A_{1g}$ transition.

Like the $PdCl_4^{2-}$ salts, the $PtBr_4^{2-}$ salts with platinum cations exhibit peaks and valleys with nonzero absorbance just on the high-energy side of the d-d region, around 27,000 cm^{-1} - 24,000 cm^{-1}. By visual analogy with the absorptions in the other three series, these bands are assigned to the interionic electron transfer transitions of the types, b_{1u} $[Pt(NH_3)_4^{2+}] \leftarrow d_{xy}$ $[PtBr_4^{2-}]$ (z), and b_{1u} $[Pt(NH_3)_4^{2+}] \leftarrow d_{xy,yz}$ $[PtBr_4^{2-}]$ (x,y).

Vibrational Structure

The $PdCl_4^{2-}$ series exhibited the strongest and most distinct vibrational structure of any of the series studied. For each of the salts, structure appeared on the $^1A_{2g}$ (x,y) band at 6K, and several salts possessed structure in weak, spin-forbidden bands. Table 14 summarizes the observed structure for each series, and Appendix B catalogs the components for each salt.

Salts of the other three series generally showed weak structure; only in $Pt(en)_2PtCl_4$ and $Pd(en)_2PtCl_4$ were progressions observed that were as robust as those seen in the $PdCl_4^{2-}$ series.

Vibrational structure is discernible in the $^1A_{2g}$ band for

Table 14. Summary of vibrational structure on the $^1A_{2g}$ transitions

Compound		No. of peaks	Intensity
$Pt(NH_3)_4PdCl_4$	247 ± 19	11	weak
$Pt(CH_3NH_2)_4PdCl_4$	258 ± 24	14	strong
$Pt(en)_2PdCl_4$	257 ± 12	15	strong
$Pd(NH_3)_4PdCl_4$	258 ± 49	7	very weak
$Pd(en)_2PdCl_4$	260 ± 18	15	strong
$Pt(NH_3)_4PdBr_4$	-	-	very weak
$Pt(CH_3NH_2)_4PdBr_4$	175 ± 29	5	very weak
$Pt(en)_2PdBr_4$	170 ± 9	5	weak
$Pd(NH_3)_4PdBr_4$	158 ± 13	7	weak
$Pd(en)_2PdBr_4$	169 ± 24	8	weak
$Pt(NH_3)_4PtCl_4$	280 ± 33	5	weak
$Pt(CH_3NH_2)_4PtCl_4$	283 ± 20	7	weak
$Pt(en)_2PtCl_4$	281 ± 11	9	strong
$Pd(NH_3)_4PtCl_4$	250 ± 35	3	very weak
$Pd(en)_2PtCl_4$	278 ± 17	11	strong
$Pt(NH_3)_4PtBr_4$	-	-	very weak
$Pt(CH_3NH_2)_4PtBr_4$	176 ± 18	3	weak
$Pt(en)_2PtBr_4$	176 ± 24	7	weak
$Pd(NH_3)_4PtBr_4$	-	-	very weak
$Pd(en)_2PtBr_4$	172 ± 22	9	very weak

seventeen of the twenty compounds studied. Table 14 gives the average separation between components for each compound. Note that, for each series, the separation is characteristic of the totally symmetric stretching vibration ν_1 for each anion. The decrease in frequency from the value for the ground state obtained from Raman spectra is attributed to the longer M-X bond length (where M= Pt,Pd; X= Cl,Br) and consequent weaker bond in the excited state, compared to the ground state.

The standard deviations for the average separation over the progressions are typically about 10 percent of the separations. While the high deviation may indicate systematic changes in the progressions, such as a decrease in separation arising from an asymmetric potential function, it is more likely that they simply reflect uncertainties in the measurements, in view of the relatively low resolution and low intensities encountered in these spectra.

The absence of observed structure in a compound's spectra does not mean, of course, that no vibrational progression occurs for the compound. Crystals of many of the salts did not form as thick or as large as crystals of other salts. For example, the crystals of two salts for which no structure was observed, $Pt(NH_3)_4PdBr_4$ and $Pd(NH_3)_4$-$PtBr_4$, formed only as very thin and fragile needles that afforded extremely small crystal faces. The combination of small surface area and thickness often required us to operate the spectrophotometer at the limit of its resolution. Larger, thicker crystals, and improved

instrumentation might reveal structure for these two salts.

However, even those salts for which large, thick crystals were produced often showed weakly developed structure, and in the case of $Pt(NH_3)_4PtBr_4$, no structure at all. Therefore, the division of the structure into categories of "strong", "weak", and "very weak" in Table 14 can, in fact, be taken as a fair description of the intensities of the observed structure.

$Pd(en)_2PdCl_4$ was richest in vibrational structure: distinct progressions were observed in the weak, spin-forbidden $^3A_{2g}$, ^3E_g bands at 16,000 cm^{-1} and in the $^1E_g/^1B_{1g}$ z-polarized band at 20,000 cm^{-1}, as well as in the $^1A_{2g}$ band at 20,200 cm^{-1} in x,y-polarization.

The structure on the $^3A_{2g}$, ^3E_g bands appear as seven weak peaks in x,y-polarization, with an average separation of about 271 ± 31 cm^{-1}, and as eleven somewhat stronger peaks in z, with an average separation of 261 ± 10 cm^{-1}. Figure 38 shows the bands at 6K and 300K for a very thick (106 μm) crystal. The asymmetric shape and poor resolution of the peaks in x,y indicates the presence of at least two transitions, at about 16,000 cm^{-1} and 17,000 cm^{-1}. This suggests that the $^1E_g/^1B_{1g}$ states in the band at 20,000 cm^{-1} occur at slightly higher energy than the $^1A_{2g}$ state. This is quite reasonable, in view of the location of $^1E_g/^1B_{1g}$ at higher energy than $^1A_{2g}$ in $Pd(en)_2PdBr_4$.

The well-resolved structure visible in the z-polarized peak at 16,000 cm^{-1} suggests that the transition in z is excited by only one vibration, although a total of nine excited-state energies

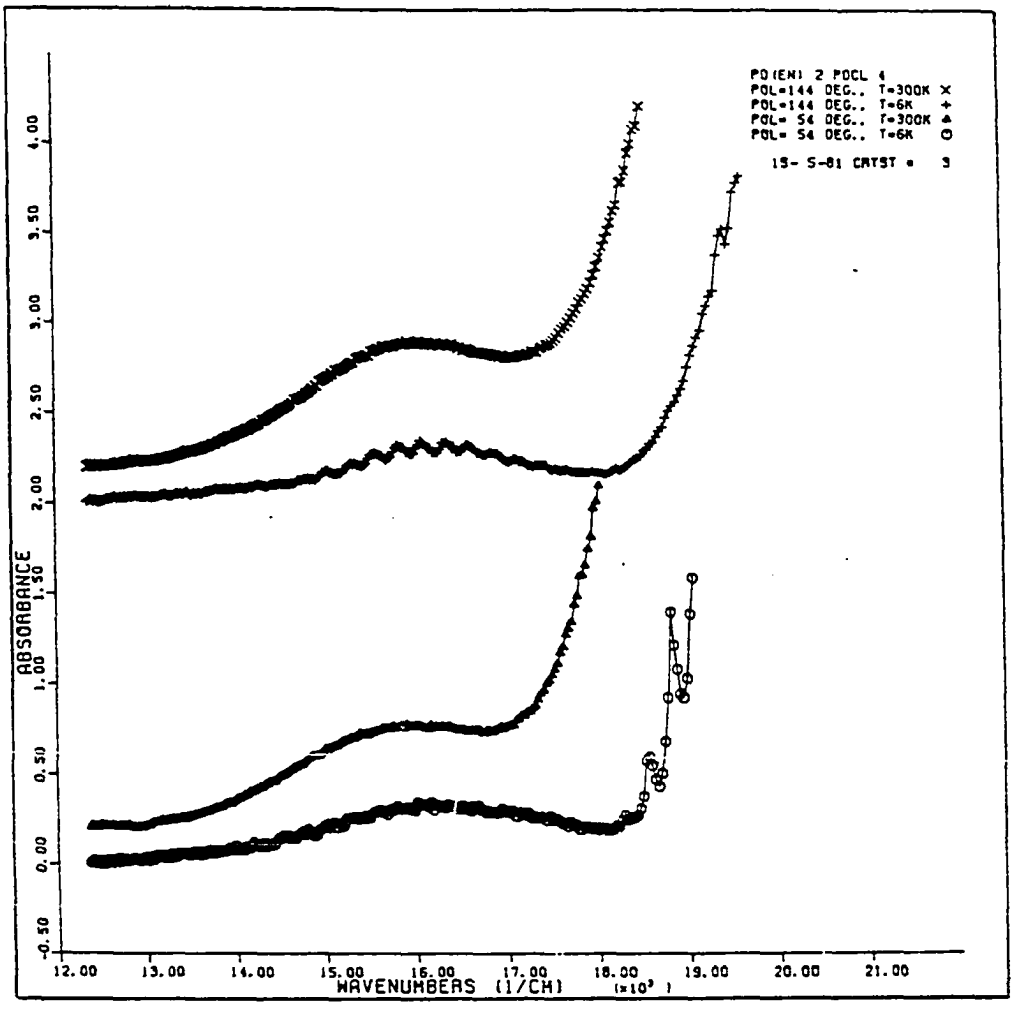

Figure 38. Vibrational structure on the low-energy, spin-forbidden bands in $Pd(en)_2PdCl_4$

are expected for the spin-forbidden transitions. The remaining transitions are probably too weak to be observed.

$Pd(en)_2PdCl_4$ was also the only Magnus-type salt to show vibrational structure in the $^1E_g/^1B_{1g} \leftarrow {}^1A_{1g}$ band in z-polarization. Figure 39 shows the z-polarized structure, as well as the much stronger x,y-polarization. Eleven weak components, with an average separation of 265 ± 25 cm^{-1} were observed. The z-polarized ^1E_g transition is excited by e_u vibrations, and although the structure may arise because one vibration is more effective than another in vibronic excitation (13), it appears that this is not likely, since no other salts show structure in this band. A possible explanation for the structure arises from the suggestion made in the next section, based on evidence from the structural detail of the $^1A_{2g}$ band, that the two e_u vibrational frequencies actually differ by such a small amount that vibrational structure is no longer significantly reduced by the presence of two asymmetric exciting vibrations of different frequencies (13). The structure appears better developed because the progressions due to each vibration are merged into a single progression by the limited resolution in the measurement.

Of course, it is also possible that the structure in $^1E_g/^1B_{1g}$ is observed as a result of incomplete polarization, which can occur because the $Pd(en)_2PdCl_4$ unit cell is triclinic. At least a partial crystal structure determination is necessary in order to calculate polarization ratios (52) for incomplete polarization.

Figure 39. Portions of the polarized absorption spectra of $Pd(en)_2PdCl_4$, showing vibrational structure in both z- and x,y-polarizations

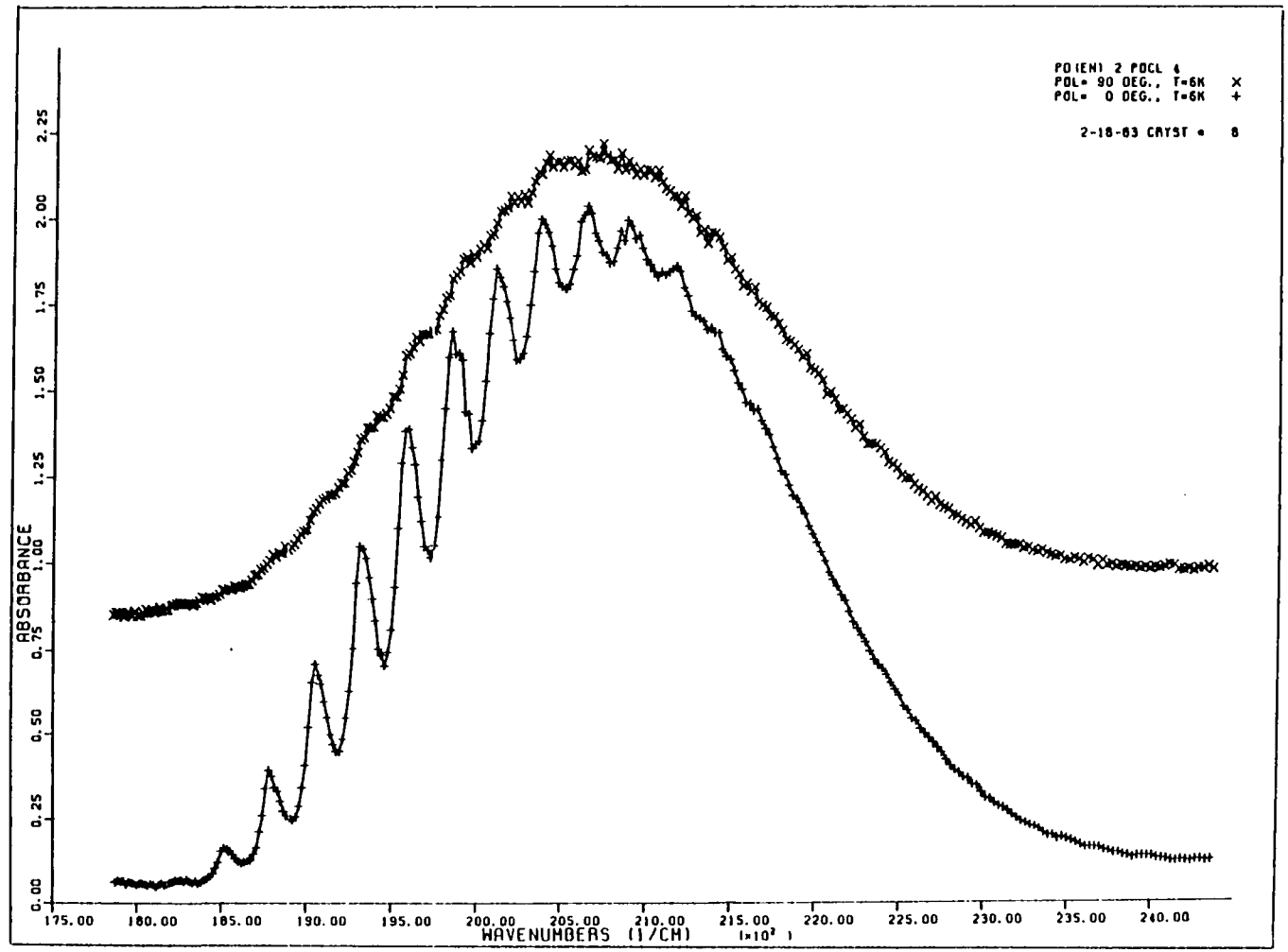
PD(EN) 2 PDCL 6
POL= 90 DEG., T=6K X
POL= 0 DEG., T=6K +
2-18-83 CRYST # 8
ABSORBANCE
0.00
0.25
0.50
0.75
1.00
1.25
1.50
1.75
2.00
2.25
175.00
180.00
185.00
190.00
195.00
200.00
205.00
210.00
215.00
220.00
225.00
230.00
235.00
240.00
WAVENUMBERS (1/CM) (*10²)

A similar calculation performed for $Pt(en)_2PdCl_4$, using Pd and Cl positions obtained from the structure attempt discussed in this section, yielded a polarization ratio, $P_z/P_{x,y}$ of 72,840, which is beyond the capabilities of our instrument to detect. Unfortunately, this calculation is of limited value, since it is $Pd(en)_2PdCl_4$, not $Pt(en)_2PdCl_4$, which shows the structure in the $^1E_g/^1B_{1g}$ band.

Vibrational detail was observed in slow wavelength scans of the $^1A_{2g}$ band for $Pt(CH_3NH_2)_4PdCl_4$, $Pt(en)_2PdCl_4$, and $Pd(en)_2PdCl_4$. The arrows in Figure 40 indicate the vibrational detail in a representative scan of a $Pt(CH_3NH_2)_4PdCl_4$ crystal. The components were observed only in the first 4-5 peaks in the vibrational progression, but they were quite distinct and reproducible over several thick crystals for each salt, so there is little doubt about their authenticity.

The components are very similar to the L, B, and S components resolved in the 15K crystal spectra of K_2PdBr_4 (36). Table 15 lists the energy separations associated with the components in each salt.

Rush et al. (36) have assigned the strong components S and B in K_2PdBr_4 to ν_6, an asymmetric stretch, and ν_7, and in-plane bend that constitute the two e_u exciting vibrations. The L component was assigned to a lattice vibration, and the C component to a combination mode.

The energy separation of S and B (i.e., ν_6-ν_7) was only 50 cm^{-1},

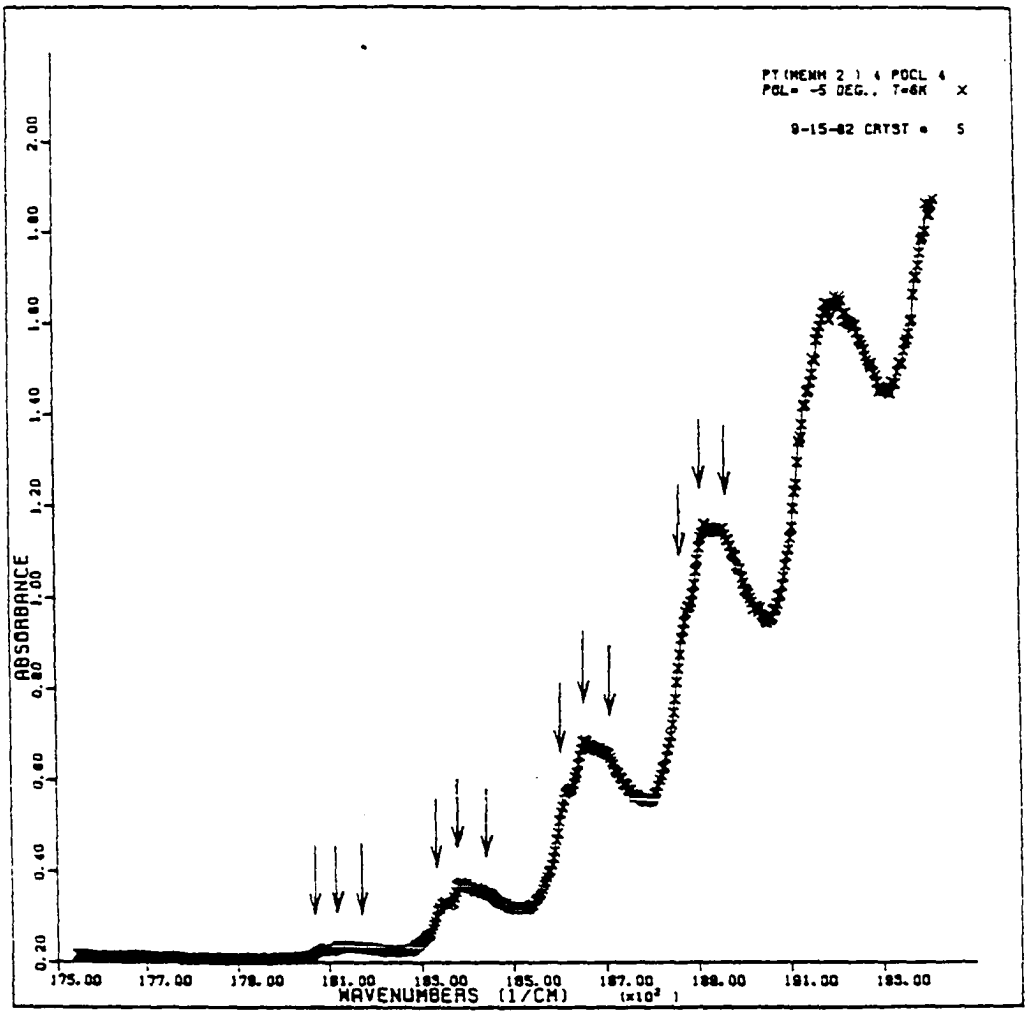

Figure 40. Structural detail on the $^1A_{2g}$ band at 6K for $Pt(CH_3NH_2)_4PdCl_4$

Table 15. Energy separations in cm^{-1} for observed vibrational components

Salt	Separation (cm^{-1})		
	1-2[a]	1-3[b]	2-3[c]
$Pd(en)_2PdCl_4$	-	-	52.4 ± 7.5
$Pt(en)_2PdCl_4$	59.3 ± 5.9	95.5 ± 7	36.3 ± 3.8
$Pt(CH_3NH_2)_4PdCl_4$	38.8 ± 2.5	72.5 ± 8.7	33.8 ± 9.5
K_2PdBr_4[d]	45	90	40

[a]Separation of bending and stretching band.

[b]Separation of bending and lattice band.

[c]Separation of stretching and lattice band.

[d]Separations calculated from Reference 36.

compared to 120 cm^{-1} in the ground-state $PdBr_4^{2-}$ ion. Rush et al. therefore concluded that ν_7 would not decrease, and might actually increase on going from the ground-state ion to the excited state in K_2PdBr_4. Such an increase indicated to Rush et al. that the e_u in-plane bending vibration in the excited state is spatially restricted by the nearby K^+ ions. As support, they cited the fact that the e_u bending displacements decrease the Br-K distance much more rapidly than do the e_u stretching vibrations.

The explanation proposed by Rush et al. for the small separation seen in K_2PdBr_4 appears to be reasonable for $Pd(en)_2PdCl_4$ and the other Magnus-type salts as well: although the radius of the chloride ligand is smaller than the bromide, and thus will decrease the spatial restriction suffered by the Pd-Cl bending mode, the bulky methylamine and ethylenediamine ligands on the cations should serve to restore the spatial restriction to the levels believed to exist in K_2PdBr_4. Note that the ν_6-ν_7 separation assigned to K_2PdCl_4 is 120 cm^{-1}, whereas the separations observed for K_2PdBr_4, $Pt(en)^{2-}PdCl_4$, and $Pt(CH_3NH_2)_4PdCl_4$ are all between 39 cm^{-1} and 59 cm^{-1}.

Changes in ν_6-ν_7 may also explain why the intensity of the vibrational structure varies widely from compound to compound, and why the $PtBr_4^{2-}$ and $PdBr_4^{2-}$ series of the Magnus-type salts show only weak, poorly resolved structure, while K_2PtBr_4 and K_2PdBr_4 show well-resolved vibrational structure.

It has been noted (13) that one of the conditions which may reduce vibrational structure is the existence of more than one

asymmetric vibration of different frequencies which excite a given transition. The result of multiple exciting vibrations is the superposition of several progressions in the same region of the band in such a way that the progressions destructively interfere, thereby reducing the observed intensity of the progressions. The $^1A_{2g}$ transition in these complexes is excited by the e_u vibrations, which include both the e_u stretch (ν_6) and the e_u bend (ν_7). As the ν_6-ν_7 separation becomes larger, reduction of the observed vibrational structure should occur. But, as ν_6-ν_7 approaches zero, merging of the peaks associated with ν_6 and ν_7 occurs throughout the progression, resulting in larger separations between the remaining peaks. Thus, the structure will exhibit its maximum intensity. Although complete crystal structures for each Magnus-type salt are needed to confirm the hypothesis, it appears that those salts which spatially restrict the e_u bend the most, and hence have the smallest ν_6-ν_7 values, exhibit the most intense vibrational structure.

As indicated in Table 14, none of the Magnus-type salts having NH_3 ligands exhibit strong vibrational structure. By the reasoning given above, the NH_3 salts should not exhibit strong vibrational structure because the NH_3 ligands do not sufficiently crowd either the chloride or the bromide ligands enough to affect ν_7. Structure would also be weak in the methylamine and ethylenediamine salts with bromide ligands because the bromides cause the unit cell to be so large that the methylamine or ethylenediamine

ligands, though bulky, do not crowd the bromide as the e_u in-plane bending vibration brings the bromide closer to the amine in the adjacent cation unit. The $PtCl_4^{2-}$ series, on the other hand, shows substantial structure because the somewhat smaller unit cell permitted by the chloride ligands allows the chloride moved by the e_u bend to get close enough to the ethylenediamine to produce a spatial restriction. $Pt(CH_3NH_2)_4PtCl_4$ is an intermediate case: moderate structure is observed because methylamine is intermediate in size between NH_3 and ethylenediamine. Finally, the ethylenediamine and methylamine salts in the $PdCl_4^{2-}$ series show strong vibrational structure because, as seen above, ν_6-ν_7 is greatly reduced from its value in K_2PdCl_4. It should be stressed, however, that complete crystal structures which give the C-Cl and C-Br in-plane distances are needed to confirm this proposal.

GENERAL SUMMARY

The conclusions drawn from the data presented here partially support the view of Day et al. (28,29), that the optical spectra of the Magnus-type salts can be explained by a vibronic model with crystal perturbations of the orbitals present in the isolated anion. We have shown, however, that other transitions also occur in the visible and near ultraviolet regions. These charge-transfer transitions join the d-d transitions in bringing about the unusual colors observed in MGS and the other Magnus-type salts. We may conclude that the unusual colors are not the result of metal-metal bonding or formation of bands delocalized over many metal centers (9,31).

Our placement of $^1B_{1g} \leftarrow {}^1A_{1g}$ ($\sigma^* \leftarrow d_{z^2}$) with the $^1E_g \leftarrow {}^1A_{1g}$ ($\sigma^* \leftarrow d_{xz,yz}$) transition in K_2MX_4, M= Pt or Pd; X= Cl or Br, as proposed earlier by Elding and Olsson (24), suggests that the d_{z^2} orbital mixes somewhat with the s orbital in the next higher shell. That such mixing can occur implies that the 6s orbital in MGS lies at an energy only moderately higher than the 5d orbitals.

It appears unlikely that the absorption at 20,700 cm^{-1} (z), 20,900 cm^{-1} (x,y) in K_2PtCl_4 is the $^1B_{1g}$ band: the temperature dependence of the peak intensities across the entire $PtCl_4^{2-}$ series does not correspond to that expected for the $^1B_{1g}$ band, nor is the shift of the $^1B_{1g}$ absorption expected to be less than the shift for ^1E_g, as would clearly be the case in the $PdCl_4^{2-}$ and $PdBr_4^{2-}$ series, if $^1B_{1g}$ were indeed at very low energy. Thus,

our research provides evidence contradicting the proposals of Tuszynski and Gliemann (26) for K_2PtCl_4 and several related complexes. While the d_{z^2} orbital may be destabilized somewhat by mixing with the 6s orbital, the systems do not experience the destabilization required to place $^1B_{1g}$ much below ^1E_g except where the metal-metal spacings are very small, as in $Pt(NH_3)_4PdCl_4$ and MGS.

Crystal effects may modify the d-d bands, but they also produce allowed bands corresponding to transfer of electrons from one ion to an adjacent ion. This mechanism should not be viewed as a delocalization over the entire chain, as one would expect from band theory. Rather, the delocalization of the transition is limited to only a central ion and its two nearest neighbors in the chain.

The formation of these electron-transfer exciton states in the Magnus-type salts is promoted by the close metal-metal spacings, which permit orbital overlap to a degree not possible in the potassium salts. Unlike the formation of ionic exciton states in molecules, however, these excited states in the Magnus-type compounds correspond to a decrease in the charge of the ions involved. We therefore note that the changes in the lattice energies of the crystals, along with changes in the ionization energies of the ions, will be important factors in determining the energies at which the interionic electron transfer transitions will occur. The relative importance of each of these factors to the Magnus-type systems is not yet resolved.

This research has demonstrated the relationship that exists between the physical orientation of the orbitals in the Magnus-type salts and the absorption spectra for the salts. It is hoped that future research will provide spectroscopic and structural data necessary to refine the assignments and rationalizations presented here, particularly those pertaining to the vibrational structure intensities and the interionic electron transfers.

REFERENCES

1. Magnus, G. Pogg. Ann. 1828, 14, 242.

2. Cox, E.G.; Pinkard, W.; Wardlaw, W.; Preston, G.H. J. Chem. Soc. 1932, 2527.

3. Yamada, S. J. Am. Chem. Soc. 1951, 73, 1182.

4. Godycki, J.; Rundle, R. Acta Cryst. 1953, 6, 487.

5. Yamada, S.; Tsuchida, R. J. Am. Chem. Soc. 1953, 75, 6351.

6. Atoji, M.; Richardson, J.W.; Rundle, R.E. J. Am. Chem. Soc. 1957, 79, 3017.

7. Yamada, S.; Tsuchida, R. Bull. Chem. Soc. Japan 1956, 29, 894.

8. Miller, J.R. J. Chem. Soc. 1961, 4452.

9. Miller, J.R. J. Chem. Soc. 1965, 713.

10. Fishman, E.; Interrante, L.V. Inorg. Chem. 1972, 11, 1722.

11. Mehran, F.; Scott, B.A. Phys. Rev. Lett. 1973, 31, 99.

12. Yamada, S. J. Am. Chem. Soc. 1951, 73, 1579.

13. Martin, D.S. Inorg. Chim. Act. Revs. 1971, 5, 107.

14. Chatt, J.; Gamlen, G.O.; Orgel, L.E. J. Chem. Soc. 1958, 486.

15. Fenske, R.F.; Martin, D.S.; Ruedenberg, K. Inorg. Chem. 1962, 1, 441.

16. Gray, H.B.; Ballhausen, C.J. J. Am. Chem. Soc. 1963, 85, 260.

17. Basch, H.; Gray, H.B. Inorg. Chem. 1967, 6, 365.

18. Cotton, F.A.; Harris, C.B. Inorg. Chem. 1967, 6, 369.

19. Martin, D.S.; Tucker, M.A.; Kassman, A.J. Inorg. Chem. 1965, 4, 1682.

20. Martin, D.S.; Foss, J.G.; McCarville, M.E.; Tucker, M.A.; Kassman, A. Inorg. Chem. 1966, 5, 491.

21. McCaffery, A.J.; Schatz, P.N.; Stephens, P.J. J. Am. Chem. Soc. 1968, 90, 5730.

22. Messmer, R.P.; Wahlgren, U.; Johnson, K.H. Chem. Phys. Lett. 1973, 18, 7.

23. Vanquickenborne, L.G.; Ceulemans, A. Inorg. Chem. 1981, 20, 796.

24. Elding, L.I.; Olsson, L.F. J. Phys. Chem. 1978, 82, 69.

25. Martin, D.S. Inorg. Chem. 1966, 5, 1298.

26. Tuszynski, W.; Gliemann, G. Z. Naturforsch. 1979, 34a, 211.

27. Harrison, T.G.; Patterson, H.H.; Godfrey, J.J. Inorg. Chem. 1976, 15, 1291.

28. Day, P.; Orchard, A.F.; Williams, R.J.P. J. Chem. Phys. 1965, 42, 1973.

29. Day, P.; Orchard, A.F.; Williams, R.J.P. J. Chem. Phys. 1965, 43, 3763.

30. Anex, B.G.; Ross, M.E.; Hedgecock, M.W. J. Chem. Phys. 1967, 46, 1090.

31. Anex, B.G.; Takeuchi, N. J. Am. Chem. Soc. 1974, 96, 4411.

32. Martin, D.S.; Hunter, L.D.; Kroening, R.; Coley, R.F. J. Am. Chem. Soc. 1971, 93, 5433.

33. Martin, D.S.; Rush, R.M.; Kroening, R.; Fanwick, P.E. Inorg. Chem. 1973, 12, 301.

34. Martin, D.S. private communication, Iowa State University, Ames, Iowa.

35. Isci, H.; Mason, W.R. Inorg. Nucl. Chem. Lett. 1972, 8, 885.

36. Rush, R.M.; Martin, D.S.; LeGrand, R.G. Inorg. Chem. 1975, 14, 2543.

37. Jacobson, R.A. "An Algorithm For Automatic Indexing and Bravais Lattice Selection: the programs BLIND and ALICE", Ames Laboratory-USAEC Report IS-3469, Iowa State University, Ames, Iowa, 1974.

38. Takusagawa, F. Ames Laboratory, USDOE, Iowa State University, Ames, Iowa, unpublished.

39. Lapp, R.L.; Jacobson, R.A. "FOUR: A Generalized Crystallographic Fourier Program", Ames Laboratory-DOE Report IS-4737, Iowa State University, Ames, Iowa, 1980.

40. Mais, R.H.B.; Owston, P.G.; Wood, A.M. Acta Cryst. 1972, B28, 393.

41. Martin, D.S. "Program Wave", Iowa State University, Ames, Iowa, unpublished.

42. The derivation was performed by Dr. D.S. Martin, Iowa State University, Ames, Iowa.

43. Erny, M.; Moncuit, C. Theoret. Chim. Acta 1982, 61, 29.

44. Drago, R.S. Physical Methods in Chemistry, Philadelphia, W.B. Saunders, 1977.

45. Moncuit, C. Theoret. Chim. Acta (Berl.) 1975, 39, 255.

46. Staritzky, E. Anal. Chem. 1956, 28, 915.

47. Kroening, R.F.; Rush, R.M.; Martin, D.S.; Clardy, J.C. Inorg. Chem. 1974, 13, 1366.

48. Harris, C.M.; Livingstone, S.E. J. Chem. Soc. 1959, 1505.

49. Franke, E.; Moncuit, C. C.R. Hebd. Seances Acad. Sci., Ser. B. 1970, 271, 741.

50. Martin, D.S. private communicaition, Iowa State University, Ames, Iowa.

51. Martin, D.S. "Optical Properties of Linear Chain Haloamine Platinum Complexes" in Extended Linear Chain Compounds, Vol. 1, J.S. Miller, ed., New York, Plenum, 1982, p. 409.

52. Robbins, G.A. Ph.D. dissertation, Iowa State University, Ames, Iowa, 1982.

ACKNOWLEDGMENTS

I wish to thank Dr. D.S. Martin for his help, guidance, and support throughout my time as a graduate student. From him I have learned much indeed.

I also wish to express my deep gratitude to my wife, Lanette, for her support and encouragement under a variety of unusual, and often trying, circumstances. Similar thanks go to my good friend Fred Miller, for similar reasons.

Finally, I thank Mrs. Sue Shankster for the courage, patience, and determination she displayed as she typed this dissertation.

APPENDIX A

In general, the intensity of an electronic transition depends on the transition moment integral:

$$\underset{\sim}{\mu} = \langle \psi_{el}' | (\hat{M}_x + \hat{M}_y + \hat{M}_z) | \psi_{el}^{\circ} \rangle \quad (1)$$

where ψ_{el}' is the excited-state electronic wavefunction, ψ_{el}° is the ground-state electronic wavefunction, and $\hat{M}_x$, $\hat{M}_y$, $\hat{M}_z$ are the dipole moment components along each of the three Cartesian coordinates. A nonzero transition moment integral gives rise to a nonzero transition intensity. The transition moment integral is nonzero only if the symmetry product of equation 1 contains the totally symmetric representation. In the D_{4h} system,

$$\Gamma_{\psi_{el}'} \cdot \Gamma_{\psi_{el}^{\circ}} \cdot \Gamma_{\hat{M}_x,\hat{M}_y,\hat{M}_z} \supset A_{1g} \quad (2)$$

must be true for a transition to gain intensity. Now, $\hat{M}_z$ transforms in D_{4h} as A_{2u}, and $\hat{M}_x$,$\hat{M}_y$ transform together as E_u. Therefore, the D_{4h} selection rules are

$$\Gamma_{el}' \cdot \Gamma_{el}^{\circ} \supset A_{2u} \quad (3)$$

and

$$\Gamma_{el}' \cdot \Gamma_{el}^{\circ} \supset E_u \quad (4)$$

for polarizations in z and x,y, respectively. These conditions hold for all electric dipole-allowed transitions.

Some transitions, such as the d-d transitions with which much of this research is concerned, do not satisfy the dipole-allowed selection rules. These transitions gain some allowed character by vibronic coupling, however.

The transition moment integral in the case of vibronic coupling is

$$\underset{\sim}{\mu} = \langle \psi_{el}{}' \psi_{vib}{}' \, | (\hat{M}_x + \hat{M}_y + \hat{M}_z) | \, \psi_{el}{}^{\circ} \psi_{vib}{}^{\circ} \rangle \qquad (5)$$

where $\psi_{vib}{}^{\circ}$ and $\psi_{vib}{}'$ are the ground-state and excited-state vibrational wavefunctions, and all other terms are defined as they were in equation 1. For transitions from an A_{1g} vibrational ground state, the vibronic selection rules are

$$\Gamma_{\psi_{el}'} \cdot \Gamma_{\psi_{el}^{\circ}} \cdot \Gamma_{\psi_{vib}'} \supset A_{2u} \qquad (6)$$

and

$$\Gamma_{\psi_{el}'} \cdot \Gamma_{\psi_{el}^{\circ}} \cdot \Gamma_{\psi_{vib}'} \supset E_u \qquad (7)$$

for z- and x,y-polarizations, respectively. The ungerade normal vibrations, a_{2u}, b_{2u}, e_u (stretching), and e_u (bending) for square-planar MX_4 groups, give allowed character in the vibronic coupling mechanism for D_{4h}.

APPENDIX B: CATALOG OF PEAK MAXIMA FOR VIBRATIONAL STRUCTURE IN THE MAGNUS-TYPE SALTS

Table 1. Energies (ν, cm^{-1}) for the observed vibrational peaks for the $^1A_{2g}$ transitions (6K) in the $PdCl_4^{2-}$ series

$Pd(en)_2PdCl_4$		$Pd(NH_3)_4PdCl_4$	$Pt(en)_2PdCl_4$	
			17924	
18250			18175	
18525	(18585)[b]		(18372)[a] 18430	(18471)[b]
18790	(18850)	18900	(18636) 18688	(18723)
19060	(19105)	19200	(18882) 18943	(18975)
19320	(19365)	19400	(19135) 19201	(19238)
19586	(19637)	19700	19443	
19865		20000	19755	
20125		20250	20008	
20400		20450	20263	
20688			20509	
20905			20768	
21175			21026	
21400			21286	
21660				
21887				

[a]Parentheses indicate the shoulder assigned to a bending vibration.

[b]Parentheses indicate the shoulder assigned to a lattice vibration.

$Pt(CH_3NH_2)_4PdCl_4$			$Pt(NH_3)_4PdCl_4$
			17960
(18080)[a]	18120	(18140)[b]	18215
(18350)	18390	(18425)	18475
(18620)	18660	(18700)	18700
(18885)	18920	(18960)	19000
	19210		19250
	19500		19500
	19750		19780
	20000		20000
	20300		20250
	20550		20500
	20800		
	21050		
	21250		

Table 2. Energies (ν, cm^{-1}) for the observed vibrational peaks for the $^1A_{2g}$ transitions (6K) in the $PdBr_4^{2-}$ series

$Pd(en)_2PdBr_4$	$Pd(NH_3)_4PdBr_4$	$Pt(en)_2PdBr_4$	$Pt(CH_3NH_2)_4PdBr_4$
18083	18025		
18215	18175	18150	
18382	18350	18315	18300
18587	18500	18490	18500
18762	18675	18670	18650
18939	18825	18830	18800
19084	18975		19000
19268			

Table 3. Energies (ν, cm^{-1}) for the observed vibrational peaks for the $^1A_{2g}$ transitions (6K) in the $PtCl_4^{2-}$ series

$Pd(en)_2PtCl_4$	$Pd(NH_3)_4PtCl_4$	$Pt(en)_2PtCl_4$	$Pt(CH_3NH_2)_4PtCl_4$	$Pt(NH_3)_4PtCl_4$
			23400	
23625		23750	23700	23750
23875		24030	24000	24025
24130		24320	24275	24275
24410		24600	24550	24575
24700	24800[a]	24875	24850	24825
24975	25075	25170	25100	25150
25250	25300	25450		
25530		25710		
25810		26000		
26120				
26375				

[a]Extremely weak and poorly defined.

Table 4. Energies (ν, cm^{-1}) for the observed vibrational peaks for the $^1A_{2g}$ transitions (6K) in the $PtBr_4^{2-}$ series

$Pd(en)_2PtBr_4$	$Pt(en)_2PtBr_4$	$Pt(CH_3NH_2)_4PtBr_4$
22805	22727	
22989	22883	
23175	23068	23068
23364	23229	23256
23557	23392	23419
23697	23613	
23849	23781	
24038		
24184		

Table 5. Energies (ν, cm^{-1}) for the vibrational peaks for triplet and z-polarized singlet transitions of $Pd(en)_2PdCl_4$

triplet x,y [a]	triplet z	singlet z
14174	14793	18250
14503	15038	18520
14749	15291	18820
15015	15557	19100
15279	15823	19350
15552	16069	19650
15798	16332	19900
	16584	20200
	16858	20410
	17123	20750
	17391	20750
		21030

[a]Transition type and polarization, respectively.

Table 6. Energies (ν, cm^{-1}) for weak transitions in the x,y - polarization (6K) for $Pd(en)_2PtCl_4$ and $Pt(en)_2PtCl_4$

$Pd(en)_2PtCl_4$	$Pt(en)_2PtCl_4$
22075	21940
22325	22240
22610	22525
22870	22800
	23100
	23370